VIRTUAL SCREENING AND DOCKING OF POTENTIAL PROTEIN KINASE B INHIBITORS

by

Seval Kenar

B.S., Chemical Engineering, Middle East Technical University, 2008

Submitted to the Institute for Graduate Studies in
Science and Engineering in partial fulfillment of
the requirements for the degree of
Master of Science

Graduate Program in Chemical Engineering

Boğaziçi University

2012

ACKNOWLEDGEMENTS

I would like to thank all the people who had valuable contribution to this thesis. I owe my gratitude to all those people who have made this dissertation possible. Since it is not just a written document, but it is freedom to explore science, a way of questioning thoughts and expression of ideas. It is my pleasure to extend my sincere gratitude to my thesis advisor Prof. Dr. Kutlu Ülgen and my co-supervisor Assist. Prof. Elif Özkırımlı Ölmez who were abundantly helpful and offered invaluable assistance, support and guidance with their wise advice and encouragement they provided at different stages of my research, my graduate experience has ripened.

I wish to express my appreciation to the members of my committee: Prof. Viktorya Aviyente, Prof. Türkan Haliloğlu, and Prof. Kemal Yelekçi for their constructive criticisms and insightful comments.

I am also grateful to all of my friends and colleagues with whom I have shared experiences in graduate studies. I wish to thank especially Gizem Özbüyükkaya, Gözde Taşkın, Begüm Alaybeyoğlu, Deniz Menekşedağ and Oya Gürsoy for their various forms of support during my graduate study. The warm friendship ties us have helped me overcome setbacks and stay focused on my graduate study.

Most importantly, none of this would have been possible without the love and patience of my parents. This dissertation has been underpinned by their love, concern, support and strength all these years. My deepest gratitude is to my dear husband, Suat. He encouraged me throughout this endeavor, and had always full faith in me to accomplish my task.

Financial support provided by projects of TUBITAK 111M444 and BAP 5554 is gratefully acknowledged.

ABSTRACT

VIRTUAL SCREENING AND DOCKING OF POTENTIAL PROTEIN KINASE B INHIBITORS

This study aims to carry out a molecular docking process of novel ATP competitive inhibitors for protein kinase B-beta (PKBβ / AKT-2), activation of which has been observed in 30-40% of ovarian and pancreatic cancers. 3D pharmacophore filtering by Phase and multistep docking and scoring by Glide were applied to two different conformations of AKT-2 to take into account the conformational change upon binding of different inhibitors. The molecule library CoCoCo was screened to find hits. The procedure employed here combines the pharmacophore building and database screening methods, considers the protein conformation change upon binding by using two different protein conformations and also takes into account the solvation effect by including conserved water molecules in the active site. The top ranked molecules were further analyzed according to their interactions with AKT-2 and the final docking results from Glide were compared with previously identified inhibitors based on structure and chemistry. As a main contribution, ten putative inhibitors were proposed and analyzed for absorption, distribution, metabolism, and excretion (ADME) properties and selectivity for PKB-β.

ÖZET

POTANSİYEL PROTEİN KİNAZ B İNHİBİTÖRLERİNİN SANAL TARAMASI VE DOKLANMASI

Bu çalışmada, pankreas ve yumurtalık kanseri vakalarının %30-40'ında aktivasyonu gözlenen protein kinaz B-β (PKB-β / AKT-2) için yeni "ATP rekabetçi" inhibitörlerin moleküler doklanması hedeflenmiştir. AKT-2 proteininin farklı inhibitörlere bağlandığında geçirdiği yapısal değişiklikleri hesaba katmak için iki farklı AKT-2 yapısına, Phase ile üç boyutlu farmakofor filtreleme ve Glide ile çok adımlı doklama ve skorlama uygulanmıştır. CoCoCo molekül kütüphanesi isabet molekülleri (hit) bulmak için taranmıştır. Bu çalışmada kullanılan uygulama ile farmakofor oluşturma ve veritabanı tarama yöntemleri birleştirildi, bağlanma sırasındaki protein yapısal değişikliği iki farklı protein konformasyonu kullanılarak ele alındı, ve aynı zamanda korunmuş su molekülleri aktif bölgeye dahil edilerek çözünme etkisi dikkate alındı. Üst sıradaki moleküllerin AKT-2 ile olan etkileşimleri detaylı olarak analiz edildi ve Glide'ın nihai doklama sonuçları, önceden tanımlanmış inhibitörlerle yapılarına ve kimyalarına göre karşılaştırıldı. Sonuç olarak, on olası inhibitör önerildi ve bu moleküllerin ADME ve PKB-β' ya seçicilik özellikleri incelendi.

TABLE OF CONTENTS

LIST OF FIGURES

LIST OF TABLES

LIST OF SYMBOLS

C	Carbon
Cl	Chlorine
H	Hydrogen
N	Nitrogen
O	Oxygen
S	Sulfur
Å	Angstrom
α	Alpha
β	Beta
γ	Gamma
ΔG, DG	Binding free energy

LIST OF ACRONYMS/ABBREVIATIONS

2D	Two dimensional
3D	Three dimensional
A	Hydrogen bond acceptor
Ala	Alanine
accptHB	Number of hydrogen bond acceptors
ADME	Absorption, distribution, metabolism, and excretion
Arg	Arginine
Asn	Asparagine
Asp	Aspartic acid
ATP	Adenosine triphosphate
AU-ROC	Area under the receiver-operating characteristic curve
CAT	Catalytic domain
Coul	Coulomb energy
CPU	Central processing unit
D	Hydrogen bond donor
donorHB	Number of hydrogen bond donors
EXT	C-terminal extension
FISA	Hydrophilic component of the total surface accessible area
FOSA	Hydrophobic component of the total surface accessible area
Gly	Glycine
GA	Genetic algorithm
Gln	Glutamine
Glu	Glutamic acid

H	Hydrophobic group
Hbond	Hydrogen bonding energy
His	Histidine
HM	Hydrophobic regulatory motif
HTS	High-throughput screening
IC	Incremental construction
IFD	Induced fit docking
Leu	Leucine
Lipo	Lipophilic energy
LogP	Partition coefficient
Lys	Lysine
MC	Monte Carlo
MD	Molecular dynamics
Met	Methionine
MM-GBSA	Molecular mechanics/generalized born surface area
MW	Molecular weight
N	Negatively charged group
NCI	National Cancer Institute
O (1,2,3,4,5)	Proposed 2JDO molecules 1, 2, 3, 4, 5
OPLS	Optimized potentials for liquid simulations
P	Positively charged group
PCaco	Predicted permeability
PDB	Protein Data Bank
PDK-1	3-phosphoinositide-depedent protein kinase 1
PH	Pleckstrin homology domain
Phe	Phenylalanine

PI3K	Phosphatidylinositol 3-kinase
PIP_2	Phosphatidylinositol-3,4-biphosphate
PIP_3	Phosphatidylinositol-3,4,5-triphosphate
PISA	Phi component of the total solvent accessible surface area
PPW	Protein preparation wizard
Q	Charge
QSAR	Quantitative structure-activity relationship
R	Aromatic ring
R (1, 2, 3, 4, 5)	Proposed 2JDR molecules 1, 2, 3, 4, 5
RCSB	Research Collaboratory for Structural Bioinformatics
ROC	Receiver operating characteristic
RMSD	Root mean square deviation
RotB	Rotatable bond penalty
S	Solute equilibrium concentration
SASA	Total solvent accessible surface area in square angstroms
Ser	Serine
SP	Standard precision
Thr	Threonine
Tyr	Tyrosine
Val	Valine
vdW	Van der Waals
VS	Virtual screening
Wat (1, 2, 3, 4)	Conserved water molecules 1, 2, 3, 4
WPSA	Weakly polar component of the total solvent accessible surface area
XP	Extra precision

1. INTRODUCTION

The main challenge for the pharmaceutical industry is to increase success rate in bringing drugs to the market. Approximately 14-year period and more than US$800 million are required for a compound to become an approved drug [1, 2]. The major aim in drug discovery is to decrease this timeline and increase the number of hit identification. Therefore, there is an increasing investment in computational methods such as combinatorial chemistry [3], and predictive ADME methods [4].

A kinase is an enzyme that catalyzes the transfer of phosphate group from high-energy donor such as ATP to a specific acceptor. Up to five hundred different kinases have been identified in the human genome [5]. Protein kinases are one of the largest group of kinases and they are known as key regulators of almost all cellular signaling cascades. Protein kinases are responsible for many diseases including cancer, if the signaling network is perturbed by any abnormalities such as mutation [6], and they are an important therapeutic target.

This research is planned to find potential inhibitors (candidate drug) among a large number of molecules (dataset) for protein kinase B-β (target protein), which is also known as AKT-2, by computational methods of pharmacophore modeling and structure based drug design. The results will guide drug design efforts and narrow down the list of molecules to be tested experimentally.

CoCoCo_Phase database [7], which compatibly works with Phase program was used within the framework of this study. All screening processes were performed by Schrodinger Suite 2011. Structure information of target proteins were retrieved from Protein Data Bank [8]. Database was virtually screened by ligand-based pharmacophore model and structure-based docking method. Phase and Glide programs were used for ligand and structure-based approaches, respectively. Post-filtering analyses including, strain energy estimation, pharmacokinetic feature calculation, and binding free energy calculations were also performed.

The succeeding sections of this study contain detailed information about the theoretical background of the research, adopted procedure with computational methods, analysis of the results and recommendations. Basic background information about computer-aided drug design and brief summary about target protein and small molecule database are given in Chapter 2 (Theory section). Chapter 3 (Method section) includes all parameters and computational approaches that were used throughout the study. In Chapter 4 (Result and Discussion section) findings of the research are reported and presented via tables and illustrated materials. Implications of the findings are explained and interpretations are also stated in this section. Conclusion and Recommendation section, Chapter 5, covers an overview about the research such as primary aim, methodology, major results and conclusion. Some recommendations are also suggested for future research. Extra information regarding the content of the study is presented in the Appendix.

2. THEORY

Traditionally used experimental high throughput screening (HTS) is expensive and time consuming to screen a large compound database. Virtual screening (VS) is an alternative computational method used to discriminate between wanted and unwanted molecules, scale down molecular database to identify novel drug candidates for experimental testing. VS can be divided into two categories; ligand-based virtual screening which is generally based on ligand similarity and structure-based virtual screening which is primarily docking [9, 10].

2.1. Ligand-Based Virtual Screening

Ligand-based approaches are useful when the crystal structure of the target protein is unknown [11–13] but can also be used when 3D structure is available. In the latter case, ligand-based approaches are used as pre-processing step before a structure-based VS to filter the molecular database to eliminate compounds that do not contain essential features required for binding or activity [14]. In order to apply ligand-based virtual screening, knowledge of a number of active binders to the active site is required. Information that is gathered from a set of active binders is then used to screen a database to find a compound that have similar property and thus activity [15] which can be explained by Similar Property Principle. Similar Property Principle [16] indicates that similar structures possibly have similar properties. Structurally similar molecules are more likely to be active with respect to a random molecule in the database. The main idea behind VS is to screen a database to find molecules that have similar property to the reference molecules, searching criteria change with respect to the applied method [17].

Molecular similarity, fragment searching, 3D shape matching, quantitative structure-activity relationships (QSAR) and pharmacophore matching are the commonly used ligand-based VS methods [15, 18]. Molecular fingerprint method is used to screen a molecular database to identify molecules that have similar fingerprints [18]. Pharmacophore methods consist of identification of common pharmacophoric features

from a set of active ligands and screening database with these features, and activity of a screened molecule can be found by building QSAR model [17–19].

The first definition of “pharmacophore” was given by Paul Ehrlich as: “a molecular framework that carries the essential features responsible for a drug’s biological activity” [20]. In other words a pharmacophore is the 3D orientation of chemical features that defines the binding interactions between the molecule and target protein. A pharmacophore model is determined by retrieving common features from a set of actives by superimposing 3D structures of the actives, and this model is used to screen a molecular database [21].

Pharmacophore feature is generally a chemical functional group and frequently used features in computer aided drug design programs can be classified as H-bonding interactions, lipophilic areas, aromatic interactions, electrostatic interactions, and custom, user-defined features [10]. Widely used computer programs to build a pharmacophore model are Phase, MOE, Discovery Studio, LigandScout, Catalyst, and ICM-Chemist.

Within the framework of the present thesis, the program Phase was employed which can be used for pharmacophore perception, structure alignment, activity prediction, and 3D database searching [22, 23].

2.2. Structure-Based VS

When the structure of the target protein is known, structure-based computational methods can be used. Molecular dynamics (MD) simulations and docking are the commonly used structure-based VS methods [18]. MD simulation is used to explain the binding interactions of a molecule and its target protein, and this method can also give properties like membrane permeability of the molecule [24]. By molecular docking, favored orientation of molecule within the binding site can be predicted computationally and affinity can be predicted via scoring functions [15]. Target protein structure and small molecule database are needed to perform molecular docking. Molecular docking method includes the internal steps of virtually placing a molecule into the binding site, computationally simulates the protein-ligand interaction to attain optimum steric and

physicochemical properties, and scoring this generated pose of the molecule [25]. High-scored molecules are then selected to be tested experimentally (Figure 2.1).

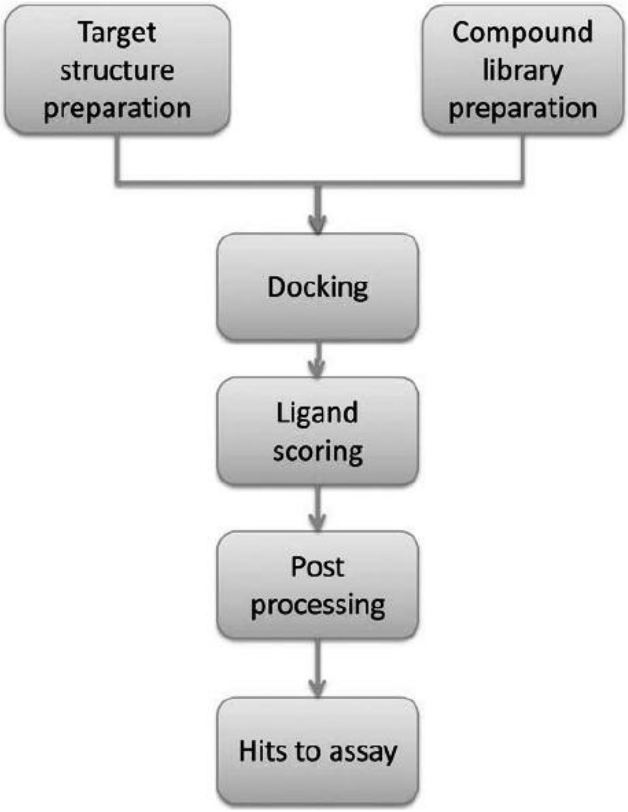

Figure 2.1. Representative workflow of docking-based virtual screening [25].

As popularity of the molecular docking increases, the number of docking programs is also increasing. The most widely used ones are summarized in Table 2.1, each program uses a different searching strategy such as genetic algorithm (GA), Monte Carlo (MC), and incremental construction (IC). Within the framework of the present research Glide (Grid-based Ligand Docking with Energetics) will be used which searches for interactions between ligand molecules and a receptor molecule. Glide can be run in rigid or flexible docking modes.

Table 2.1. Commonly used docking programs where GA: genetic algorithm, MC: Monte Carlo, IC: incremental construction [25].

Program	Search strategy	Free for academia	Website
AutoDock [26]	GA/MC	Yes	http://autodock.scripps.edu
Dock [27]	IC	Yes	http://dock.compbio.ucsf.edu
FlexX [28]	IC	No	http://www.biosolveit.de/flexx
Glide [29]	Hybrid	No	http://www.schrodinger.com
Gold [30]	GA	No	http://www.ccdc.cam.ac.uk/products/life_sciences/gold
Surflex [31]	IC	No	http://www.tripos.com/index.php
ICM [32]	MC	No	http://www.molsoft.com/docking.html
LigandFit [33]	MC	No	http://accelrys.com/products/discovery-studio
eHiTS [34]	IC	No	http://www.simbiosys.ca/ehits/index.html

2.3. Small Compound Database

The selection of database which is used in virtual screening process has a great importance on the success of a project [35]. A small compound database usually consists of physically available compounds that are supplied by chemical vendors [25]. A number of small compound databases that are commonly used in virtual screening is listed in Table 2.2.

Table 2.2. Commonly used virtual screening databases [25].

Database	Type	# compounds	Website
PubChem	Public	30 million	http://pubchem.ncbi.nlm.nih.gov
ChEMBL	Public	1 million	https://www.ebi.ac.uk/chembldb/index.php
NCI Set	Public	140,000	http://dtp.nci.nih.gov/index.html
ChemSpider	Public	26 million	http://www.chemspider.com
CoCoCo	Public	7 million	http://cococo.unimore.it/tiki-index.php
TCM	Public	32,000	http://tcm.cmu.edu.tw
ZINC	Public	13 million	http://zinc.docking.org
ChemBridge	Commercial	700000	http://www.chembridge.com
Specs	Commercial	240000	http://www.specs.net
Asinex	Commercial	550000	http://www.asinex.com
Enamine	Commercial	1.7 million	http://www.enamine.net

Table 2.2. Commonly used virtual screening databases [25] (cont.).

Database	Type	# compounds	Website
Maybridge	Commercial	56000	http://www.maybridge.com
WOMBAT	Commercial	263000	http://www.sunsetmolecular.com
ChemDiv	Commercial	1.5 million	http://www.chemdiv.com
ChemNavigator	Commercial	55.3 million	http://www.chemnavigator.com
ACD	Commercial	3870000	http://accelrys.com/products/databases/sourcing/available-chemicals-directory.html
MDDR	Commercial	150000	http://accelrys.com/products/databases/bioactivity/mddr.html

2.3.1. CoCoCo Database

CoCoCo [7], Commercial Compound Collection, is a free, ready to use, multiconformational chemical database, which is designed particularly for pharmacophore screening. CoCoCo database is made of the chemical providers which are listed in Table 2.3. The versions of the original chemical vendor databases and the original number of records for corresponding version are also listed in Table 2.3.

Table 2.3. Chemical vendors of CoCoCo database [7].

Chemical vendors	Version of the database	Number of records
Asinex	27/03/2009	261606
ChemBridge	21/05/2009	603253
ChemDiv	22/09/2009	789834
Life Chemicals	16/09/2009	316539
National Cancer Institute (NCI)	09/2003	260071
Princeton Biomolecular Research Inc.	29/07/2009	1082074
Enamine	21/10/2009	1350112
Specs	28/09/2009	201570
Total		4865059

CoCoCo database was first created by Dr. Alberto Del Rio and then it was developed by BioChemoInformatics Laboratory at the University of Bologna. The preparation process of CoCoCo database has two parts. First part is the common preparation and consists of cleaning of the vendors' files and elimination of the duplicate molecules.

Corina software is used for hydrogen addition and conversion of all chemical structures to 3D. SDF toolkit is used for eliminating the duplicate chemical structures within the same vendor and among the vendors (Table 2.4). Second part of their preparation process consists of generation of tautomers and stereoisomers. For 3.7 million compounds, which are remained after elimination of duplicates, tautomers are generated by the tautomerizer utility and stereoisomers are generated by Corina. There are approximately 7 million (6 981 566) records at the end of this step. Next part is the conformation generation and calculations vary depending on output file. They define three output options for multiconformer version of CoCoCo; namely, CoCoCo_MC, CoCoCo_Catalyst, and CoCoCo_Phase. CoCoCo_Catalyst is designed to work with the Discovery Studio (DS) software and conformer generation is done by DS suite. CoCoCo_Catalyst contains 600 million conformers. CoCoCo_MC is in sdf file format and designed to be used in any pharmacophore screening software while CoCoCo_Phase is designed to work with the Phase software and both of CoCoCo_MC and CoCoCo_Phase are prepared by ionizer and ConfGen utilities and both databases have 144 million conformers.

Table 2.4. First part of CoCoCo database preparation [7].

	# original	# after Corina	#internal duplicates	# duplicates among vendors							
				Asinex	ChemBridge	ChemDiv	Life Chemicals	NCI	Princeton Biomolecular Research Inc.	Enamine	Specs
Asinex	261606	261585	208	0	73630	69365	16274	3873	102492	22017	43758
ChemBridge	603253	602922	352		0	52824	18161	3545	185629	29621	35313
ChemDiv	789834	789810	27618			0	51644	2611	97890	17712	18808
Life Chemicals	316539	316537	276				0	687	28757	18374	1874
NCI	260071	257548	17450					0	4486	3538	1182
Princeton Biomolecular Research Inc.	1082074	1082040	107324						0	33609	38002
Enamine	1350112	1350100	18							0	5233
Specs	201570	201556	1								0

2.4. Protein Kinase B (PKB)

In 1987, Stephen Staal identified AKT, which is also known as protein kinase B [36], as a viral oncogene [37]. However, research on AKT was significantly increased after activation of AKT by insulin [38] was discovered in 1995. AKT kinase is a member of AGC kinase superfamily [39], and there are three isoforms in the AKT family; namely, AKT-1/PKB-α [37], AKT-2/PKB-β [40], and AKT-3/PKB-γ [41]. AGC kinase superfamily in the human kinome and AKT family in AGC kinase group are illustrated in Figure2.2 and Figure 2.3, respectively. Figure 2.3 also shows the sequence of activation sites of AGC kinase and AKT family is highlighted in the figure.

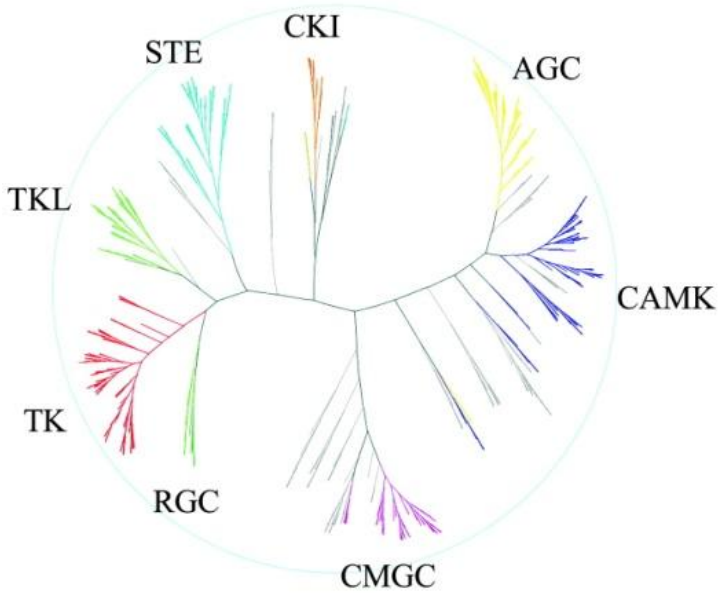

Figure 2.2. The human kinome.

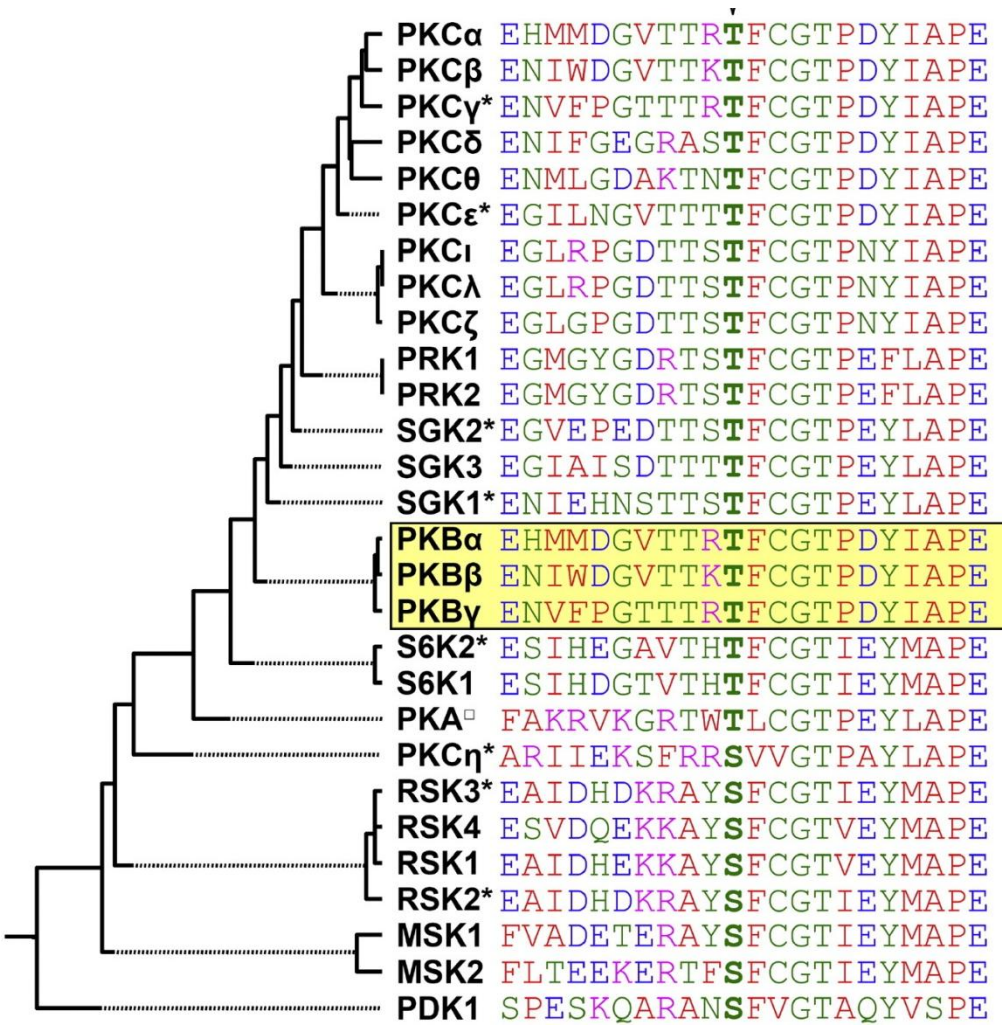

Figure 2.3. Phylogenetic tree of several AGC kinase with activation site sequence [42] (AKT family is shown in yellow box).

AKT structure is composed of conserved three domains (Figure 2.4). They are pleckstrin homology (PH) domain which is located in the N-terminus, kinase catalytic domain and hydrophobic regulatory motif in the C-terminal tail [43]. Poorly conserved linker (LINK) region is placed between CAT domain and PH domain. All three isoforms are homologous with high sequence identity. Table 2.5 lists the percent sequence identity among AKT isoforms for the different regions.

Table 2.5. Pairwise percent identity within AKT domains [39].

Pair	PH	LINK	CAT	EXT
AKT-1/AKT-2	80	46	90	66
AKT-1/AKT-3	84	40	88	76
AKT-2/AKT-3	76	17	87	70

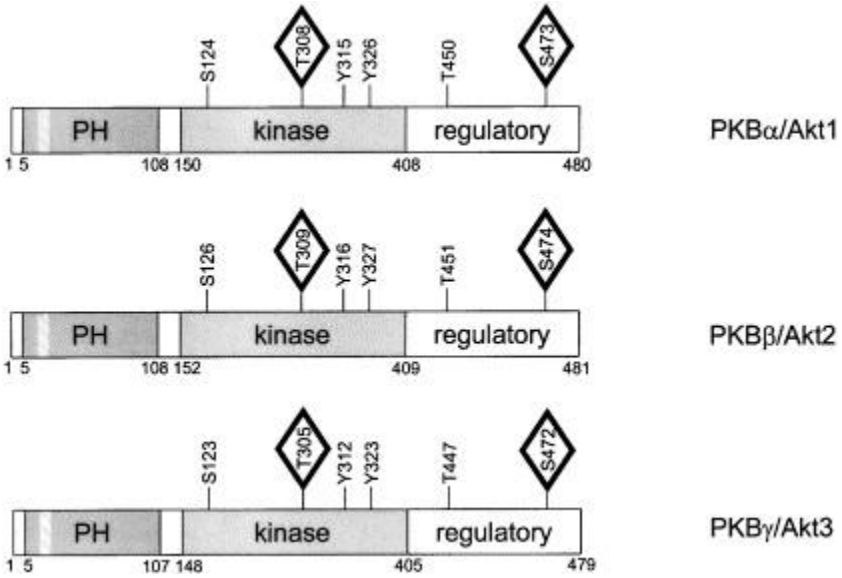

Figure 2.4. Domains of AKT protein [44].

Catalytic domains of protein kinases (Figure 2.5) have structurally and functionally diverse bilobal form in the mechanisms of regulation and activation [45]. N-lobe mainly consists of β-sheet structure, whereas helices are common in the C-lobe. There are two conserved sequence motifs in N-lobe; namely, Gly-rich loop and P-loop. Gly-rich loop, which has a conserved motif of GxGxxG, is placed between β1 and β2. Gly-rich loop is the most flexible part of the protein and it has a highly conserved hydrophobic residue Val that interacts with ATP. C-helix is located in the N-lobe and its position with respect to the activation loop determines the open and closed conformations. C-lobe is very stable and helices D, E, F, and H are highly buried. Four β-strands in the C-lobe, which are positioned between the two lobes, participate in the phosphate translation from ATP to protein. The catalytic loop is located between β6 and β7. P+1 loop in C-lobe has a role in substrate recognition. The activation loop and Mg-binding loop are also part of the C-lobe.

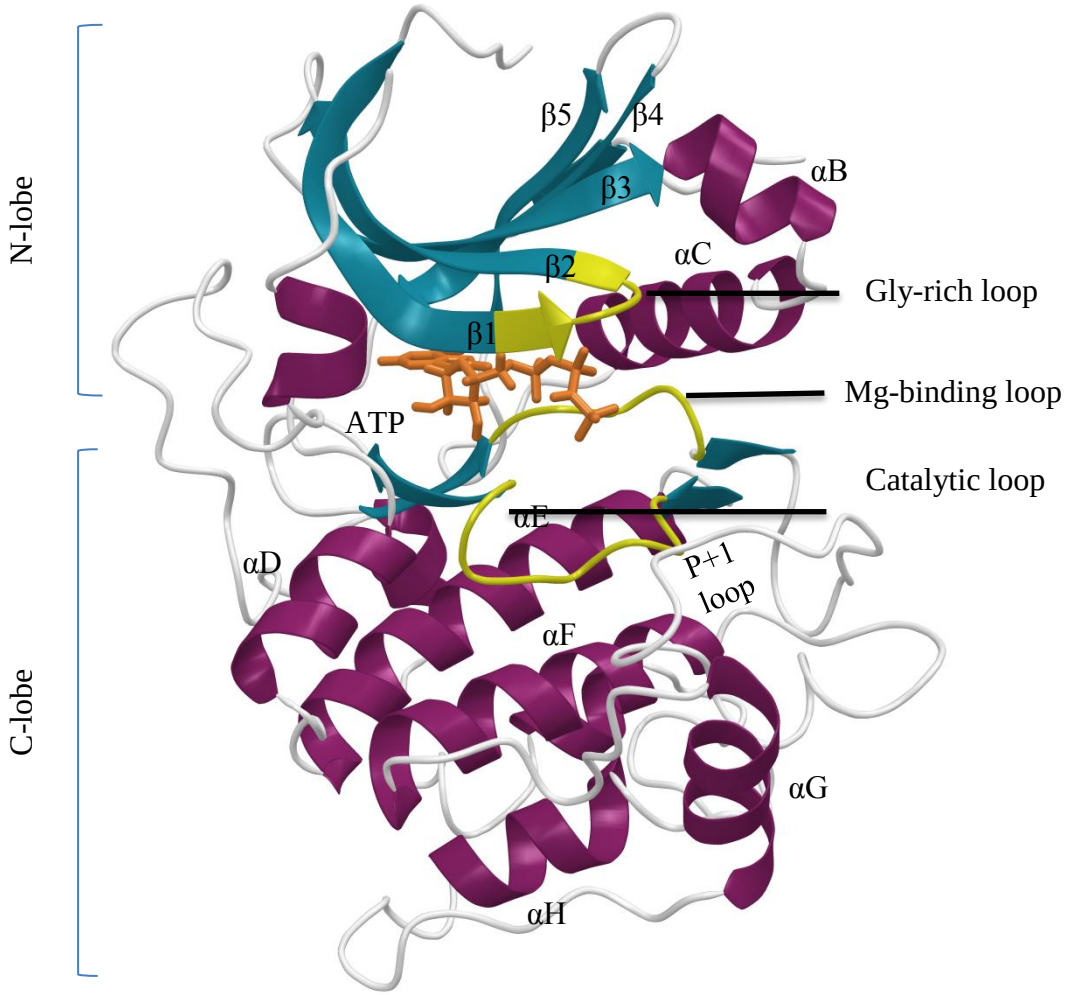

Figure 2.5. Cataltytic domain of AKT-2 (Helicies in maroon, sheets in blue, ATP in orange, and important loops in yellow, PDB codes of protein: 2JDO (PKB-β), ligand:1O6L (ATP)).

AKT is activated by the phosphatidylinositol 3-kinase (PI3K) lipid products of phosphatidylinositol-3,4,5-triphosphate (PIP_3) and phosphatidylinositol-3,4-biphosphate (PIP_2) through PH domain [46, 47]. Phosphorylation of Thr in the activation loop (Thr308 in AKT-1, Thr309 in AKT-2, and Thr305 in AKT-3) and Ser in the regulatory tail (Ser473 in AKT-1, Ser474 in AKT-2, and Ser472 in AKT-3) are required for AKT to become activated [47–51]. PIP_3 and PIP_2 directly bind to the PH domain, and as a result activation loop adopts a different conformation [52], in which it becomes available to be catalyzed by 3-phosphoinositide-dependent protein kinase 1 (PDK-1) through mentioned Thr, Ser residues [53, 54]. Summary of the activation mechanism and the upstream regulators are shown in Figure 2.6.

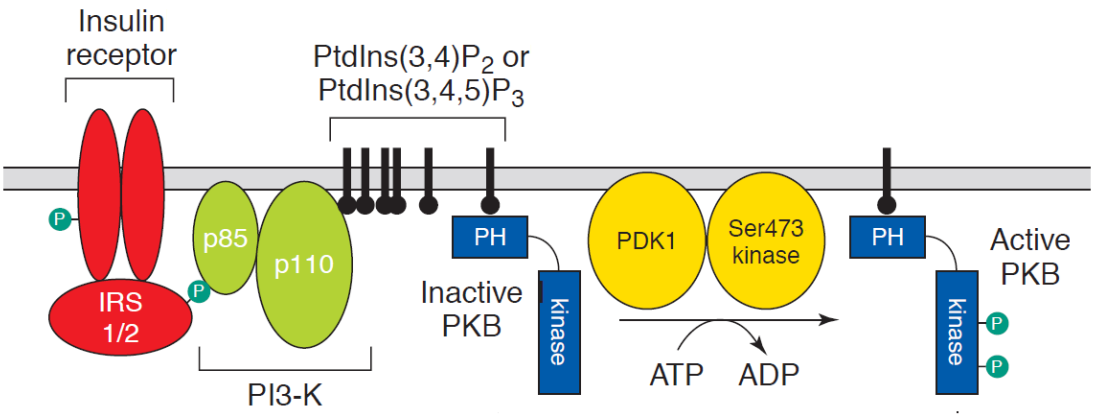

Figure 2.6. Activation mechanism and the upstream regulators of AKT protein [55].

Activated AKT may cause several diseases like cancer, diabetes, cardiovascular disease and neurological disorders (reviewed in [56]). Figure 2.7 shows the downstream effectors of AKT and related diseases. Among the AKT-related diseases most severe one is cancer and all three isoforms of AKT play a role in cell growth, survival, and progression of tumor [37, 57–60]. Over-expression of AKT-1 is observed in 40% of breast and ovarian cancers, increased activity of AKT-2 is observed in 30-40% of pancreatic and ovarian cancers and AKT-3 is amplified in breast and prostate cancers [61]. However, over expression of AKT-2 gene is more frequently observed in human cancer among other isoforms and with this property, it stands out from remaining isoforms [62,63].

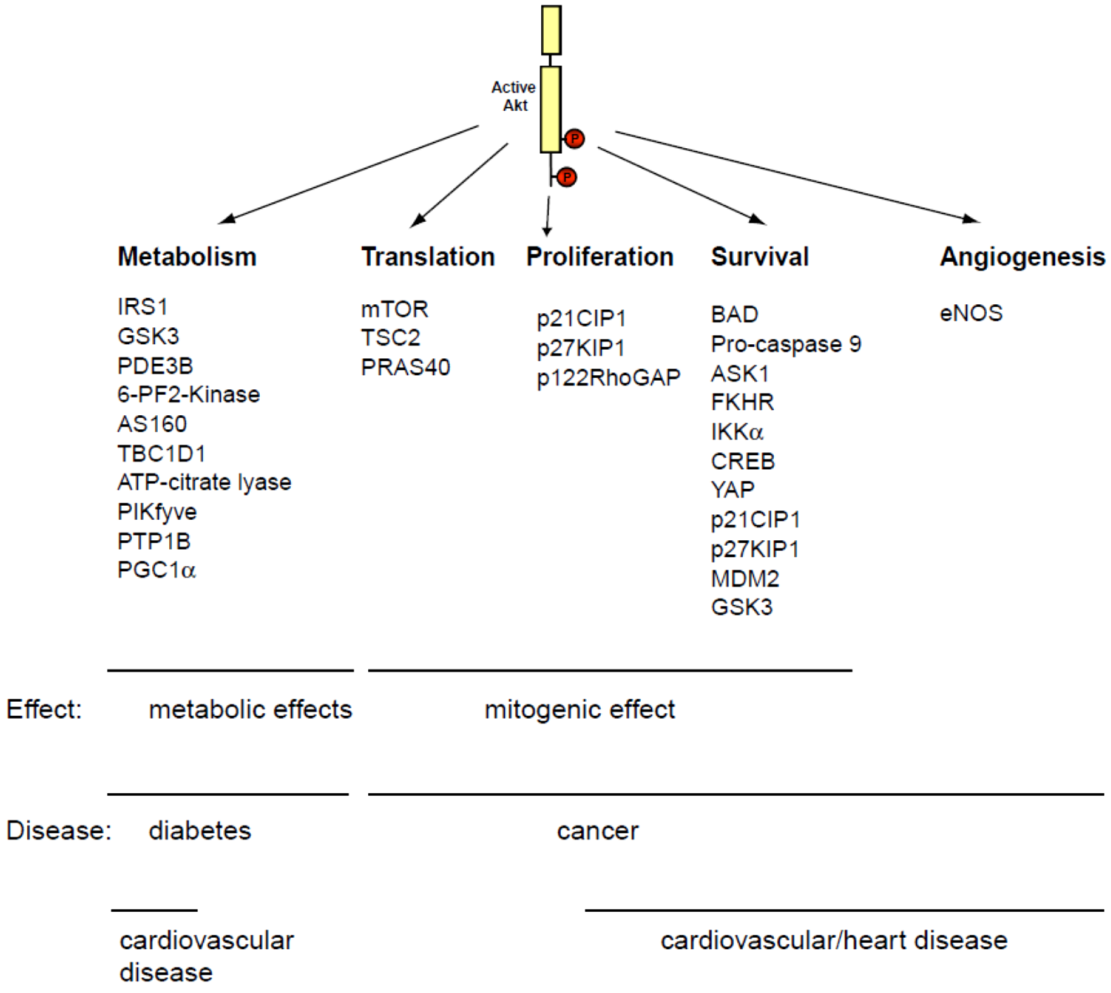

Figure 2.7. Downstream effectors of AKT and related diseases [56].

2.5. PKB Inhibitors

Since AKT-2 is an attractive target for the treatment of cancer, several small molecule inhibitors have been identified. Although, AKT inhibitors particularly target ATP binding site and allosteric PH domain [39, 64], inhibition through LINK region and substrate binding site is also possible (reviewed in [63, 65]).

Previous research has focused mainly on ATP competitive inhibitors of AKT-2 and several ATP-competitive leads that inhibit the catalytic domain were discovered. For instance, indazole and pyridine based compounds commonly known as A-443654 and A-674563 [66] are two ATP-competitive inhibitors. Several other ATP-competitive inhibitors have been reported such as isoquinoline-5-sulfonamides [67, 68], pyrazole [69], indazole

[66] and aminofurazan derivatives [61]. The catalytic domains of PKA and PKB-β are structurally similar with only a three residue difference (Ala232, Met282, and Thr213 in PKB numbering) between them [70, 71] in the ATP binding region. The similarity between PKB-β and other isoforms (PKB-α, and PKB-γ) is even higher. Therefore, specificity is the main difficulty in discovering potent ATP-competitive drug candidates for PKB-β. Co-crystallized PKB-β inhibitors mainly consist of indazole-based amino furazan class of compounds (Table 2.6), where class information of ligands X37 (2XH5) and X37 (2X39) were not found in literature.

Table 2.6. Class of co-crystallized PKB-β inhibitors.

PDB Code of Complex	**Ligand Code**	**Class of the Compound**
3D0E	G93	Aminofurazan [72]
3E87	G95	Aminofurazan [73]
3E88	G96	Aminofurazan [73]
3E8D	G98	Aminofurazan [73]
2UW9	GVP	4-phenylpyrazoles [72]
2JDO	I5S	Isoquinoline sulphonamide [71]
2JDR	L20	Indazole-based [71]
2XH5	X37	-
2X39	X39	-

Allosteric PKB inhibitor that targets PH domain includes phosphatidylinositol ether lipid analogs [74]. The similarities between PH domains of PKB isoforms are lower as compared with catalytic domain. This brings the advantage of exhibiting isoform selectivity. Binding pocket of PH domain is shallow and highly charged, and it is not a proper binding site. The nature of shallow binding site in PH domain makes it unfavorable for drug design studies [39]. Molecules that were designed to this pocket have low solubility and poor pharmacokinetics properties. Moreover, PH domains are present in many other proteins and specificity towards PKB-β remains unsolved.

Allosteric LINK region inhibitors [75, 76] are found to be highly selective against PKB isoforms. Although their isoform-specific characteristics are attractive, inhibitors reported to date have poor pharmacokinetics properties, and require further modifications.

A 14-mer, substrate competitive peptide [77] with sequence ARKRERTYSFGHHA was identified as a PKB inhibitor. However, protein substrate binding region is shallow and solvent exposed; and it not an ideal binding site.

In addition to inhibitors directly targeting AKT itself, inhibition of downstream effectors and upstream regulators in the AKT signaling cascade also prevent the activation of AKT. PDK1 inhibitors [78], PI3K inhibitors [79], protein prenylation inhibitors [80], and RTK inhibitors [81] are the examples of this kind of inhibition.

A novel PKB-β inhibitor was discovered through structure-based virtual screening and experimentally tested [82]. In this study MOE database was screened via FRED and GOLD docking and yielded with a novel chemotype but shows no selectivity for AKT-2. Optimization studies regarding corresponding compound was also performed and binding mode was predicted by validated Glide docking protocol [83].

3. METHODOLOGY

In this study, the pharmacophore hypothesis and database screening to find matches to hypothesis were done by Phase program [22, 23, 84]. Virtual screening was carried out with CoCoCo database and the docking process was completed with Glide (Grid-based Ligand Docking with Energetics) program [29, 85–87] using two different conformation of PKB (PDB codes: 2JDO and 2JDR).

3.1. Protein Structure Preparation

Coordinates of all protein and inhibitor complex structures were retrieved from RCSB Protein Data Bank (PDB) [8]. Proteins were prepared by Protein Preparation Wizard (PPW) [88], which is a module of Maestro software [89]. Proteins may have multimeric units, and duplicate structural units were reduced to a single unit. 2 water molecules were kept for target proteins used in docking calculations (PDB codes: 2JDO and 2JDR), and all other water molecules were deleted for further calculations. Selectivity calculations were performed on protein kinase A (PDB codes: 2JDT and 2JDV) and protein kinase B-α (PDB codes: 3OCB) and similar preparation steps were followed for both proteins.

The bond orders were assigned, missing hydrogen molecules were added, and selenomethionines were converted to methionines using PPW. Possible ionization and tautomeric states of the ligands at pH 7.0 ± 4.0 were predicted by Epik module [90–93].

Optimization step is an iterative process and in this step hydroxyl and thiol groups, water molecules, amide groups of asparagine (Asn) and glutamine (Gln), and the imidazole ring in histidine (His) were reoriented, and protonation states of histidine (His), aspartic acid (Asp) and glutamic acid (Glu) and tautomeric states of histidine were predicted. Hydrogen bonding optimization was done for a normal pH range of 6-8.

In the minimization step, all heavy atoms of the protein were restrained so that the RMSD between the minimized coordinates and the initial coordinates is less than 0.3 Å. Impref module of Impact [94] with OPLS2005 force field was used in the minimization.

Protein active site was represented as a series of grid base points and then these generated grid files were used for docking process. Receptor grids for proteins (PDB codes: 2JDO, 2JDR, 2JDT, 2JDV and 3OCB) were generated by Glide software. No scaling of the van der Waals radii of the receptor was applied and partial charge cutoff was taken as 0.25. The scoring grid site is defined by two concentric cubes both of which are centered on the center of co-crystal ligand. Size of enclosing box, in which all docked ligands must stay, was defined by similar size to co-crystal ligand, and size of the inner box, in which the center of the docked ligands must stay, was taken as of 10 Å on each side. H-bond constraints were applied only for 2JDO and 2JDR with residues Lys181, Glu200, Glu230, Ala232, Glu236, Glu279, Asn280, Asp293, and Phe294. Glide also allows the rotation of hydroxyl groups of Ser, Thr, and Tyr residues of the receptor during the ligand docking process, and rotation of two residues, Thr213 and Thr292, in the vicinity of the native ligands was allowed.

3.2. Hypothesis Generation

A set of pharmacophore features was used to create pharmacophore sites (site points) for all ligands according to the pharmacophore features available in Phase. Under Phase application, Develop Pharmacophore Model was used for this purpose. There are four sequential steps in a Phase run; namely, Prepare Ligands, Create Sites, Find Common Pharmacophore, and Score Hypothesis.

First step to generate a pharmacophore hypothesis is preparing ligands for pharmacophore model. The ligands were removed from their prepared complex structures. After adding the ligands to a Phase run, they should be cleaned up before proceeding. Low-energy 3D ligand structures were created with LigPrep [95] utility, where hydrogen atoms were added, protons were added or removed to produce ionization state at pH 7.0, stereoisomers were generated, and an energy minimization was performed.

The second step is to create pharmacophore sites for the ligands. There are six standard set of pharmacophore features supplied by Phase to define sites. They are hydrogen bond acceptor (A) which is represented by light red projected points and has arrows along the H-bond axis; hydrogen bond donor (D) which is represented by light blue projected points and has arrows along the potential H-bond axis; hydrophobic group (H) which is represented as a green sphere; negatively charged group (N) which is represented as a red sphere; positively charged group (P) which is represented as a blue sphere, and aromatic ring (R) which is represented as an orange torus.

After creating pharmacophore sites for all ligands, the next step in Develop Pharmacophore Model workflow is to find common pharmacophores. Common pharmacophores are those pharmacophores that have the same site feature with the same arrangement. Identical sites are clustered together and if a cluster has at least one pharmacophore from each ligand, it is taken as a common pharmacophore. In Phase, common pharmacophores are found from the variant list. A variant consists of a number of feature types. To illustrate, the variant ADPR contains one hydrogen-bond acceptor (denoted by "A"), one hydrogen-bond donor (denoted by "D"), one positively charged group (denoted by "P") and one aromatic ring (denoted by "R"). The number of the pharmacophore sites which compose a variant list can be taken between 3 and 7. In this study maximum 6, minimum 3 site points were specified to be included in the hypothesis, and at least 4 of the 8 ligands were set to be matched. With these options variant list was made and from this list common pharmacophores were found by using tree-based partition technique with maximum tree depth five and minimum intersite distance 2.0Å.

In Scoring Hypotheses step, common pharmacophores were scored to find optimum alignments to active set of inhibitors. Common pharmacophore hypotheses describe critical binding information in 3D. Survival score is the final scoring function which consists of weighted factors of vector score, site score, volume score, selectivity score, and number of matches. Default weighting factors were used which is 0.0 for selectivity score, and 1.0 for the other scores.

3.3. Ligand Based Excluded Volumes

Graphical user interface utility, create_xvolShell from $SCHRODINGER/utilities directory was used to generate ligand-based excluded volumes. This utility creates excluded volume spheres from shell around the actives with grid size 1 Å. Generated excluded volume was then added as a part of pharmacophore hypothesis to eliminate structures that stay outside the specified volume when screening database for finding matches to hypotheses.

3.4. Pharmacophore Database Screening

Find Matches to Hypothesis workflow of Phase was used to perform pharmacophore database screens. This workflow consists of three segments. They are conformation generation, matching and hit treatment. Conformation generation step was skipped since a ready-to-use database, CoCoCo, which is compatible with Phase, was used.

In matching panel of the workflow, pharmacophore sites for the molecules in the database were generated during search. In addition, all site points of the hypothesis (4 site points for hypothesis DRRR) were set to match to the molecules. Site matching tolerance was not changed and taken as 2 Å.

In hit treatment panel of the workflow, ligand-based excluded volumes were applied. Hit is the conformer of the database molecules that pass search process for finding matches to hypothesis. One hit structure was saved per molecule. No align score restriction was set, but hits with lower than 0.65 vector score and lower than 0.25 volume score were set to be rejected.

3.5. Ligand Structure Preparation

Ligands that pass the pharmacophore database screen were prepared using LigPrep application of the Schrödinger Suit. Ionizer and stereoizer utilities in LigPrep were used to generate different protonation states, tautomers and stereoisomers of the molecules in the database at pH range 7±2. By default LigPrep generates at most 8 tautomers and 32

stereoisomers per ligand structure. OPLS_2005 force field was used for MacroModel [96] to perform energy minimization for each ligand.

3.6. Rigid-Receptor Docking and Scoring

Glide program was used in all docking and scoring calculations with OPLS_2005 force field. Prepared ligands and proteins were used as the initial coordinates for Glide. During the docking process, the target protein was treated as rigid while ligand was flexible. Database was first screened by the standard precision (SP) mode of Glide docking protocol. In this step, flexible docking, which generates ring conformation and nitrogen inversions for standard precision mode, was selected. Thus, ligand conformations are generated during docking. For freezing amide bonds, not in cis or trans form, penalties were applied as a docking option. Advanced docking settings were kept as default, which discards ring conformations if their energies are higher than 2.5 kcal/mol, keeps maximum 500 poses per ligand for the initial phase of docking, keeps 40 poses per ligand for energy minimization, takes distance-dependent dielectric constant as 2.0 in the minimization step, and takes maximum number of minimization steps as 100.

Ligands with more than 300 atoms and 50 rotatable bonds were not considered in docking. Glide enables users to change the van der Waals radii of nonpolar atoms of the ligands to take into account the receptor flexibility. In this study, since receptor flexibility was handled by docking with multiple receptor conformations, scaling of the van der Waals (vdW) radii of ligands was not relaxed and default parameters (scale 0.8) were used where ligand vdW radii was scaled by 0.8 with partial atomic charge cutoff of 0.15.

H-bonding constraints were also applied for SP docking run. At least one H-bond between Ala232 or Glu230 residues and docked molecule was imposed as a constraint in Glide SP run. For each ligand five poses were generated and after post-docking energy minimization only one of them was saved in the pose viewer file. A pose can be defined as ligand arrangement in the binding site of the receptor. Pose ranking of docked structure for each ligand was made using a model energy score (Emodel), and pose selection was done according to this score.

Schrodinger's docking post-processing script of select top poses was used to select top 1000 structures by keeping one structure per compound. Top 1000 poses were then screened using extra precision mode (XP) of Glide. Command-line premin utility (MMFF force field) was used for selected 1000 structures before a Glide XP docking experiment to relieve any strain and relax ligand structures.

In the Glide XP run, all parameters except the constraints were kept the same as Glide SP run. A constraint of at least 3 H-bond between residues Lys181, Glu200, Glu230, Ala232, Glu236, Glu279, Asn280, Asp293, Phe294 and docked molecule was imposed in XP mode of Glide docking. Further information about methodology used by Glide can be found elsewhere [29, 85, 86].

3.7. Post-Docking Evaluation

In order to predict absorption, distribution, metabolism, and excretion (ADME) properties of the molecules, QikProp [97] module of the Maestro Suite was used in normal mode. Monte Carlo (MC) calculations were run with BOSS program [98] and for parameters OPLS-AA force field was used. The MC calculations were performed for a single solute in a periodic cube at 25 °C and 1 atm. Further information about methodology used by QikProp can be found elsewhere [99].

Strain energies of docked molecules were calculated by using strain re-dock utility of Schrodinger Suite. The following default parameters were used: force field is OPLS_2005, penalty scale factor was 0.25, energy offset was 4.00 kcal/mol and lower strain energy was ignored, Cartesian coordinates were used and force constant was 120.00 kcal/mol/ $Å^2$, half-width of flat-bottom restraint potential applied to the bound state was 3 tenths of an Å.

Binding energies of each ligand was calculated by Prime/MM-GBSA [100–102] with a continuum solvation model (surface generalized born model) and OPLS_2005 force field by using the following equation,

$$\Delta G_{bind} = E_{complex\,(minimized)} - E_{ligand\,(minimized)} - E_{receptor\,(minimized)} \qquad (2.1)$$

In the equation ΔG_{bind} is the binding energy, $E_{complex(minimized)}$ is the minimized energy of the complex structure, $E_{ligand(minimized)}$ is the minimized energy of the ligand, and $E_{receptor(minimized)}$ is the minimized energy of the unliganded receptor. Calculations were performed with protein-ligand complex structure from docked poses with a flexible protein structure. The flexible region was defined to include protein residues which are 5.0 Å far from the ligand. Prior to calculations all water molecules were deleted since an implicit solvent model was used. No harmonic potential constraint was applied to the flexible region.

Enrichment metrics were calculated with Schrodinger Python script of enrichment calculator. Schrodinger 1000 drug-like compounds [29, 85] were used as a decoy set, and nine native AKT-2 kinase inhibitors were used as an active set of compounds. Combined database (decoy set and nine ligands) were prepared by LigPrep with default settings, and this database was docked to receptor 2JDO with unconstrained, extra precision mode. In Glide XP docking run, all settings were kept as default. After docking, Prime MM-GBSA calculations were performed to calculate Prime binding free energy. Receiver Operating Characteristic (ROC) curves were plotted for the XP Gscore and MM-GBSA rankings to compare which scoring is more appropriate for, specifically, AKT-2 kinase protein.

3.8. Similarity Analysis

ChemMine Tools, which is an open access online server and available at: http://chemmine.ucr.edu, was used for similarity analysis of small molecule data. 2D similarity search within ChemMine Tools uses atom pairs as structural descriptor and Tanimoto, Tversky or Dice metrics as similarity coefficient. In this study, Tanimoto coefficient was used to calculate similarity. Tanimoto coefficient is computed by dividing the fraction of the structural features shared among two compounds to their union. ChemMine Tools uses three algorithms; namely, hierarchical clustering, multidimensional scaling (MDS) and binning clustering for clustering of compounds by structural similarity and in this study, hierarchical clustering algorithm was set to be used. For similarity clustering, generated atom pair descriptors are used to compute similarity measures which are required to obtain similarity matrix using Tanimoto coefficient. Hierarchical tree analysis was carried out by ChemMine, and clustering is done by hclust function with R

program and branch lengths of the tree are proportional to the compound-to-compound similarities.

3.9. Induced-Fit Docking

Induced fit protocol (IFD) [103, 104] was adopted to proposed ten molecules by using Induced Fit Docking Workflow to proteins 2JDO and 2JDR. Both flexible receptor and ligand docking was performed in this step. Center of enclosing and inner box was set as the centroid of the native ligands. Box size was determined automatically. Flexible ligand mode was used. No H-bond constraint was set. Initial rigid Glide docking was performed with softened docking parameters (receptor van der Waals radii scaling of 0.7 and ligand van der Waals radii scaling of 0.5). Residue Phe163 was selected to trim. This means Phe163 was removed from the active site, then ligand docking proceeds, and relocated after docking. 20 poses were kept for each ligand. Then, residues within 5.0 Å of the ligand poses were subjected to Prime refinement which includes conformational search and energy minimization. Glide redocking was performed with structures within 30.0 kcal/mol. XP precision mode was selected for docking processes. Mentioned settings are valid for IFD with receptors, 2JDO and 2JDR.

4. RESULTS AND DISCUSSION

AKT is frequently amplified and overexpressed in human cancer cells, and its inhibition is a promising therapeutic approach for the treatment of cancers. Accordingly, this study aims to propose new ligands to inhibit the AKT-2 protein. The workflow of the study is summarized in Figure 4.1 and each step will be discussed in the following sections.

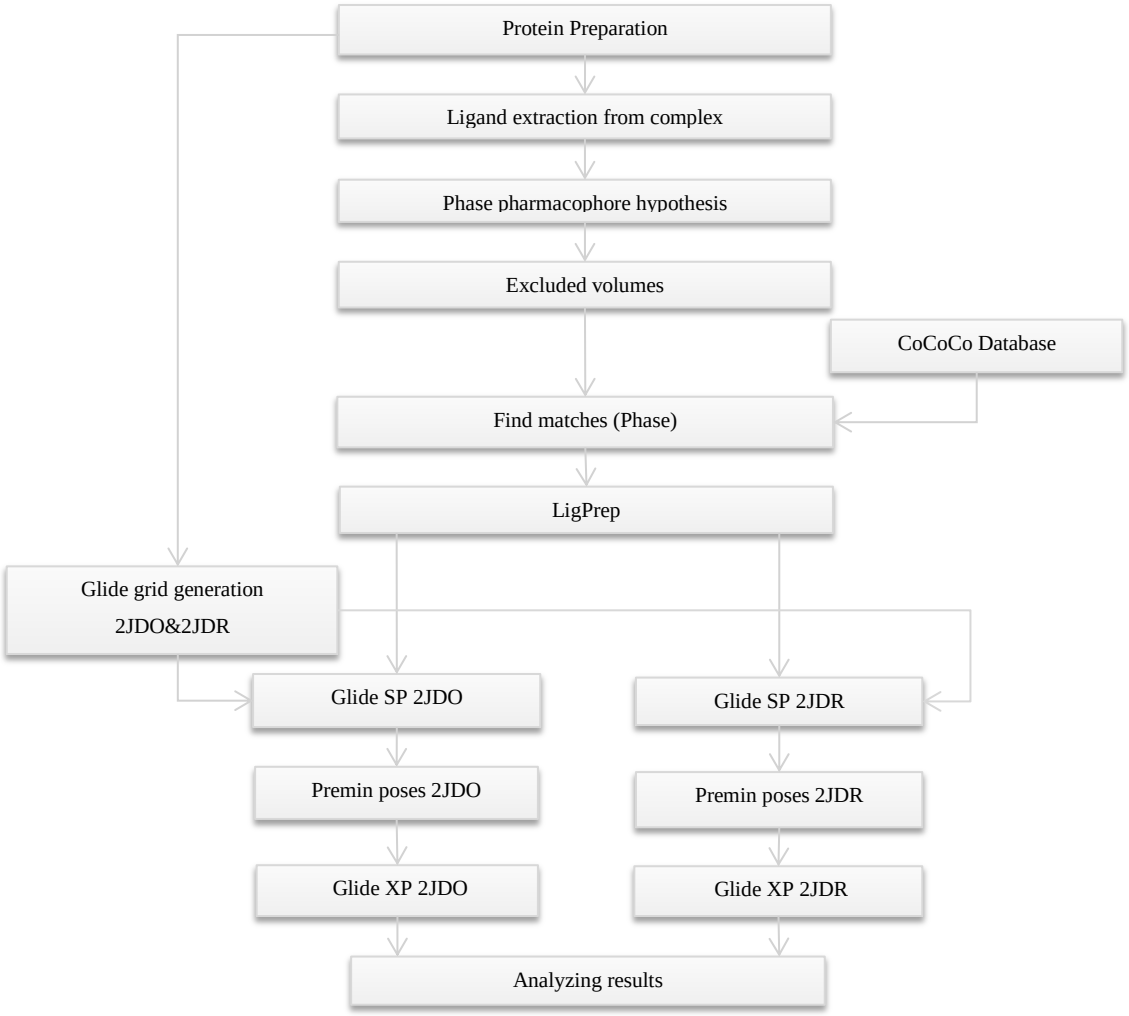

Figure 4.1. Workflow of the virtual screening and docking of protein kinase B inhibitors.

4.1. Analysis of the Binding Site

There are nine X-ray structures of AKT-2 in complex with inhibitor available in PDB and these were used to examine the binding site interactions and identify the important characteristics of the binding site. Structure file from the PDB must be prepared for use in molecular modeling calculations. A typical PDB structure file consists only of heavy atoms and may include a co-crystallized ligand, water molecules, metal ions, and cofactors. Some structures are multimeric, and may need to be reduced to a single unit. Because of the limited resolution of X-ray experiments, it can be difficult to distinguish between NH and O, and the placement of these groups must be checked. PDB structures may have missing information on connectivity, which must be assigned, along with bond orders and formal charges. The Protein Preparation Wizard (PPW) was used to prepare the protein for docking experiments.

The crystal structures of AKT-2 in complex with nine different AKT-2 inhibitors (Table 4.1) that bind to the ATP binding side of the molecule are available in PDB (PDB codes: 3D0E [105], 3E87 [73], 3E88 [73], 3E8D [73], 2UW9 [69], 2JDO [71], 2JDR [71], 2XH5 [72], 2X39 [72]). In Table 4.1, the PDB codes and resolution of the complexes, the ligands including their chemical names and formulas are summarized.

Table 4.1. General information of AKT-2 inhibitors.

PDB Code of Complex	Ligand Code	Resolution (Å)	Ligand Chemical Name	Ligand Chemical Formula
3D0E	G93	2.00	(3S)-3-({[2-(4-amino-1,2,5-oxadiazol-3-yl)-1-ethyl-4-(3-hydroxy-3-methylbut-1-yn-1-yl)-1H-imidazo[4,5-c]pyridin-7-yl]oxy}methyl)piperidin-1-ium	$C_{21}H_{28}N_7O_3$
3E87	G95	2.30	N-[(1S)-2-azaniumyl-1-phenylethyl]-5-{1H-pyrrolo[2,3-b]pyridin-4-yl}thiophene-2-carboxamide	$C_{20}H_{19}N_4OS$
3E88	G96	2.50	4-[2-(4-amino-1,2,5-oxadiazol-3-yl)-6-[(2R)-2-azaniumyl-3-phenylpropoxy]-1-ethyl-1H-imidazo[4,5-c]pyridin-4-yl]-2-methylbut-3-yn-2-ol	$C_{24}H_{28}N_7O_3$
3E8D	G98	2.70	4-[2-(4-amino-1,2,5-oxadiazol-3-yl)-6-[(1S)-3-azaniumyl-1-phenylpropoxy]-1-ethyl-1H-imidazo[4,5-c]pyridin-4-yl]-2-methylbut-3-yn-2-ol	$C_{24}H_{28}N_7O_3$
2UW9	GVP	2.10	4-(4-chlorophenyl)-4-[4-(1H-pyrazol-4-yl)phenyl]piperidin-1-ium	$C_{20}H_{21}ClN_3$
2JDO	I5S	1.80	N-[2-({2-[(4-chlorophenyl)methoxy]ethyl}azaniumyl)ethyl]isoquinoline-5-sulfonamide	$C_{20}H_{23}ClN_3O_3S$
2JDR	L20	2.30	5-{5-[(2S)-2-azaniumyl-3-(1H-indol-3-yl)propoxy]pyridin-3-yl}-3-methyl-1H-indazole	$C_{24}H_{24}N_5O$
2XH5	X37	2.72	4-[(4-tert-butylphenyl)methyl]-1-{7H-pyrrolo[2,3-d]pyrimidin-4-yl}piperidin-4-aminium	$C_{22}H_{30}N_5$
2X39	X39	1.93	4-{[(4-chlorophenyl)methyl]carbamoyl}-1-{7H-pyrrolo[2,3-d]pyrimidin-4-yl}piperidin-4-aminium	$C_{19}H_{22}ClN_6O$

As a representative example, ligand G98 in ATP pocket of AKT-2 (PDB: 3E8D) is shown Figure 4.2, and a detailed view of the binding pocket is represented in Figure 4.3. Gly-rich loop, which is flexible, is shown in pink and Met180, Glu200, Glu230, Ala232, Glu236, Glu279, Asn280, Thr292, Asp293, and Phe294, which are important residues for H-bond network, are shown in Figure 4.3. In Figure 4.3, hinge region residues of Ala232

and Glu230 are shown in orange color and ribose binding residues of Glu236, Glu279, Asn280, and Asp293 are shown in yellow color and other residues are shown in black color. Phe163 residue is missing in one crystal structure (PDB code: 3E8D), Glu471, Gln467, Thr449, and Glu468 residues are missing in two crystal structures (PDB code: 2XH5 and 2X39). Some of the PDB files include the dimeric form of the protein (PDB code: 3D0E, 3E87, 3E88, and 3E8D), and chains of the duplicate structural units were deleted (Table 4.2). The last step before optimizing the structure is to generate the correct protonation states on the ligand. The state penalty and the charge of all the protonation states for all ligands are listed in Table 4.3 (as S1, S2, S3, etc.), where the selected protonation state is shown in bold. S_1 indicates the lowest state penalty and subscript of states increases with increasing state penalty. Formal charge of the ligand states are denoted as Q and possible intermolecular H-bond count of ligands are listed in the Table 4.3. The selection was made by considering possible H-bond count, state energy and the ligand interaction map obtained which is available in PDB web site (www.rcsb.org). Next, hydrogen-bonding network optimization and minimization are performed. Protein structure is refined in the minimization step and all heavy atoms of the protein are restrained.

Table 4.2. Information about available AKT-2 protein and ligand complexes.

PDB code	**Dimeric Form**	**Missing Residues**
3D0E	√	
3E87	√	
3E88	√	
3E8D	√	Phe163
2UW9		
2JDO		
2JDR		
2XH5		Glu471, Glu467, Thr449, Glu468
2X39		Glu471, Glu467, Thr449, Glu468

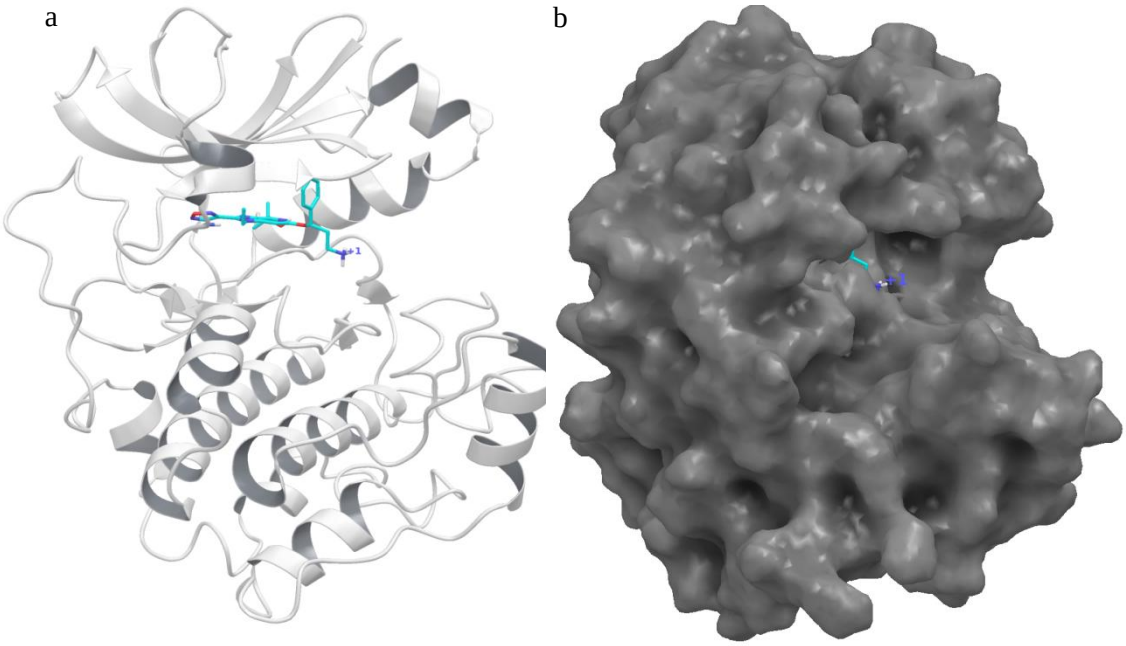

Figure 4.2. AKT-2 kinase (PDB: 3E8D) (a) cartoon, (b) surface representation.

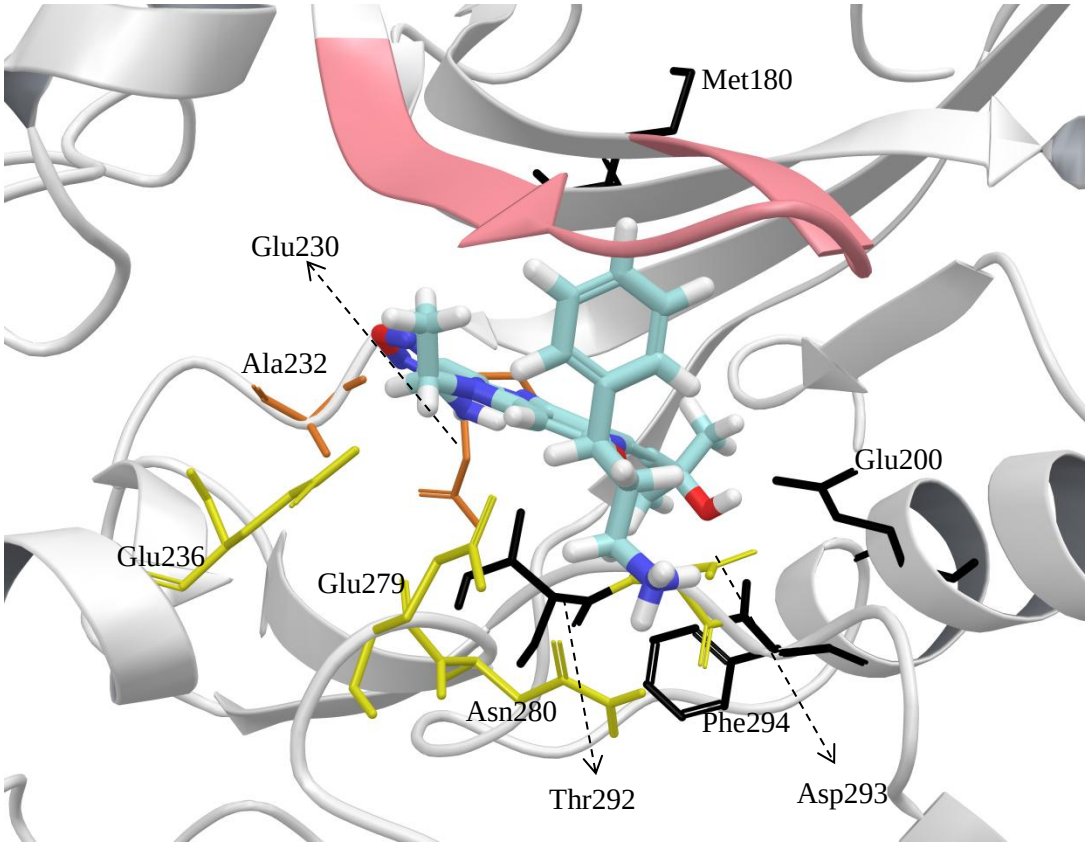

Figure 4.3. Binding pocket of AKT-2 kinase with G98 (PDB: 3E8D).

Table 4.3. Generated ligand states from Protein Preparation Wizard.

PDB Code-Ligand	Het States – States Penalties		
	S_1	S_2	S_3
3DOE – G93	**0.65 kcal/mol** **Q=+1** **H bond count=4**	4.20 kcal/mol Q=+2 H bond count=4	4.34 kcal/mol Q=0 H bond count=3
3E87 – G95	**0.84 kcal/mol** **Q=+1** **H bond count=3**	3.26 kcal/mol Q=0 H bond count=3	
3E88 – G96	**0.84 kcal/mol** **Q=+1** **H bond count=2**	3.15 kcal/mol Q=0 H bond count=1	
3E8D – G98	**0.82 kcal/mol** **Q=+1** **H bond count=3**	4.52 kcal/mol Q=0 H bond count=3	
2UW9 – GVP	1.06 kcal/mol Q=+1 H bond count=1	**1.06 kcal/mol** **Q=+1** **H bond count=3**	4.61 kcal/mol Q=0 H bond count=1
2JDO – I5S	**0.67 kcal/mol** **Q=+1** **H bond count=2**	2.68 kcal/mol Q=0 H bond count=2	4.41 kcal/mol Q=+2 H bond count=1
2JDR – L20	**0.84 kcal/mol** **Q=+1** **H bond count=3**	3.02 kcal/mol Q=0 H bond count=3	
2XH5 – X37	**0.83 kcal/mol** **Q=+1** **H bond count=4**	3.78 kcal/mol Q=+2 H bond count=3	4.41 kcal/mol Q=0 H bond count=4
2X39 – X39	0.16 kcal/mol Q=0 H bond count=5	**1.28 kcal/mol** **Q=+1** H bond count=5	2.76 kcal/mol Q=+1 H bond count=4

Binding sites of all nine ligand-protein complexes were aligned and ligands were extracted. When all ligands were superimposed (Figure 4.4), it was observed that ligand alignments in the binding sites are similar and they cluster together closely. In Figure 4.4a and Figure 4.4.b, AKT-2 structure (3E8D) is shown in surface and ribbon representation respectively; while nine native ligands are shown in the binding site with different coloring. In Figure 4.4c, blue volume indicates the overlap of molecular surface of all native ligands. The distances between various positions on the volume were reported to obtain some information about the size of the volume. Distance between the peak points on the surface was measured while the peak points were determined by visual inspection.

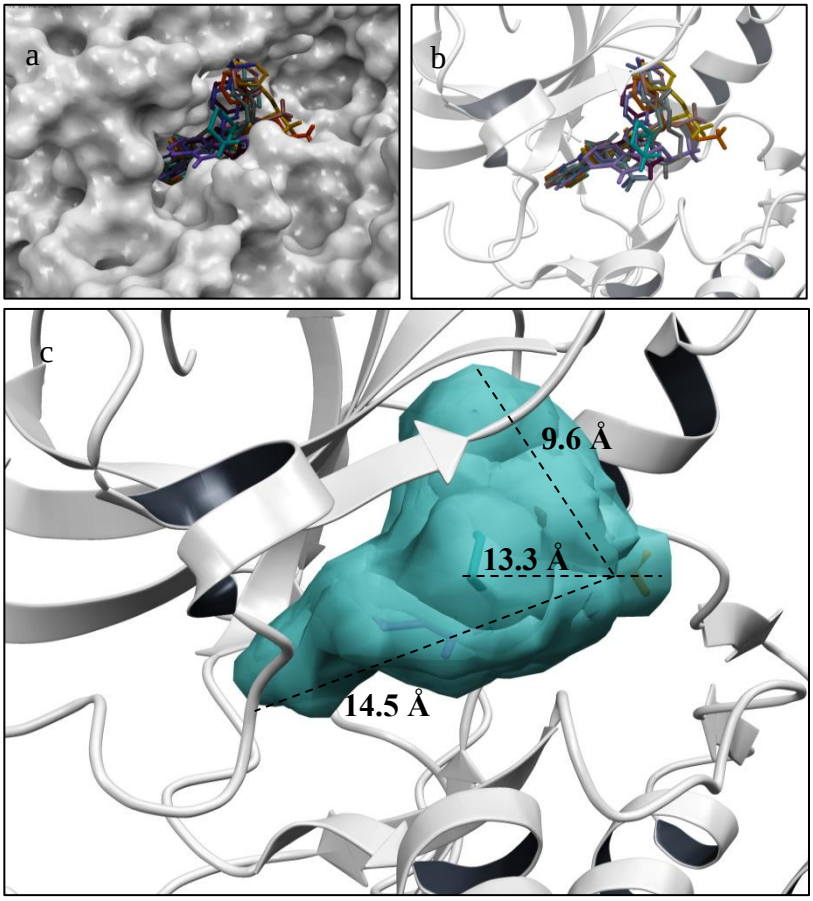

Figure 4.4. Ligands of AKT-2 in the active site (a) protein in surface representation, (b) protein in ribbon representation, (c) ligands in surface representation.

Prepared protein-ligand complexes were examined and then ligands were extracted. The structures of these ligands (Table 4.1) and their interactions with AKT-2 are examined in detail in Figure 4.5 to Figure 4.13 and explained below.

The ligand G93 with chemical formula $C_{21}H_{28}N_7O_3$ has 59 atoms and 62 bonds of which 7 are rotatable. It has 7 hydrogen bond acceptors and 5 hydrogen bond donors. Molecular weight is 426.49 g/gmol and the partition coefficient, log P value is 1.17. The compound satisfies the Lipinski's rule of five and it is drug-like. Figure 4.5 shows the interactions between the ligand and the protein. Red colored sphere indicates acidic residues, green colored sphere indicates hydrophobic residues, purple colored sphere indicates basic residues, blue colored sphere indicates polar residues, and gray colored sphere indicates Gly residues. H-bond between protein backbone and the ligand is marked with solid pink line and H-bond between protein side chains and the ligand is marked with

dotted pink line. Solvent exposed group of ligand atoms are displayed as yellow spheres. The same coloring scheme is used in all interaction maps (Figures 4.5-4.13 and Figures 4.28-4.37). N5 on the oxadiazole ring and NH_2 group of the ligand make hydrogen bonds with the backbone of the Ala232 and Glu230 residues. Hydrogen bonding interactions are also observed between the piperidinyl group of the G93 and the substrate binding residues Glu236 and Glu279. Alkynol –OH group of the ligand and the backbone of the Phe294 and Glu200 side chain are in contact through hydrogen-bond interactions. Imidazopyridine ring is located near the Gly-rich region of the protein (residues 158-165) and forms a hydrophobic interaction with the protein as well as a hydrogen bond with Lys181.

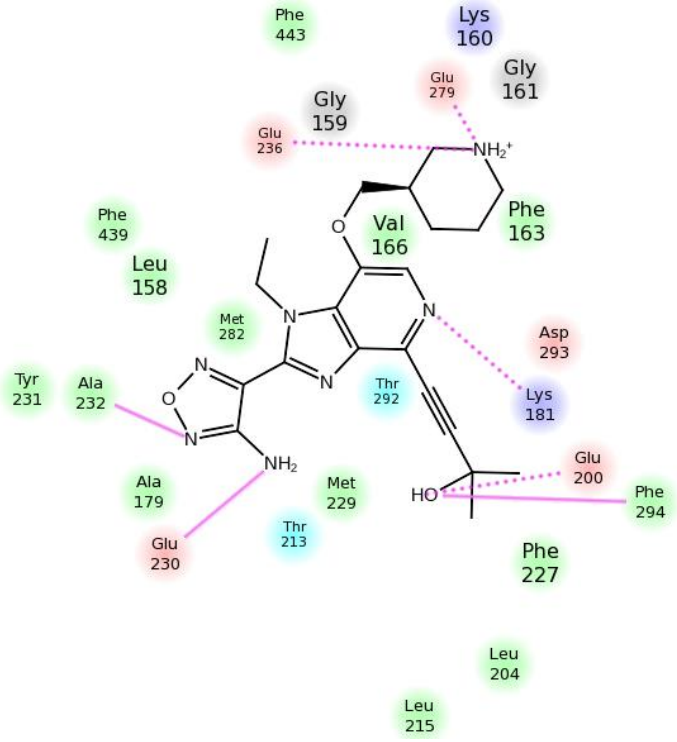

Figure 4.5. Ligand (G93) protein interaction diagram. (PDB code: 3D0E).

The ligand G95 with chemical formula $C_{20}H_{19}N_4OS$ has 45 atoms and 48 bonds of which 5 are rotatable. It has 2 hydrogen bond acceptors and 5 hydrogen bond donors. Molecular weight is 363.46 g/gmol and the partition coefficient, log P value is 2.84. The compound satisfies the Lipinski's rule of five and it is drug-like. Figure 4.6 shows the interactions between the ligand and the protein, and the residues are represented as colored spheres. There is a hydrogen-bond interaction between 7-azoindole group of G95 and the

hinge region residues of Ala232 and Glu230 of AKT-2. Phenyl ring of the G95 is in hydrophobic interaction with the Gly rich region of the protein (residues 158-165). Basic NH_3 group is located between residues of Glu279 and Asp293.

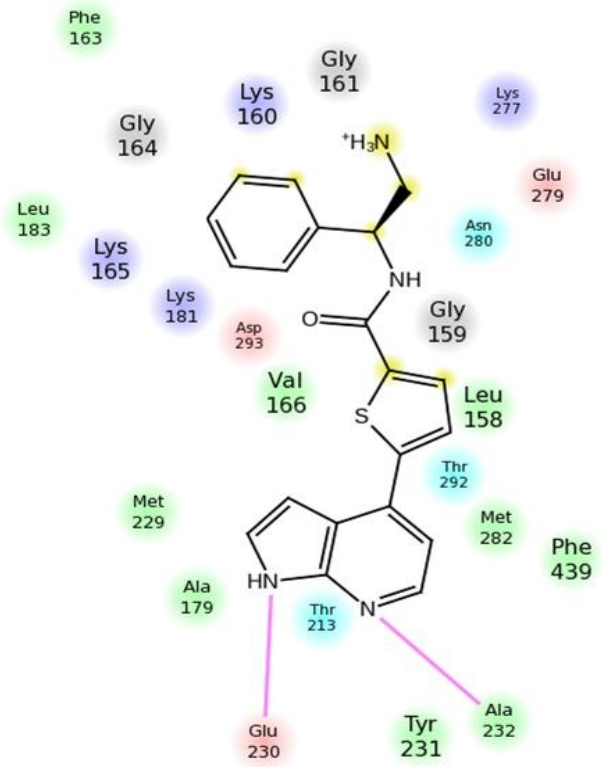

Figure 4.6. Ligand (G95) protein interaction diagram (PDB code: 3E87).

The ligand G96 with chemical formula $C_{24}H_{28}N_7O_3$ has 62 atoms and 65 bonds, of which 9 are rotatable. It has 7 hydrogen bond acceptors and 6 hydrogen bond donors. Molecular weight is 462.52 g/gmol and the partition coefficient, log P value is 2.89. The compound satisfies the Lipinski's rule of five and it is drug-like. Figure 4.7 shows the interactions between the ligand and the protein. There is a hydrogen bond interaction between 4-aminofurazan group of G96 and the hinge region residues of Ala232 and Glu230 of AKT-2. Side chain of Glu200 makes a hydrogen bond with the alkynol-OH group of the ligand. Another hydrogen bonding interaction exists between Asp293 side chain and the amine group of the ligand. Fifth H-bonding interaction of G96 is observed with the side chain of Thr292. Phenyl ring of the ligand is in hydrophobic contact with Gly-rich loop of the AKT-2 (residues 158-165).

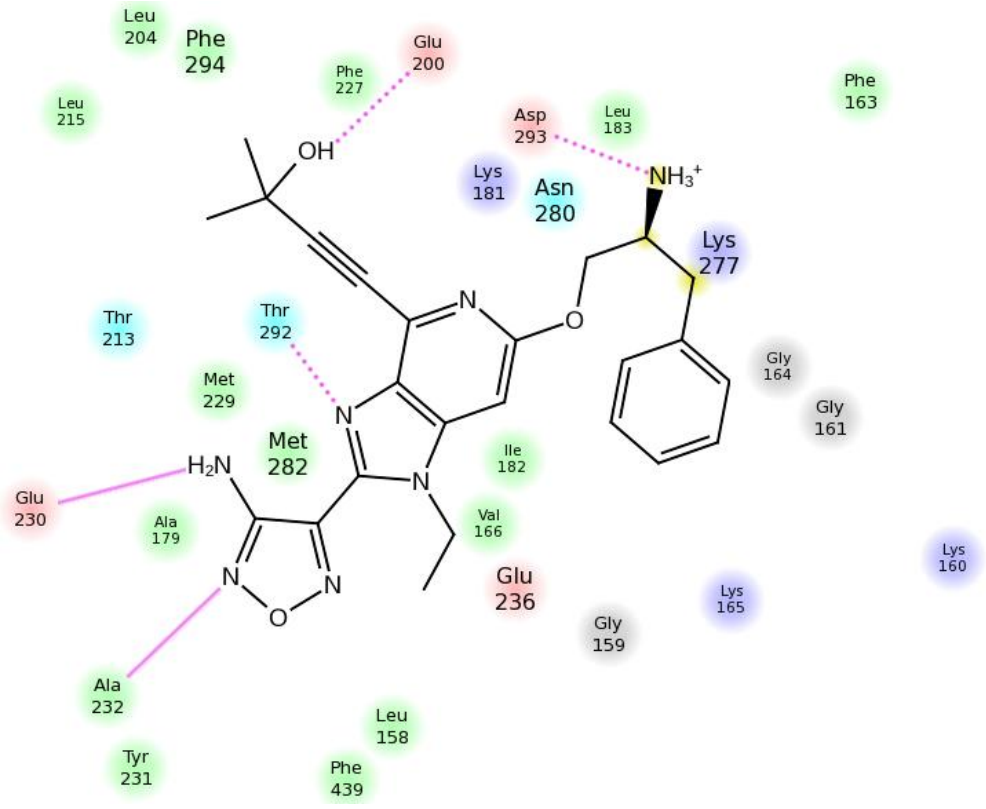

Figure 4.7. Ligand (G96) protein interaction diagram (PDB code: 3E88).

The ligand G98 with chemical formula $C_{24}H_{28}N_7O_3$ has 62 atoms and 65 bonds of which 9 are rotatable. It has 7 hydrogen bond acceptors and 2 hydrogen bond donors. Molecular weight is 465.55 g/gmol and the partition coefficient, log P value is 2.66. The compound satisfies the Lipinski's rule of five and it is drug-like. Figure 4.8 shows the interactions between the ligand and the protein. Binding mode of G98 resembles that of G93. Residues in the hinge region, specifically Ala232 and Glu230 make H-bonding interactions with 4-aminofurazan group of ligand G98. Alkynol-OH group of the ligand and side chain of the Glu200 is in H-bonding interaction. There is also a H-bond between the ammonia of the ligand and side chain of the Asp293 residue of the protein. Fifth H-bonding interaction of G98 is observed with the side chain of Lys181. Phenyl ring of the ligand is in hydrophobic contact with Gly-rich loop of the protein.

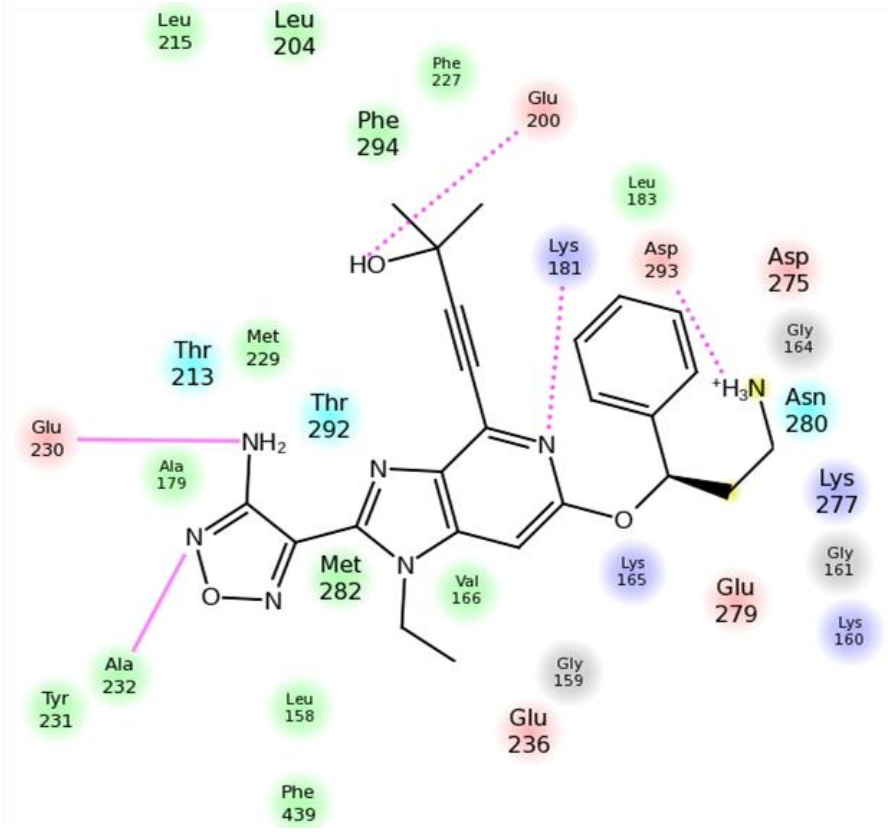

Figure 4.8. Ligand (G98) Protein interaction diagram (PDB code: 3E8D).

The ligand GVP with chemical formula $C_{20}H_{21}ClN_3$ has 45 atoms and 48 bonds of which 3 are rotatable. It has 1 hydrogen bond acceptors and 3 hydrogen bond donors. Molecular weight is 338.85 g/gmol and the partition coefficient, log P value is 4.07. The compound satisfies the Lipinski's rule of five and it is drug-like. Figure 4.9 shows the interactions between the ligand and the protein. Imidazole ring of the GVP makes H-bond with the backbone of the hinge region residues of Ala232 and Glu230. Protonated basic amine on piperidine ring of the GVP interacts with Glu236, Glu279, Asn280 and Asp293 residues in the ribose binding region, which is acidic, and makes H-bond with Glu236. 4-chlorophenyl group on phenyl ring of the ligand interacts with lipophilic region (Leu 183, Lys181, Gly161, and Gly164) next to Gly-rich loop (residues 158-165).

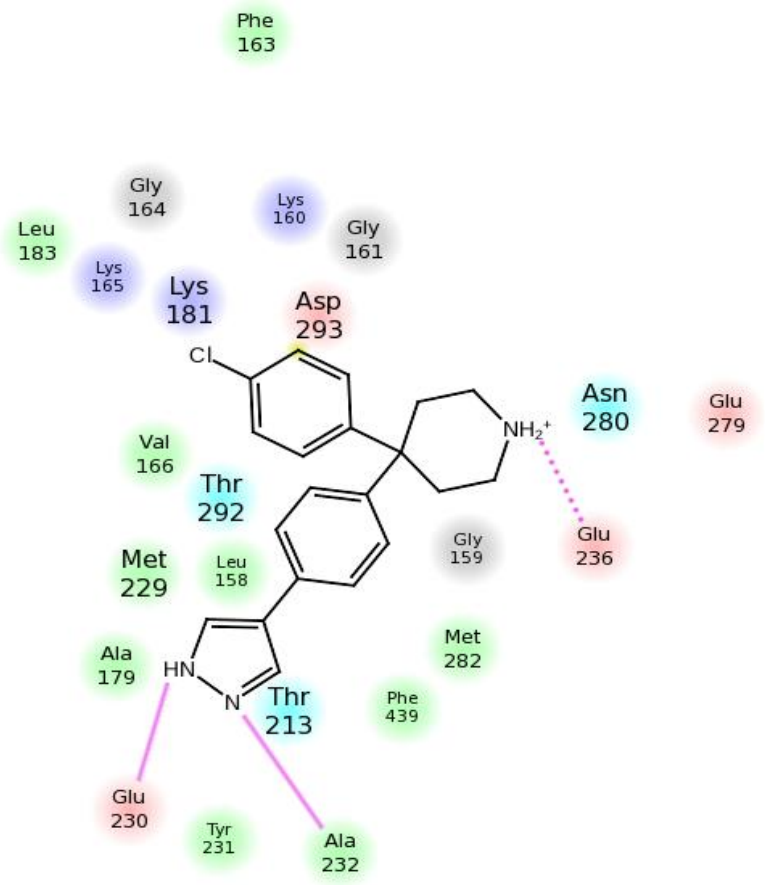

Figure 4.9. Ligand (GVP) protein interaction diagram (PDB code: 2UW9).

The ligand I5S with chemical formula $C_{20}H_{23}ClN_3O_3S$ has 51 atoms and 53 bonds of which 9 are rotatable. It has 4 hydrogen bond acceptors and 3 hydrogen bond donors. Molecular weight is 420.93 g/gmol and the partition coefficient, log P value is 2.36. The compound satisfies the Lipinski's rule of five and it is drug-like. Figure 4.10 shows the interactions between the ligand and the protein. Isoquinoline group of I5S makes H-bonding interaction with the hinge region residue of Ala232 and surrounded by the hydrophobic residues of Val166 and Met282. Protonated basic amine nitrogen of I5S makes hydrogen bond interactions with backbone of Glu279 and side chain of Asp 293 in the acidic, ribose binding region of the AKT kinase. Terminal 4-chlorophenyl ring of the ligand is located in the hydrophobic region formed by Lys181, Gly161, Gly164 residues. Aromatic rings of the ligand are surrounded by the hydrophobic residues of Val166, Met229, Ala179, Tyr231, Phe439, and Met282.

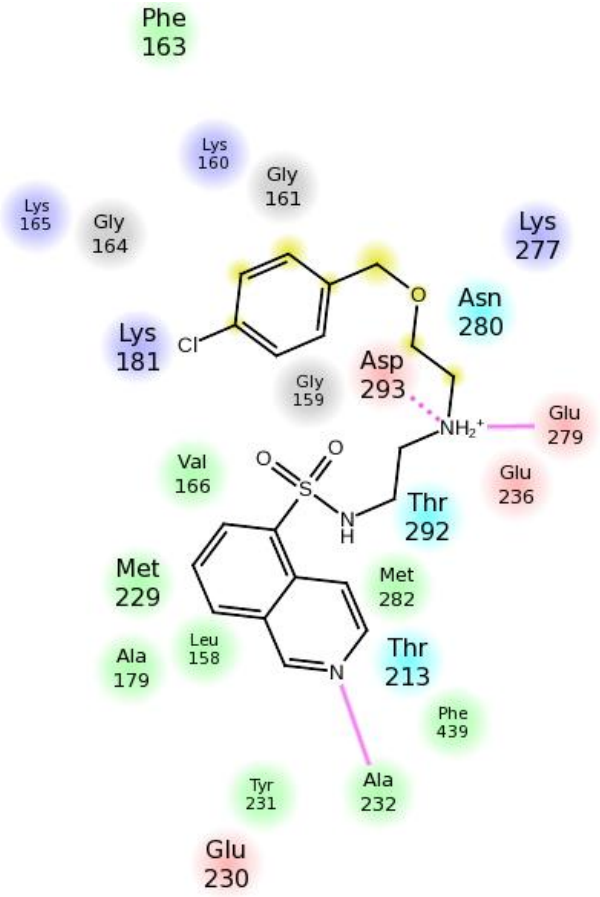

Figure 4.10. Ligand (I5S) protein interaction diagram (PDB code: 2JDO).

The ligand L20 with chemical formula $C_{24}H_{24}N_5O$ has 54 atoms and 58 bonds of which 6 are rotatable. It has 3 hydrogen bond acceptors and 5 hydrogen bond donors. Molecular weight is 398.48 g/gmol and the partition coefficient, log P value is 3.07. The compound satisfies the Lipinski's rule of five and it is drug-like. Figure 4.11 shows the interactions between the ligand and the protein. Interactions of the AKT-2 with L20 resemble the interactions of the I5S. Indazole ring of L20 makes hydrogen bond interactions with backbone of hinge region residues of Ala232 and Glu230 of AKT-2 kinase protein. Pyridine ring makes a hydrogen bond with the conserved Lys181 residue in the catalytic region. Another observed intermolecular H-bond is formed by Asn280 residue. Indole ring of L20 does not directed towards the Gly-rich loop, but it curves to methyl substituent of the indazole ring by making a U-shape. The indole ring is located between hydrophobic region formed by residues Met282, Phe439, Va166 and Gly159 in the Gly-loop and it makes a H-bond interaction with the Glu236 side chain. The U-shaped binding mode of L20 is specific to PKB over PKA [71], and by this conformation of the

ligand, Phe163 residue on the Gly-rich loop of AKT-2 kinase protein is directed into the ATP binding cleft.

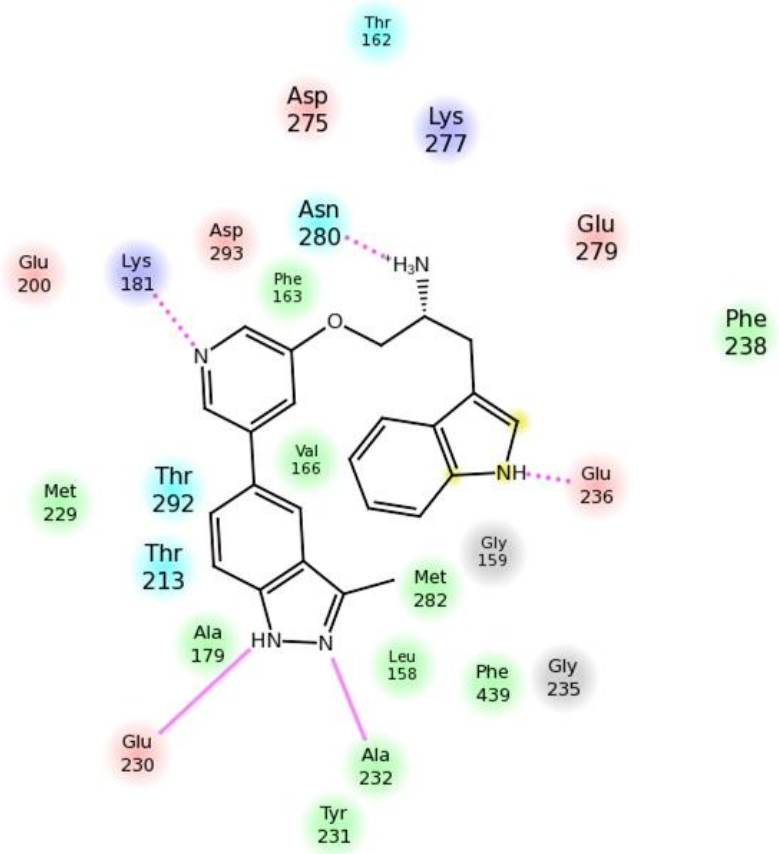

Figure 4.11. Ligand (L20) protein interaction diagram (PDB code: 2JDR).

The ligand X37 with chemical formula $C_{22}H_{30}N_5$ has 57 atoms and 60 bonds of which 4 are rotatable. It has 2 hydrogen bond acceptors and 4 hydrogen bond donors. Molecular weight is 364.51 g/gmol and the partition coefficient, log P value is 3.91. The compound satisfies the Lipinski's rule of five and it is drug-like. Figure 4.12 shows the interactions between the ligand and the protein. Pyrrolopyrimidine group (7H-pyrrolo[2,3-d]pyrimidine) of ligand X37 makes hydrogen bonding interaction with the hinge region residues of Ala232 and Glu230. Tertiary-butyl of the ligand interacts hydrophobically with the protein Gly-rich loop residues of Gly164 and Gly161. 4-amino group of X37 makes H-bond with the side chains of Glu236 and Met282.

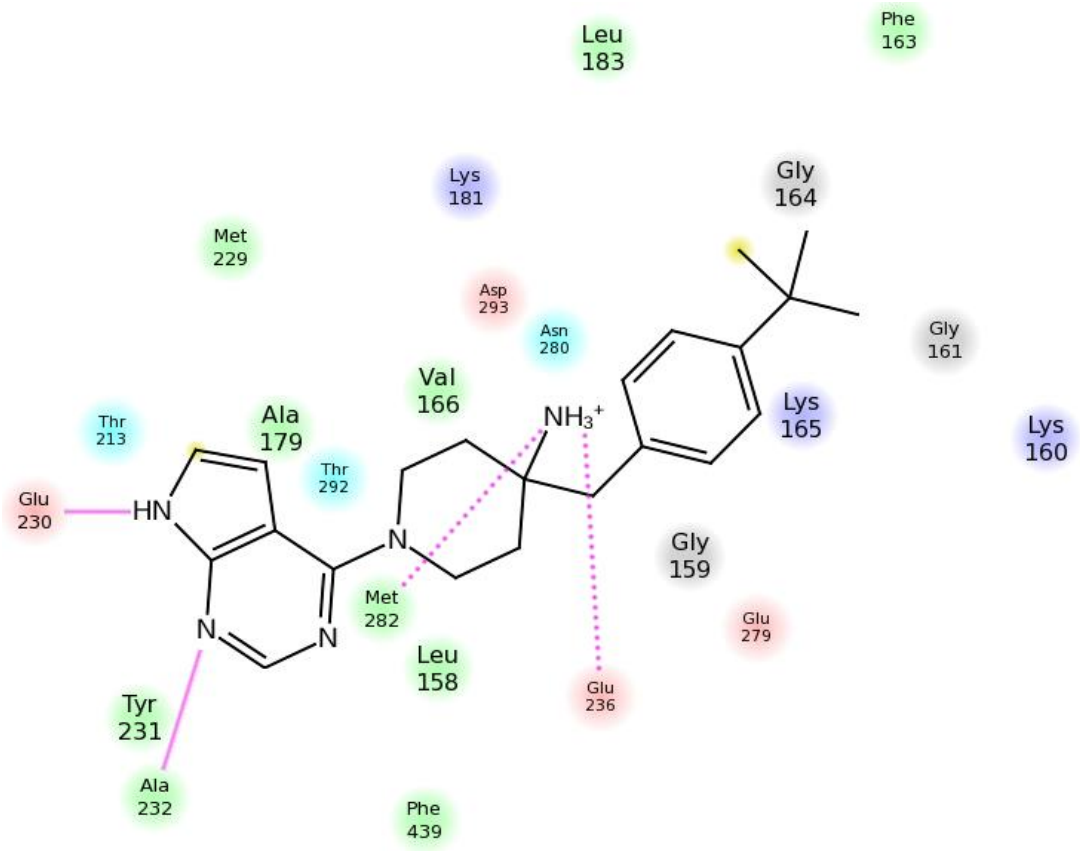

Figure 4.12. Ligand (X37) protein interaction diagram (PDB code: 2XH5).

The ligand X39 with chemical formula C19H22ClN6O has 49 atoms and 52 bonds of which 4 are rotatable. It has 3 hydrogen bond acceptors and 5 hydrogen bond donors. Molecular weight is 385.87 g/gmol and the partition coefficient, log P value is 1.88. The compound satisfies the Lipinski's rule of five and it is drug-like.

Figure 4.13 shows the interactions between the ligand and the protein. Pyrrolopyrimidine group (7H-pyrrolo[2,3-d]pyrimidine) of ligand X39 makes hydrogen bonding interaction with the hinge region residues of Ala232 and Glu230. Basic amino group of the X39 makes H-bonding interaction with Glu236 and Met282. 4-chlorophenyl ring, like other ligands containing this group, is located near the hydrophobic region of the Gly-rich loop. Amide NH group of the ligand also makes a hydrogen bonding interaction with the side chain of the Asp293 residue.

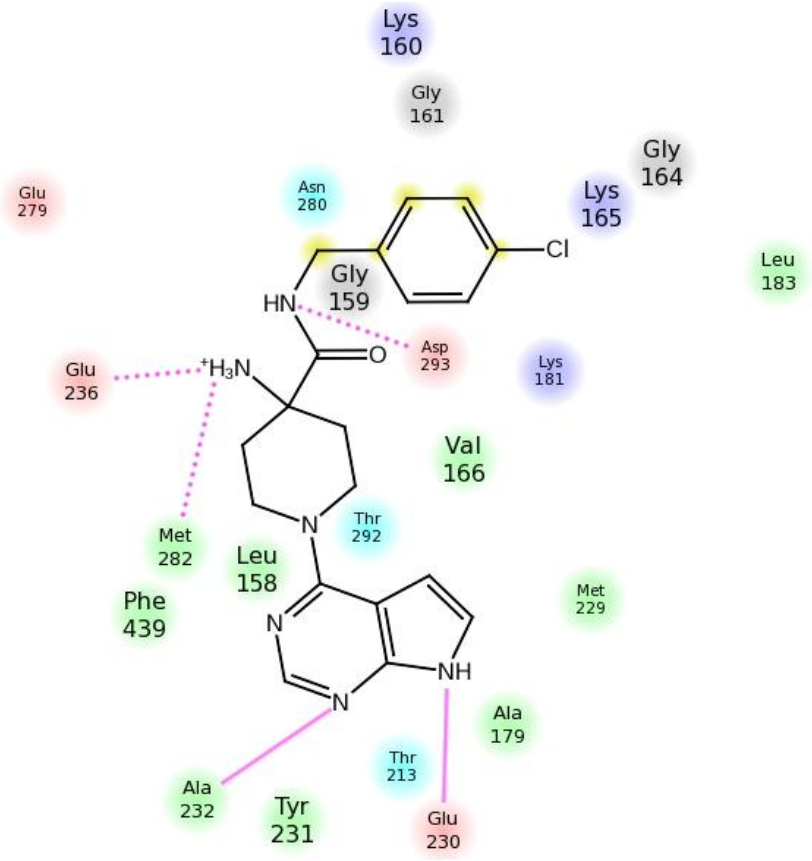

Figure 4.13. Ligand (X39) protein interaction diagram (PDB code: 2X39).

Chemical properties of the ligands and H-bond interactions with AKT-2 kinase protein are summarized in Table 4.4 and Table 4.5, respectively. Ligands' chemical data in Table 4.4 were taken from the public web service of chemicalize.org [106] which is created by ChemAxon. Total number of atoms and bonds for each ligand is listed and number of the rotatable bonds is given in brackets (Table 4.4). Table 4.4 also gives information about number of H-bond acceptor and donor groups, molecular weight (MW) of the ligand in unit of g/mol, octanol-water partition coefficient (LogP) and validity for Lipinski's rule of five (plus sign if it satisfies the Lipinski's rule of five). Table 4.5 shows a summary of H-bond network of AKT-2 kinase protein with active set of ligands; the protein residues are listed in columns, and the ligands and the corresponding PDB code for the complex, from which they were extracted, are listed in rows. Plus sign was assigned for each H-bond between a protein residue and ligand. Total column indicates the total number of H-bonds that corresponding ligand makes with AKT-2 kinase protein, and total row indicates the number ligands that make H-bond with the corresponding protein residue. For

example, ligand G93 makes seven H-bonds with Lys181, Glu200, Glu230, Ala232, Glu236, Glu279, and Phe294 residues of the AKT-2 protein. Three of nine active set of ligands make H-bonds with Lys181 residue of AKT-2.

Table 4.4. Summary of chemical properties of native ligands.

Ligand	**# of atoms**	**# of bonds**	**H bond acceptors**	**H bond donors**	**MW**	**LogP**	**Lipinski rule (Drug-like)**
G93	59	62 (7)	7	5	426.49	1.17	+
G95	45	48 (5)	2	5	363.46	2.84	+
G96	62	65 (9)	7	6	462.52	2.89	+
G98	62	65 (9)	7	2	462.52	2.66	+
GVP	45	48 (3)	1	3	338.85	4.07	+
I5S	51	53 (9)	4	3	420.93	2.36	+
L20	54	58 (6)	3	5	398.48	3.07	+
X37	57	60 (4)	2	4	364.51	3.91	+
X39	49	52 (4)	3	5	385.87	1.88	+

Table 4.5. Summary of H-bond interactions of native ligands.

PDB	**Ligand**	**Lys181**	**Glu200**	**Glu230**	**Ala232**	**Glu236**	**Glu279**	**Asn280**	**Met282**	**Thr292**	**Asp293**	**Phe294**	Total
3D0E	G93	+	+	+	+	+	+					+	7
3E87	G95			+	+								2
3E88	G96		+	+	+					+	+		5
3E8D	G98	+	+	+	+						+		5
2UW9	GVP			+	+	+							3
2JDO	I5S				+		+				+		3
2JDR	L20	+		+	+	+		+					5
2XH5	X37			+	+	+			+				4
2X39	X39			+	+	+			+		+		5
Total		3	3	8	9	5	2	1	2	1	4	1	

4.2. Pharmacophore Based Virtual Screening

Traditionally, pharmacophore based screening methodology, which is a ligand-based method, is applied when the structure information of the receptor is unknown or not available for virtual docking experiment [11, 12, 107, 108] (also reviewed in [13, 18]). This approach consumes significantly less CPU time and makes it possible to screen a large number of molecules, and in literature, examples that combine pharmacophore modeling and molecular docking are many [109–113]. Thus, in this study, screening the database via 3D pharmacophore hypothesis was used as a pre-filtering step before molecular docking simulations. First step to generate a pharmacophore hypothesis is preparing ligands for pharmacophore model. All AKT-2 inhibitors except G98 (3E8D) were used to build the pharmacophore model. The inhibitors included in pharmacophore model building were G95 (3E87), G96 (3E88), G93 (3D0E), X37 (2XH5), X39 (2X39), L20 (2JDR), I5S (2JDO), GVP (2UW9). Structures of G93 (3D0E), G96 (3E88), and G98 (3E8D) in the active set are highly similar (Figure 4.14). Their alignments and orientations in the binding pocket are also similar. The ligand G98 (3E8D), which has an intermediate conformation between G93 (3D0E) and G96 (3E88), was not included in the pharmacophore set and it was used to check the validity of docking carried out by Glide. Note that Figure 4.14 was prepared by aligning protein structures of 3D0E, 3E88, and 3E8D to 2JDO, and displaying only ligands. RMSD values to protein structure of 2JDO for 3D0E, 3E88, and 3E8D are 0.968, 0.038, and 0.913, respectively.

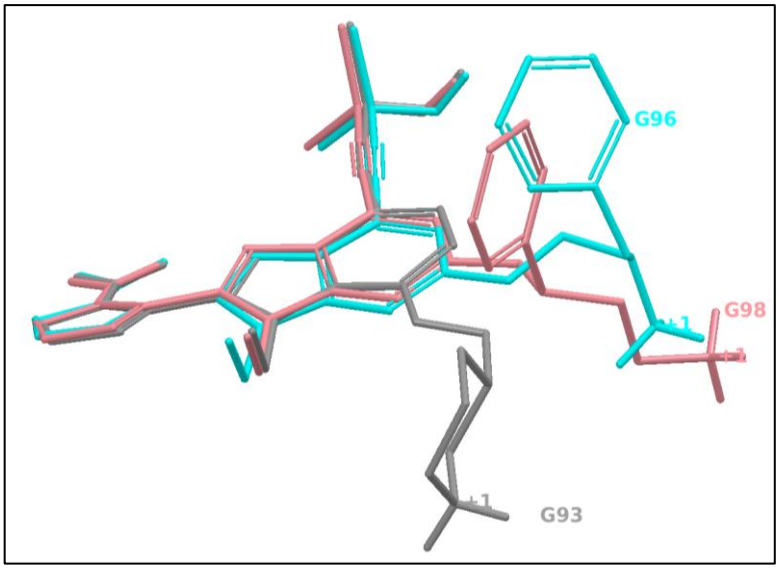

Figure 4.14. Structure of G93 (3D0E) in gray, G96 (3E88) in blue, and G98 (3E8D) in pink.

Since the pharmacophore model was generated from X-ray structures and correct conformations of the ligands were known, conformer generation step, which is normally a part of ligand preparation, was not performed.

For each ligand, sites were created and as a representative example ligand G93 (3D0E) with created sites points is shown in Figure 4.15. G93 pharmacophore feature shows that there are seven hydrogen acceptor groups (red spheres) on the ligand. All of hydrogen bond acceptors have one lone pair with only one arrow on them except A5 and A6 (Figure 4.15). There are five hydrogen atoms with high probability to make hydrogen bonds and they are labeled as D. Three aromatic rings (orange torus in the plane of the ring), two hydrophobic regions (green spheres) and a positively charged group (blue sphere) are part of the G93 pharmacophore features.

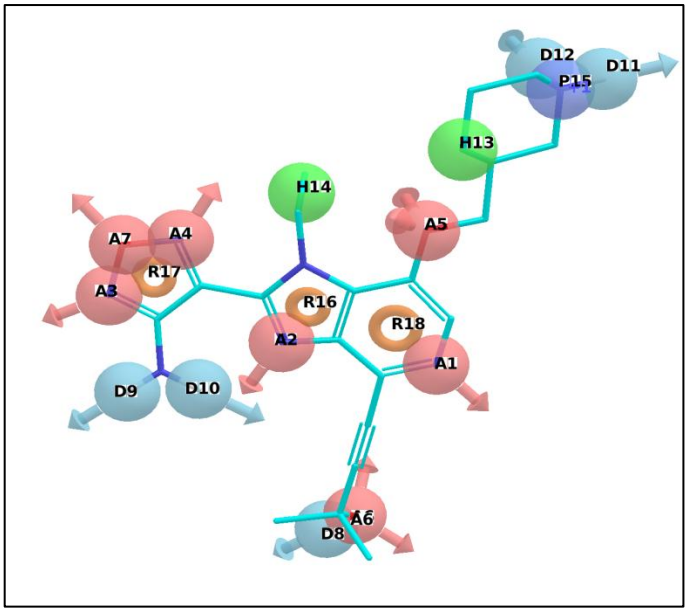

Figure 4.15. Pharmacophore site points on ligand G93.

Results of pharmacophore sites of active set of ligands are shown in Table 4.6. In Table 4.6 number of site points for each pharmacophore feature for each ligand is listed. For example, ligand G93 has 7 H-bond acceptor (A), 5 H-bond donor (D), 2 hydrophobic group, 1 positively charged group, and 3 aromatic ring.

Table 4.6. Number and type of pharmacophore sites of ligands.

Name	**A**	**D**	**H**	**N**	**P**	**R**
G93 (3D0E)	7	5	2	0	1	3
G95 (3E87)	2	5	0	0	1	4
G96 (3E88)	7	6	1	0	1	4
GVP (2UW9)	1	3	2	0	1	3
I5S (2JDO)	4	3	1	0	1	3
L20 (2JDR)	3	5	1	0	1	5
X37 (2XH5)	2	4	2	0	1	3
X39 (2X39)	3	5	2	0	1	3

After scoring, hypotheses were ranked and more tangible selection could be made. The hypotheses including their scores are listed in Table 4.7. All hypotheses contain at most four pharmacophore features. It is the maximum number that Phase can find for the given active set. Hypotheses are listed in descending order of survival score. Survival score

is the final scoring function which consists of weighted factors of vector score, site score, volume score, selectivity score, and number of matches. Selectivity score gives information about the rarity of the hypothesis. A higher value in selectivity score indicates that the corresponding hypothesis is unique to set of ligands used to compose the hypothesis. Vector score shows the fitness of the vector features (aromatic rings, acceptors and donors) of the structures which are aligned to the pharmacophore hypothesis. Site score evaluates how well the centers of the site points are aligned. Volume score indicates in which extent the volumes of the structures, that compose the hypothesis, overlap. Note that only top ten hypotheses according to survival score are listed in Table 4.7.

Table 4.7. Phase hypothesis scoring.

ID	**Survival**	**Site**	**Vector**	**Volume**	**Selectivity**
DDRR.1	2.72	0.53	0.84	0.35	1.32
DRRR.61	2.68	0.28	0.94	0.46	1.41
DHRR.1	2.64	0.46	0.85	0.33	1.50
DRRR.62	2.64	0.29	0.89	0.46	1.43
ADDR.11	2.56	0.45	0.84	0.27	1.13
ADDR.29	2.54	0.40	0.82	0.32	1.19
ADDR.35	2.52	0.41	0.79	0.32	1.20
ADRR.9	2.51	0.44	0.67	0.39	1.26
AADD.14	2.46	0.35	0.82	0.29	1.03
ADHR.7	2.43	0.44	0.70	0.29	1.41

Hypothesis DRRR.62 was selected to be used in database screening to find matches. The selection was made by considering the following arguments. First, distance between the pharmacophore features was examined. Hypotheses with very close features (DHRR.1 and ADRR.9) were rejected since these result in very small, fragment-like molecules. Another concern is whether the hypothesis features predict important protein-ligand interactions by looking at projection of hypothesis on native ligand structures (Figure 4.16). Only hypotheses with features mimicking interaction of native ligands (necessary for activity) were taken into consideration. Additionally, hypotheses that are consisting of only one type of feature, for example, DDDD, are undesirable and eliminated since they are unrealistic.

Fitness values of the structures that contribute to some of the top ranked hypotheses were listed in Table 4.8. Fitness score indicates the degree of how well the actives match the pharmacophore hypothesis and it consists of vector score, site score, and volume score. It can be seen that, in Table 4.8, only 4 of the native ligands contributed to hypothesis generation and so have fitness score since during pharmacophore hypothesis generation, at least 4 of the 8 ligands were set to be matched. Higher values of this parameter yielded no common pharmacophore. This situation arises when the native ligands assume different binding modes.

Table 4.8. Hypotheses fitness to active ligand.

Hypothesis	**G95**	**L20**	**X37**	**X39**
DDRR.1	1.80	1.65	3.00	1.70
DRRR.62	3.00	1.83	1.65	1.44
ADDR.11	1.77	1.21	3.00	1.70

3D-pharmacophore hypothesis of DRRR.62 is shown in Figure 4.16. Hypothesis DRRR.62 was represented on the aligned ligands L20, X37, X39, and G95, which has the highest fitness to hypothesis. Hydrogen bond donor site of the hypothesis DRRR.62, specifically D7, is on the indole of the G95 and involved in important protein-ligand interaction where it has an interaction through hydrogen bonding with hinge region residues Glu230 of AKT-2. Two aromatic ring sites are also represented on the indole. Other aromatic ring site of the hypothesis is in the phenyl ring of the G95 which is in hydrophobic interaction with the Gly-rich region of the AKT-2 kinase protein (Figure 4.16). Figure 4.16 also shows the other ligands that contribute to hypothesis and listed in Table 4.8.

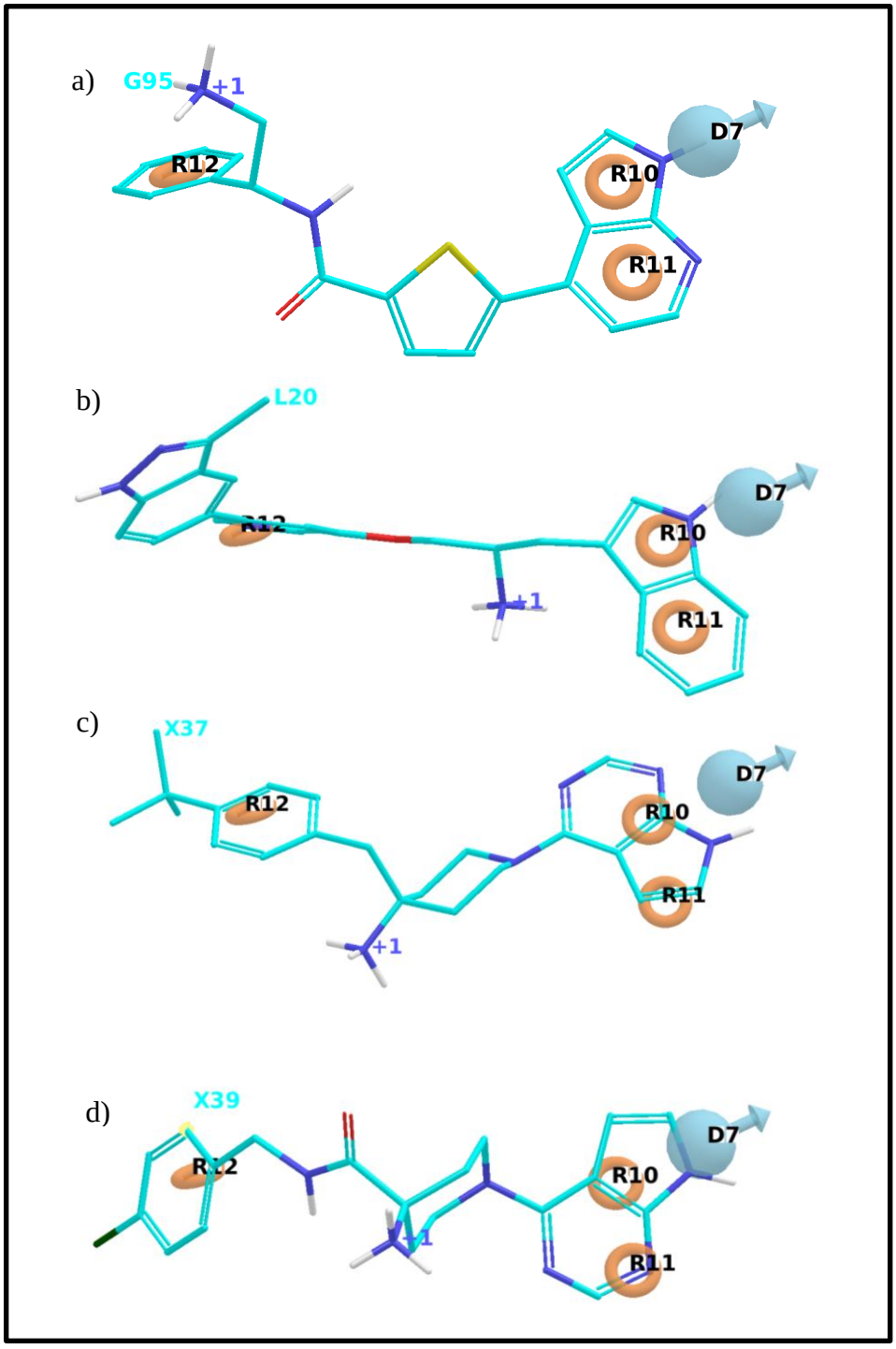

Figure 4.16. Alignments of a) G95, b) L20, c) X37, and d) X39 with hypothesis DRRR.62.

As described in the analysis of binding site section, co-crystalized inhibitors occupy similar space in the binding pocket. According to this property of the known actives, and since relatively simple, four-feature hypothesis was chosen it was decided to add ligand-based excluded volumes to the pharmacophore hypothesis before a database screen. This

utility takes less computational time and eliminates unfavorable molecules. Excluded volume spheres, off-limits to database screening, were included in the pharmacophore model. When Phase finds matches to hypothesis, ligands which occupy a region on the excluded volume were rejected. Generated ligand-based excluded volumes to the hypothesis DRRR.62 is shown in Figure 4.17. This feature was used to force matches to occupy a specific volume, to find matches to stay within the binding site, and to speed up the elimination process.

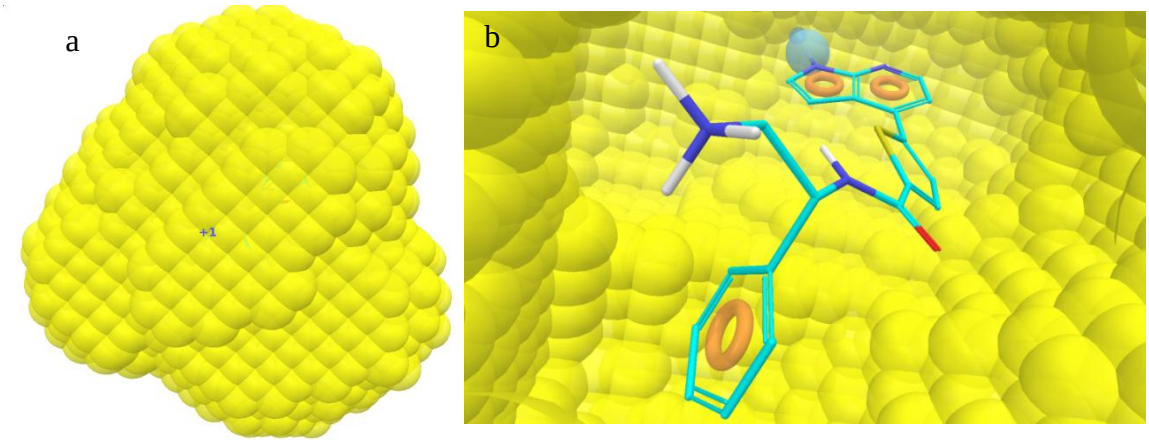

Figure 4.17. Ligand based excluded volumes to the hypothesis DRRR.62 (a) outside, (b) inside view.

After hypotheses were generated and selected, CoCoCo_Phase database was screened to find matches to hypothesis DRRR.62. CoCoCo_Phase database is a multiconformer, ready to use database and has 3.7 million compounds with 144 million conformers. This database was pre-filtered by matching the compounds to the hypothesis before docking process. 20660 hits from CoCoCo database passed the Phase filtering step for the hypothesis DRRR.62. The top ten hits from a Phase run with hypothesis DRRR.62 are shown in Table 4.9. Hits were sorted according to Fitness score. Fitness score is a weighed function of site score, vector score and volume score. Fitness score indicates how well the molecules match the pharmacophore hypothesis. Site, vector, and volume scores are same with the ones previously mentioned in Phase Hypotheses part of the report. In the matched ligand sites column of Table 4.9, letters indicate feature type of the matched site to hypothesis and the index in parenthesis indicates the site point of the hit.

Table 4.9. Phase Find Matches for DRRR.62 (Top 10 Hits).

CoCoCo ID	Matched Ligand Sites	Site Score	Vector Score	Volume Score	Fitness
4454219	D(8) R(13) R(14) R(15)	0.14	0.99	0.73	2.60
4586695	D(5) R(7) R(8) R(9)	0.14	0.95	0.74	2.57
4453880	D(8) R(10) R(11) R(12)	0.27	0.97	0.75	2.50
4453995	D(7) R(11) R(13) R(12)	0.22	0.90	0.77	2.49
1090520	D(7) R(11) R(12) R(13)	0.22	0.99	0.68	2.48
810659	D(2) R(7) R(9) R(8)	0.11	0.99	0.57	2.47
1579801	D(6) R(10) R(11) R(12)	0.34	0.99	0.76	2.47
1579799	D(6) R(10) R(11) R(12)	0.34	0.99	0.76	2.47
4586696	D(5) R(7) R(8) R(9)	0.17	0.91	0.71	2.47
3513202	D(4) R(5) R(7) R(6)	0.13	0.98	0.59	2.47

According to the fitness score, the top-scored three hits are shown with their alignment to hypothesis DRRR.62 in Figure 4.18, where D7, R10, R11, and R12 are the site points of the hypothesis DRRR.62. It was observed that they were in a good accordance with the hypothesis by looking at the pharmacophore features of DRRR.62 and how well the H-bond donor groups and aromatic rings of the molecules were superimposed.

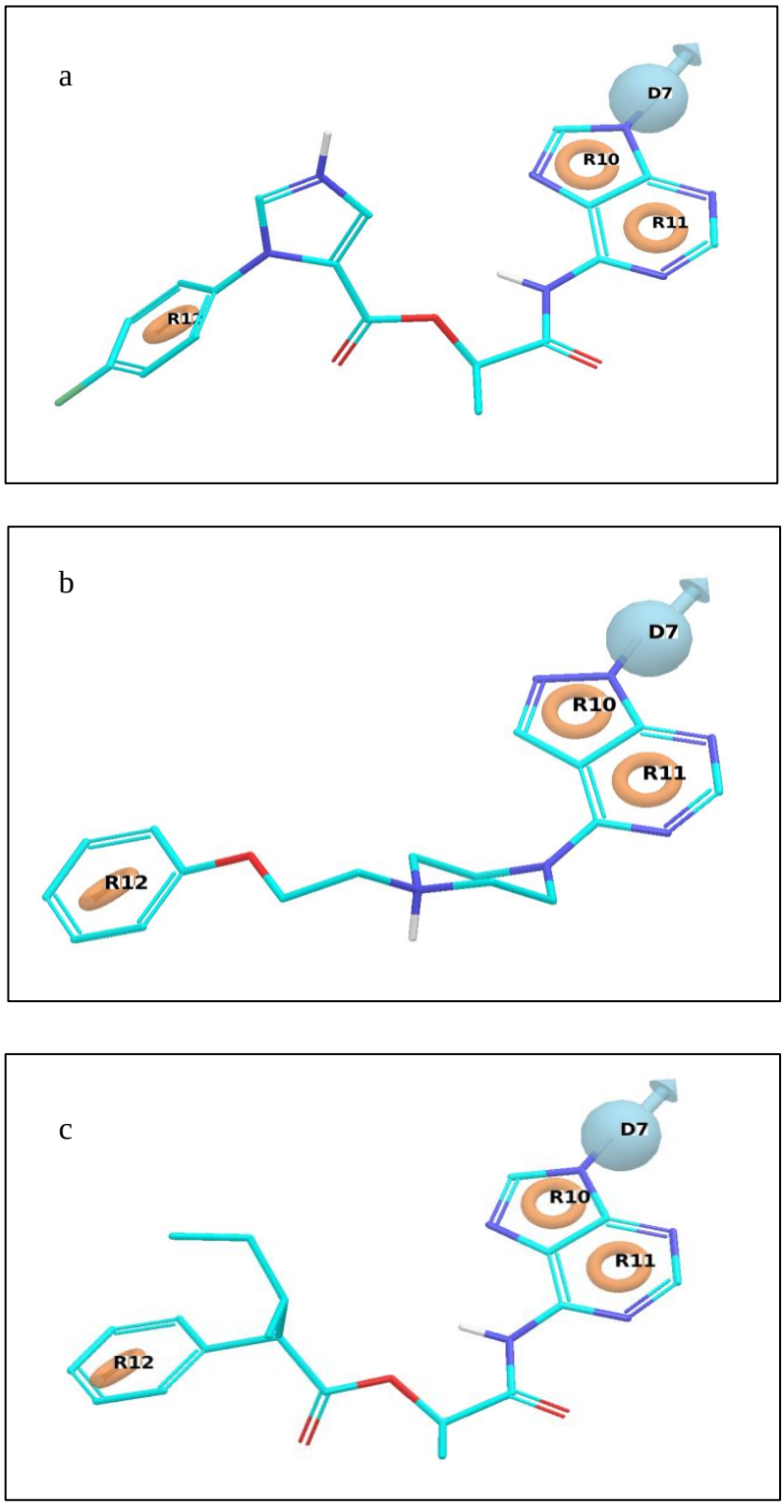

Figure 4.18. Top Three Hit (According to Fitness Score) Matching to Hypothesis DRRR.62 (a) 4454219, (b) 4586695, (c) 4453880.

4.3. Virtual Docking Studies

From Phase application (search for matches to hypothesis DRRR.62), 20.660 hits from CoCoCo database were saved. These molecules were prepared for the docking job using the LigPrep application of the Schrödinger Suit. Simply, LigPrep was used for getting high quality 3D structures of the ligands in CoCoCo database. Finally, 61042 energy-minimized structures were generated for 20660 input compounds.

4.3.1. Determination of Template Protein for Docking

Grid file should be generated for the receptor which is going to be used in a ligand docking job. For this reason, the first task to be done was to determine which X-ray structure of the AKT-2 kinase protein would be prepared for the docking experiment. When all available X-ray complex structures of AKT-2 protein were superimposed, it could be seen that protein structures were in a good accordance except the loop region in circle in Figure 4.19.

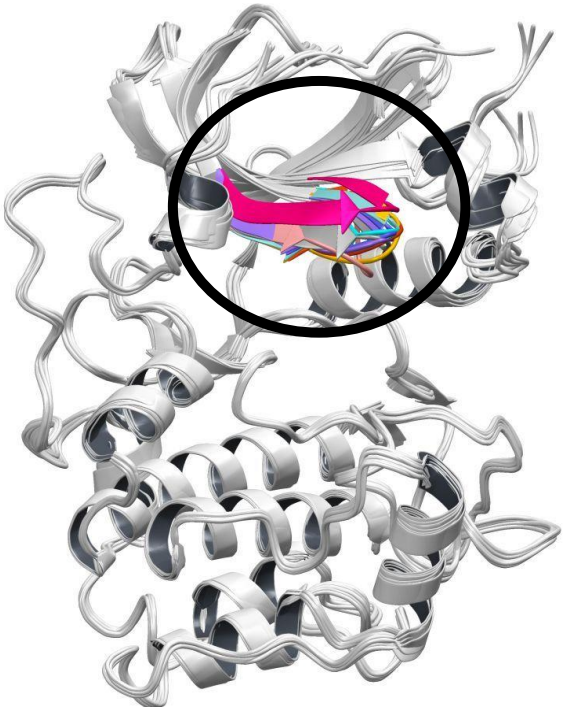

Figure 4.19. AKT-2 kinase protein structure alignment.

AKT-2 adopts different binding modes with different loop motion for each ligand. In addition to loop motion, Phe163 residue on the loop is also very flexible [64]. It is directed toward or away from the binding site (Figure 4.20). Figure 4.20 shows the Gly-loop (residues 158-165) of AKT-2 protein (also indicated in circled area in Figure 4.19), and Phe 163 residue of AKT-2.

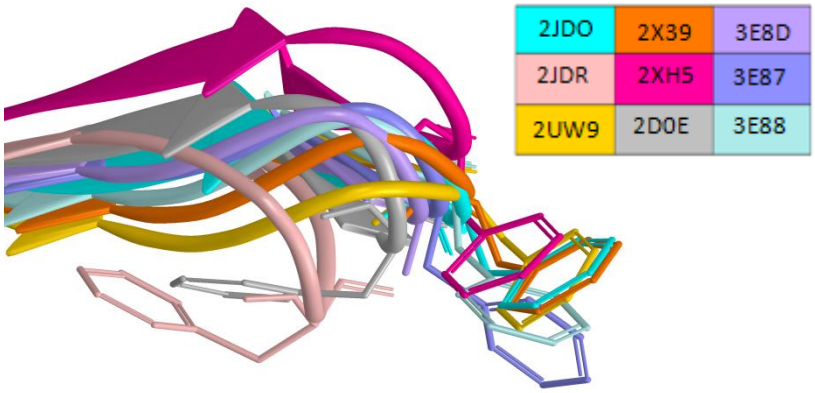

Figure 4.20. Phe 163 residue on Gly-rich loop.

In order to consider these conformational changes upon binding, two of the AKT-2 structures (2JDO and 2JDR) were used for ligand docking. The most open and most closed loop and Phe163 residue conformations exist in 2JDO and 2JDR, which are also shown in Figure 4.21. Except for the loop region, these two structures, 2JDO and 2JDR, are similar and RMSD between the C_α coordinates of the two proteins was found to be 0.66 Å. In the virtual docking studies, these two AKT-2 structures were used. 2XH5, 2X39, and 3E8D have missing residues so they were not preferred for docking experiments.

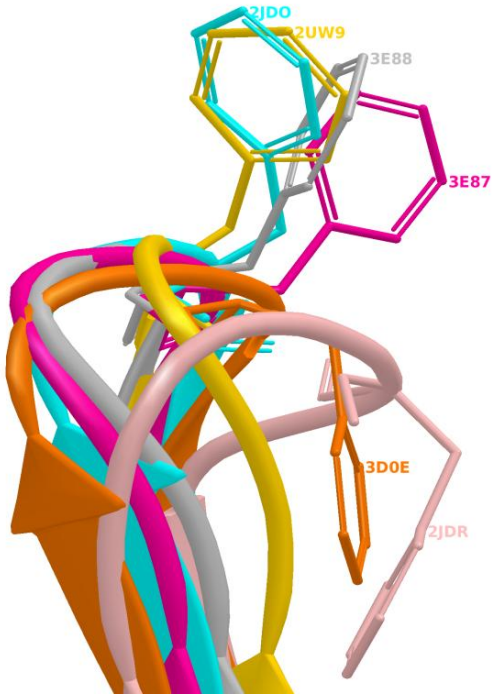

Figure 4.21. Phe163 residue on 2JDO (cyan), 2UW9 (yellow), 3E88 (gray), 3E87 (pink), 3D0E (orange), and 2JDR (light pink).

4.3.2. Determination of Conserved Water Molecules

Another important point is that, some conserved water molecules are observed in the X-ray structure files of AKT-2 complex. If the water molecules are observed in more than the half of the complex structures it can be accepted as a conserved molecule [114]. 3E87 and 3E88 complex structures do not contain any water molecule, so they were excluded from further evaluation. Remaining complex structures were superimposed to 2JDO, which has highest X-ray resolution (1.80 Å), and only the water molecules that are not farther than 2.4 Å [115] from each other were taken into account. There are four water molecules closer than 2.4 Å to each other and they are listed in Table 4.10. PDB code column of Table 4.10 shows the PDB code and the atom numbering of the corresponding water in PDB crystal structure file. Additionally the number of protein structures that contain the corresponding water molecule is also indicated. 3D representations of the water molecules are also shown in Table 4.10 with coloring as follows; 2JDO in blue, 2JDR in pale pink, 2X39 in orange, 3D0E in pink, 2UW9 in yellow, and 3E8D in gray. Note that only oxygen atoms of the water molecules are shown and they were connected by black dashed lines

and the distance between them was displayed in unit of Å. According to the definition given above, W1 and W2 in Table 4.10 can be classified as conserved water molecules for AKT-2 kinase protein. Note that in this study only water molecules that are in the ATP binding site (within 5 Å to ligands) were considered.

Table 4.10. Conserved water molecules (2JDO in blue, 2JDR in pale pink,2X39 in orange, 3D0E in pink, 2UW9 in yellow, and 3E8D in gray).

Molecule	**PDB Code**	**3D Representation**
W 1	3E8D_32 2JDR_2001 2UW9_2006 2JDO_2011 2X39_2002 5 of 7==>71%	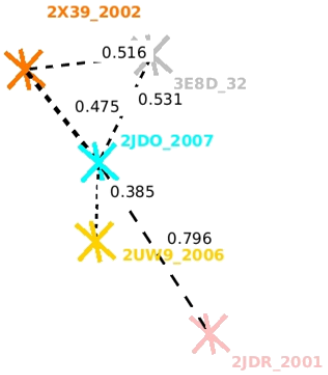
W 2	3DOE_698 2UW9_2064 2JDO_2007 2JDR_2027 4 of 7==>57%	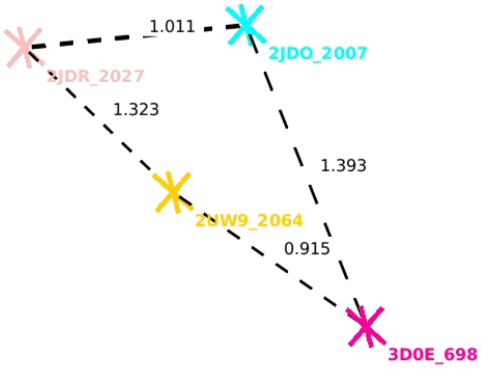
W 3	3D0E_539 2JDO_2075 2X39_2043 3 of 7 ==> 42 %	

Table 4.10. Conserved water molecules (2JDO in blue, 2JDR in pale pink,2X39 in orange, 3D0E in pink, 2UW9 in yellow, and 3E8D in gray) (cont.).

Molecule	PDB Code	3D Representation
W 4	2X39_2007 2JDO_2006 2 of 7==> 28%	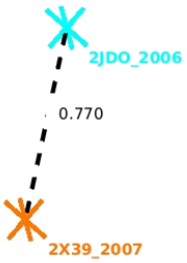

4.3.3. Protein Preparation

For ligand docking process, AKT-2 kinase structures of 2JDR and 2JDO were prepared by Protein Preparation Wizard (PPW), but this time conserved water molecules 2001 and 2027 for 2JDR, and 2007 and 2011 for 2JDO were kept. Ionization and tautomeric states were selected according to lowest state penalty. Properties of selected ligand states; namely, state penalty, charge of the ligand (Q), and number of H-bond for corresponding ligand state were listed in Table 4.11.

Table 4.11. Selected ligand states from Protein Preparation Wizard.

PDB Code-Ligand	State Property
2JDO – I5S	Penalty= 0.67 kcal/mol Q=+1 H-bond count=3
2JDR – L20	Penalty= 0.84 kcal/mol Q=+1 H-bond count=3

The region of the protein being treated during the grid generation and the explored docking run was defined by enclosing box and it is shown in purple cube in Figure 4.22a and 4.22b for 2JDO and 2JDR, respectively. Inner green cube is the bounding box and it defines the region where the center of docked molecules should stay within. Center of the

enclosing and bounding boxes is also the center of the ligand that is co-crystalized with protein (shown in cyan in Figure 4.22). Conserved water molecules are represented as red spheres.

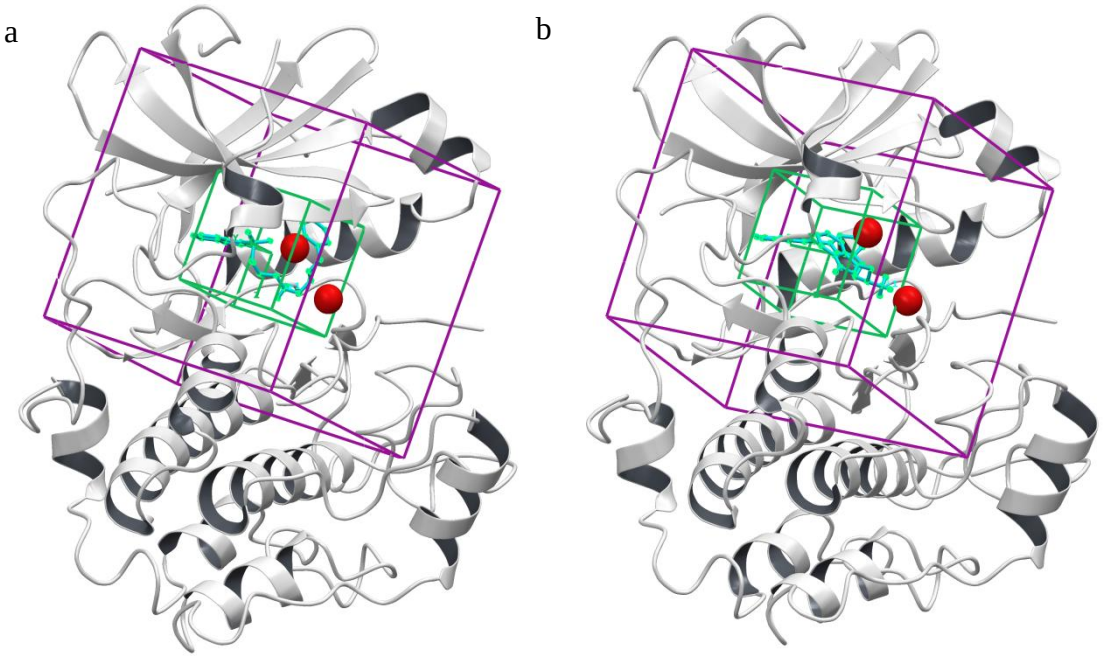

Figure 4.22. Enclosing (Green) and Bounding (Purple) Boxes for (a) 2JDO, (b)2JDR with Water Molecules (Red Spheres) and Ligand in Cyan.

In order to increase the success rate of the docking results, conserved H-bond interactions among the native ligands and AKT-2 are imposed as constraints. All constraints applied to docking process are determined in this step. The protein residues that are making H-bonding with ligand were determined by looking at protein-ligand interaction map which was examined in detail in Section 4.1. The protein residues that could be used as docking constraints were Lys181, Glu200, Glu230, Ala232, Glu236, Glu279, Asn280, Asp293, and Phe294. All Ser, Thr, and Tyr residues (whose hydroxyl groups can rotate during ligand docking with Glide) in the active site were listed and from this list two-most flexible ones; namely, Thr213 and Thr292, were to allow of rotation of their hydroxyl group. AKT-2 crystal structures were superimposed and the selected residues of Thr213 is shown in blue and Thr292 is shown in yellow color in the Figure 4.23. As a representative example, Thr213 and Thr292 residues in the Figure 4.23 shown in 2JDO active site with its native ligand I5S.

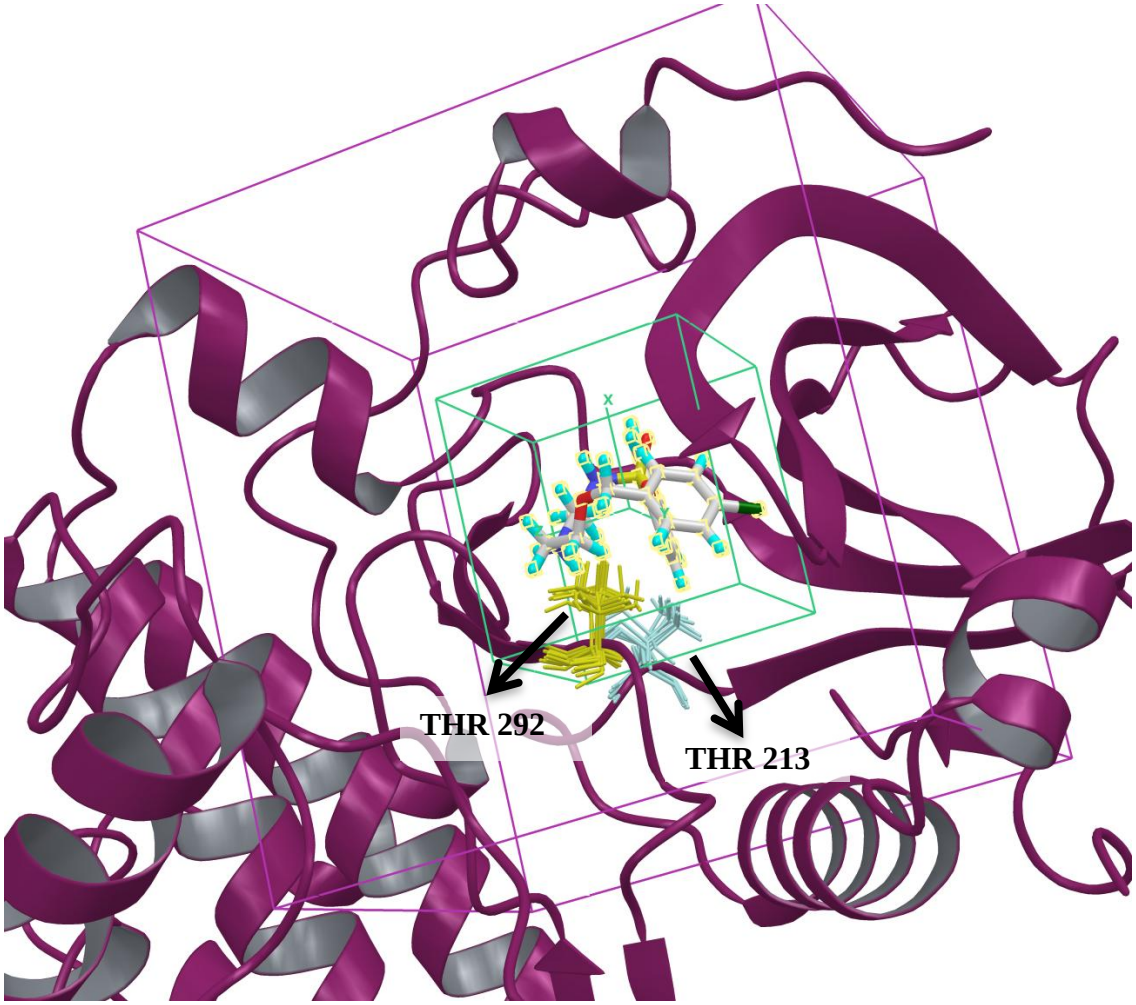

Figure 4.23. Residues of Thr213 and Thr292 in the binding pocket of AKT-2 kinase with I5S (PDB:2JDO).

4.3.4. Validation of Docking Protocol

In order to validate Glide XP docking protocol, co-crystallized molecules were re-docked to their target protein. In docking experiments no constraints were applied. Predicted docking poses were in good accordance with the experimental X-ray poses. Bound conformations of docked pose and co-crystal pose of I5S and L20 within active site of 2JDO and 2JDR are represented in Figure 4.24. RMSD (all heavy atoms) between the two I5S structures was calculated as 0.476 Å (with constraint 0.476) and between the two L20 structures was calculated as 0.217 Å (with constraint 0.228). Consequently, Glide docking protocol was used to predict the accurate binding mode of native ligands for AKT-2 kinase protein. A number of examples from literature [116–119] indicate that RMSD

values lower than 2.0 Å between the actual conformation and the predicted pose is acceptable.

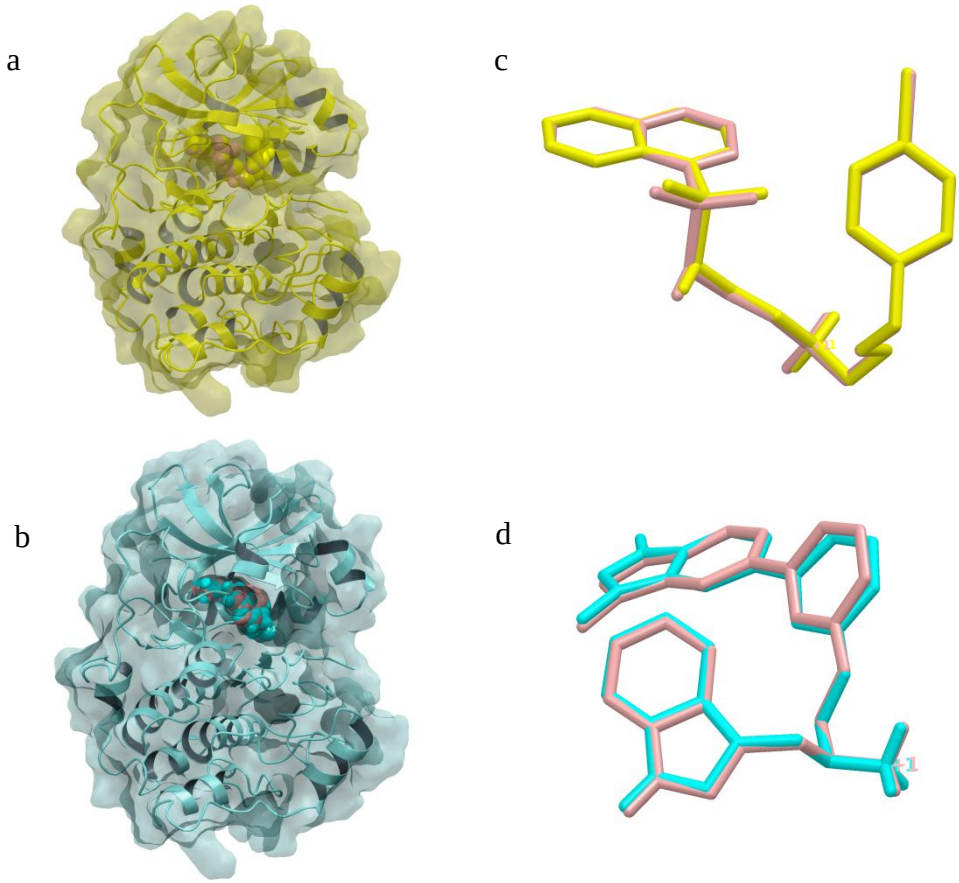

Figure 4.24. Protein with binding site (a) 2JDO, (b) 2JDR (left), (c)-(d) overlay of the bound conformations of docked pose shown in pink and co-crystal pose shown in yellow for I5S, blue for L20 (right).

4.3.5. Multistep Docking

In this study two step docking procedure was applied. First, Glide standard precision (SP) docking, which consumes less computational time, was performed, and then selected molecules were re-docked with Glide extra precision (XP) mode. After protein and ligand database preparation, Glide docking in flexible ligand mode was performed. Ligands, which pass the 'Phase find matches' procedure and which were prepared with the LigPrep utility, were used in this step. H-bonding constraints were applied for SP docking run. It is

known that H-bonding interaction at hinge region is important for kinase inhibitors, and all nine AKT-2 inhibitors make at least one hydrogen-bond with Ala232 and Glu230 in the hinge region of the protein. At least one H-bond between Ala232 or Glu230 and docked molecule was imposed as a constraint. In the output file a total of 10000 poses were kept for each Glide SP run with receptors 2JDO and 2JDR. Some molecules are represented by more than one pose. Among 10000 poses, there were 4742 distinct compounds for 2JDO and 4772 distinct compounds for 2JDR.

Ranked SP docking scores (GScore) for distinct compounds were plotted for the runs with receptors 2JDO and 2JDR, shown in Figure 4.25. GScores in these graphs show exponential decrease up to about 200 compounds after which the GScore declines more slowly. 1000 compounds with GScore values above about -9 kcal/mol for 2JDO docking and 1000 compounds with GScore values above about -8 kcal/mol for 2JDR docking were selected to be used in Glide XP run.

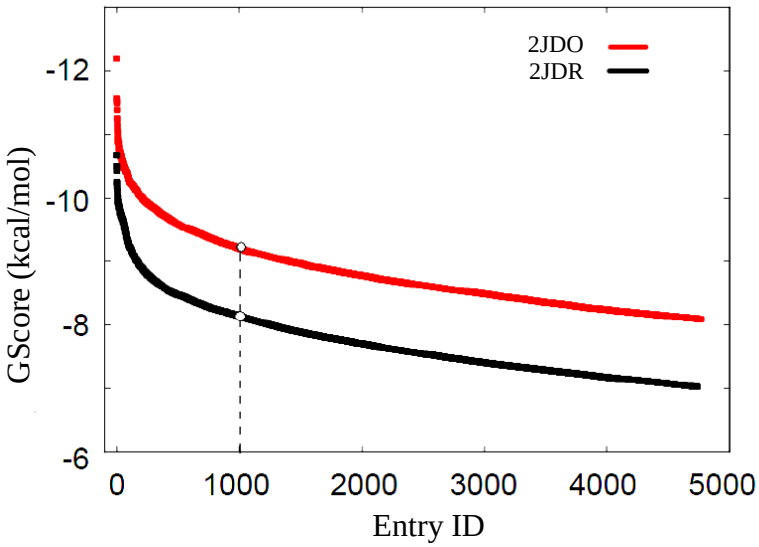

Figure 4.25. Cut-off value for selecting top poses after Glide SP docking experiment with receptors 2JDO and 2JDR.

Glide conformation generation during a SP or XP run depends on input ligand geometries. After a SP run, ligand in the output file may have internal strain and relaxing the ligand structures before feeding them into an XP run reported to give better results

[29]. The command-line premin utility was used to release excess strain for selected 1000 structures before a Glide XP docking experiment.

Selected compounds with Glide SP were re-docked with Glide XP with the same crystal structure. Glide XP docking with flexible ligand mode was then performed. H-bonding constraints were applied for XP docking run. The nine known AKT-2 inhibitors make 2 to 5 H-bonds with AKT-2 kinase protein. H-bonds are determined during the grid generation step and a constraint of at least 3 H-bonds between defined residues and docked molecule was imposed. In the output file of Glide XP run 394 poses were kept for receptor 2JDO and 137 poses were kept for receptor 2JDR.

Glide predicts binding affinity by Glidescore (GScore) [29] which is based on Chemscore [120] function with modifications (Table 4.12). Terms included in the Glide docking results are explained in Table 4.12. GScore was used to rank the hits. Top structures were selected using GScore, where lower GScore values indicate higher affinity and more favorable binding. 25 molecules that were docked using Glide extra precision mode and flexible ligand docking together the above mentioned constraints, are listed in Table 4.13 for receptor 2JDO and Table 4.14 for receptor 2JDR. Ranked XP docking scores (GScore) for distinct compounds were plotted for the runs with receptors 2JDO and 2JDR, shown in Figure 4.26. Molecules docked to receptor 2JDO, where Gly-loop is directed away from the binding site, have better scores than those docked to receptor 2JDR, where Gly-loop is directed towards the binding site. Although same molecules were used as input for docking with each structure (2JDO and 2JDR), only three molecules with CoCoCo ID 5609932, 5657271, and 5331049 were found in Table 4.13 and Table 4.14. Molecule 5609932 is in the 4^{th} rank for docking with receptor 2JDO and in the 3^{rd} rank for docking with receptor 2JDR. Molecule 5657271 is in the 19^{th} rank for docking with receptor 2JDO and in the 22^{nd} rank for docking with receptor 2JDR. Molecule 5331049 is in the 22^{nd} rank for docking with receptor 2JDO and in the 8^{th} rank for docking with receptor 2JDR. These results show that docking with two AKT-2 structures was a good choice since docking result was significantly affected by the conformation of the protein structure. Molecules that were eliminated or had low scores as a result of docking with one AKT-2 structure could achieve high docking score according to docking with the other

structure. The strategy employed here can decrease the rate of false positives during database screening.

According to Table 4.13, no direct correlation between docking score and any of the energy terms was observed, however it can be said that the major contribution to energy is made by the van der Waals energy term, which has a wide range. Site energy terms, which account for polar interactions in the binding site, are very small in both cases, but slightly better (more negative) for 2JDO. Conversely, lipophilic term is lower (more negative) for 2JDR. This was an expected result, since hydrophobic benzyl ring on residue Phe163 is directed toward the binding site in the X-ray structure of 2JDR, and this orientation may reward lipophilic contacts and impose penalty for hydrophilic contacts.

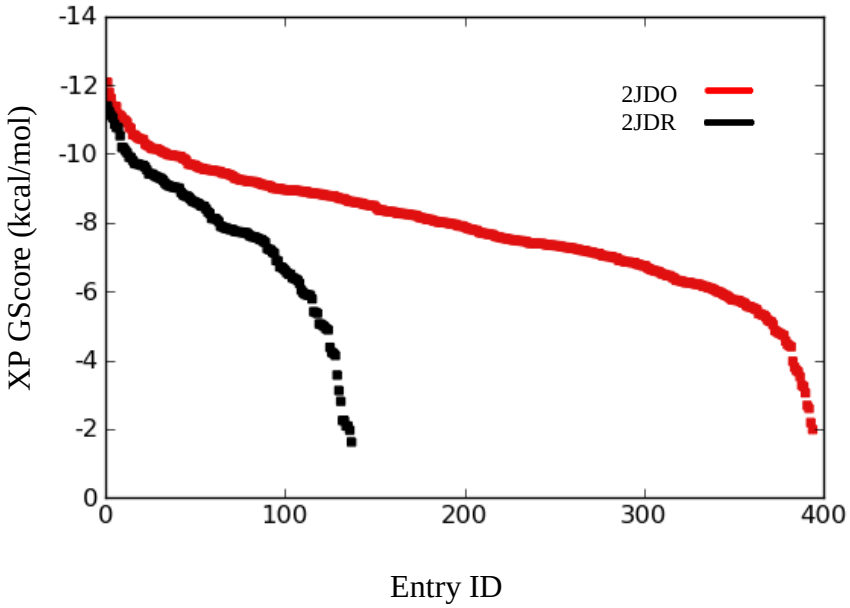

Figure 4.26. Ranked XP docking scores (GScore) for distinct compounds with receptors 2JDO and 2JDR.

Table 4.12. Terms used in Glide docking results.

Term	Description
vdW	Van der Waals energy.
coul	Coulomb energy.
Lipo	Lipophilic term.
esite	Polar term.
XP HBond	H-bonding term.
XP GScore	It is a binding affinity prediction term and it consists of van der Waals energy, coulomb energy, lipophilic term, hydrogen-bonding term, metal-binding term, term that penalize buried polar groups and freezing rotatable bonds, and term that rewards polar interactions in the active site.

Table 4.13. Glide docking results (receptor: 2JDO) for hits DRRR.62 hypothesis match (top 25 Results).

	CoCoCo ID	vdW	coul	lipo	esite	XP Hbond	XP GScore	Energy
1	2290040	-34.28	-23.07	-1.94	-0.28	-2.31	-12.09	-57.36
2	4849420	-41.89	-17.28	-2.51	-0.23	-2.11	-11.80	-59.17
3	5611052	-55.07	-20.50	-0.98	-0.06	-3.94	-11.61	-75.57
4	5609932	-38.67	-26.85	-1.88	-0.20	-2.84	-11.41	-65.52
5	3399013	-44.51	-23.78	-2.79	-0.24	-2.48	-11.38	-68.29
6	1629090	-38.08	-11.44	-3.74	-0.10	-2.39	-11.37	-49.52
7	1642127	-39.11	-15.74	-3.20	-0.10	-1.90	-11.15	-54.86
8	1273283	-25.59	-24.64	-2.47	-0.18	-1.95	-11.07	-50.23
9	1318556	-37.34	-14.70	-3.36	-0.10	-1.93	-10.91	-52.04
10	5356769	-34.35	-22.70	-0.71	-0.30	-2.60	-10.77	-57.06
11	1327900	-39.66	-13.57	-2.87	-0.10	-1.93	-10.56	-53.23
12	4703230	-10.06	-20.59	-2.25	-0.29	-2.72	-10.55	-30.65
13	5717141	-46.07	-24.17	-2.24	-0.25	-4.53	-10.51	-70.25
14	5242298	-40.19	-24.00	-2.02	-0.18	-1.43	-10.46	-64.19
15	5658764	-43.83	-17.80	-2.27	-0.23	-2.23	-10.44	-61.63
16	5331047	-37.68	-16.70	-0.51	-0.23	-2.63	-10.43	-54.38
17	5657276	-46.81	-18.38	-2.41	-0.28	-1.98	-10.41	-65.19
18	5581393	-44.56	-26.60	-0.98	-0.10	-2.44	-10.29	-71.16
19	5657271	-44.74	-25.01	-3.37	-0.23	-2.14	-10.25	-69.76
20	370431	-23.29	-16.24	-2.29	-0.15	-2.85	-10.23	-39.53
21	4586762	-34.69	-22.01	-0.81	-0.09	-1.80	-10.18	-56.70
22	5331049	-35.19	-19.53	-0.62	-0.24	-2.29	-10.15	-54.72
23	1573035	-31.77	-19.85	-0.59	-0.11	-1.33	-10.14	-51.63

Table 4.13. Glide docking results (receptor: 2JDO) for hits DRRR.62 hypothesis match (top 25 Results) (cont.).

	CoCoCo ID	vdW	coul	lipo	esite	XP Hbond	XP GScore	Energy
24	5403832	-30.26	-20.85	-1.77	-0.10	-3.64	-10.14	-51.12
25	4849433	-38.76	-16.00	-2.35	-0.18	-2.40	-10.08	-54.76
Avarage		-37.46	-20.08	-2.04	-0.18	-2.43	-10.74	-57.54

Table 4.14. Glide docking results (receptor: 2JDR) for hits DRRR.62 hypothesis match (top 25 Results).

	CoCoCo ID	vdW	coul	lipo	esite	XP Hbond	XP GScore	Energy
1	5326362	-37.61	-24.95	-2.06	-0.16	-1.98	-11.39	-62.55
2	5341958	-50.46	-10.60	-1.90	-0.07	-1.97	-11.23	-61.06
3	5609932	-45.30	-21.06	-3.23	-0.08	-2.09	-11.11	-66.36
4	1120440	-35.23	-18.16	-2.95	-0.06	-1.99	-11.05	-53.39
5	1542071	-39.70	-19.74	-2.87	-0.08	-1.55	-10.77	-59.43
6	4454000	-43.56	-14.91	-1.58	-0.08	-1.86	-10.76	-58.47
7	4586703	-33.88	-16.18	-2.10	-0.06	-1.33	-10.10	-50.06
8	5331049	-37.43	-12.36	-1.52	-0.05	-1.48	-10.03	-49.79
9	5403837	-55.56	-7.81	-2.18	-0.03	-1.81	-9.91	-63.37
10	4364750	-38.87	-9.78	-3.26	-0.02	-1.87	-9.82	-48.65
11	4586818	-33.92	-15.83	-2.13	-0.08	-2.14	-9.73	-49.75
12	4774811	-50.04	-16.28	-3.49	-0.07	-1.09	-9.71	-66.32
13	4586815	-33.28	-16.26	-1.96	-0.07	-2.15	-9.71	-49.54
14	5356771	-41.35	-13.77	-1.52	-0.16	-1.40	-9.67	-55.12
15	5384569	-37.15	-12.01	-1.90	0.00	-1.60	-9.66	-49.16
16	5559431	-44.21	-12.21	-3.75	0.00	-1.28	-9.54	-56.42
17	6372717	-40.34	-7.01	-3.60	-0.01	-1.24	-9.42	-47.34
18	5326363	-35.72	-11.78	-1.96	-0.16	-2.09	-9.42	-47.50
19	1542071	-40.21	-14.75	-2.87	-0.08	-0.78	-9.41	-54.95
20	5270832	-37.07	-12.63	-2.39	-0.10	-2.13	-9.38	-49.70
21	6177256	-33.00	-14.82	-2.24	-0.10	-1.09	-9.34	-47.82
22	5657271	-48.83	-12.59	-3.88	-0.06	-0.45	-9.33	-61.42
23	5559432	-43.38	-13.72	-3.53	-0.06	-1.19	-9.29	-57.10
24	3789656	-47.56	-10.87	-1.99	0.00	-1.68	-9.23	-58.43
25	5427909	-36.21	-15.43	-1.27	0.00	-2.11	-9.11	-51.65
Average		-40.80	-14.22	-2.40	-0.07	-1.61	-9.93	-55.01

Two dimensional chemical structures of top 10 molecules based on Glide XP score and their vendors are listed in Table 4.15 and Table 4.16.

Table 4.15. 2D structures of top 10 Molecule (receptor: 2JDO, database: hits of DRRR.62 hypothesis match).

1	Chemical Formula: $C_{15}H_{15}N_6O_2S$ Vendor: ChemDiv 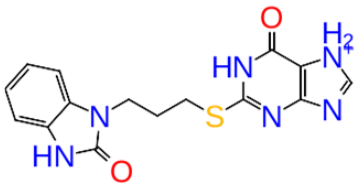	**2**	Chemical Formula: $C_{22}H_{29}N_5O$ Vendor: Enamine 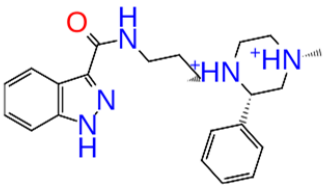
3	Chemical Formula: $C_{20}H_{22}N_6O_7$ Vendor: NCI 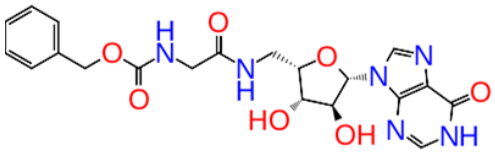	**4**	Chemical Formula: $C_{20}H_{23}N_4O_3$ Vendor: NCI 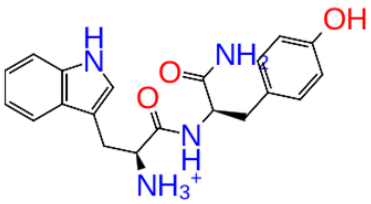
5	Chemical Formula: $C_{21}H_{24}N_3O_5$ Vendor: Enamine 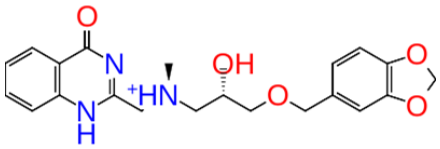	**6**	Chemical Formula: $C_{24}H_{32}N_3O$ Vendor: ChemBridge 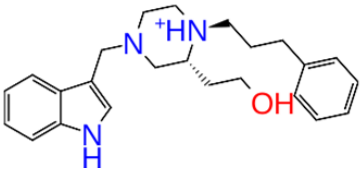
7	Chemical Formula: $C_{23}H_{30}N_3O_2$ Vendor: ChemBridge 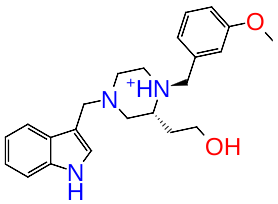	**8**	Chemical Formula: $C_{23}H_{28}N_4O_2$ Vendor: ChemBridge 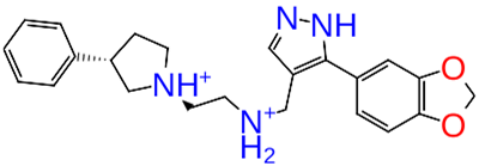

Table 4.15. 2D structures of top 10 Molecule (receptor: 2JDO, database: hits of DRRR.62 hypothesis match) (cont.).

9	Chemical Formula:	$C_{21}H_{29}N_3O_2$	**10**	Chemical Formula:	$C_{12}H_{11}N_8S_2$
	Vendor:	ChemBridge		Vendor:	NCI
	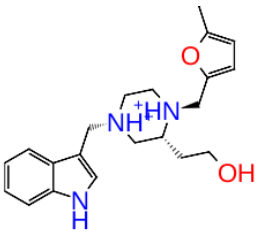			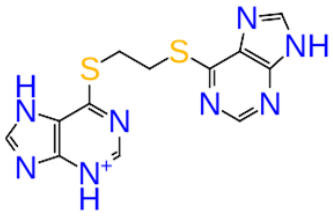	

Table 4.16. 2D structures of top 10 Molecule (receptor: 2JDR, database: hits of DRRR.62 hypothesis match).

1	Chemical Formula:	$C_{14}H_{15}N_8S_2$	**2**	Chemical Formula:	$C_{14}H_{17}N_{10}S_2$
	Vendor:	NCI		Vendor:	NCI
	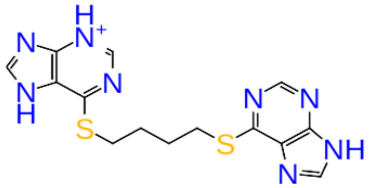			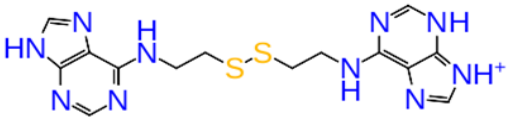	
3	Chemical Formula:	$C_{20}H_{23}N_4O_3$	**4**	Chemical Formula:	$C_{16}H_{17}N_4O_2$
	Vendor:	NCI		Vendor:	ChemBridge
	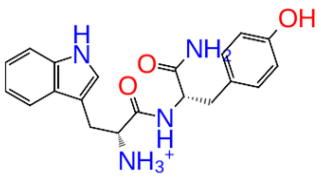			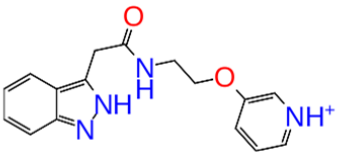	
5	Chemical Formula:	$C_{20}H_{25}N_5$	**6**	Chemical Formula:	$C_{14}H_{13}N_6O_3$
	Vendor:	ChemBridge		Vendor:	Enamine
	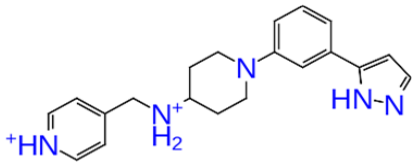			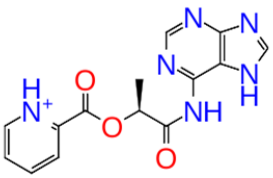	

Table 4.16. 2D structures of top 10 Molecule (receptor: 2JDR, database: hits of DRRR.62 hypothesis match) (cont.).

7	Chemical Formula: $C_{15}H_{19}N_7$ Vendor: Enamine 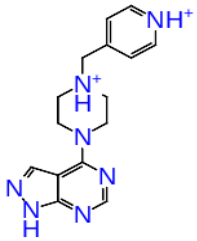	8	Chemical Formula: $C_{11}H_9N_8S_2$ Vendor: NCI 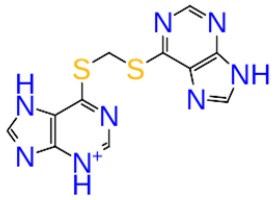
9	Chemical Formula: $C_{16}H_{16}N_6O_5$ Vendor: NCI 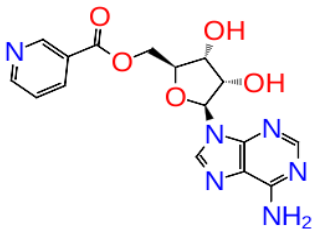	**10**	Chemical Formula: $C_{11}H_8N_8S_2$ Vendor: Enamine 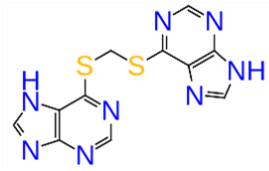

4.4. Post-Processing of Docking Results

4.4.1. Predicted ADME Properties

In order to predict absorption, distribution, metabolism, and excretion (ADME) properties of the molecules, QikProp module of the Maestro Suite was used. QikProp also allows a comparison of the results with the known drugs. Minimum and maximum values of molecular properties of 95% of the drugs are shown in the second rows of Table 4.17 to Table 4.20. Molecules with values outside the mentioned range were eliminated from further evaluation and the remaining molecules are listed in Table 4.17 and Table 4.18. In Table 4.17 and Table 4.18 molecular properties that make up Lipinski's rule of five [121] are also presented. It should be noted that the number of hydrogen donors and acceptors can be non-integer because QikProp evaluates the average value from a number of configurations. Number of violations to Lipinski's rule of five is shown in the last column in Table 4.17 and Table 4.18. Four molecules violate Lipinski's rule of five, (shown in bold in Table 4.17) 5611052, 5609932, 5717141, and 5403832 with rankings 3, 4, 13, and 24 respectively. Four molecules docked to 2JDR violate the Lipinski's rule of five (shown

in bold in Figure 4.18) 5609932, 5403837, 5559431, and 5559432 with rankings 3, 10, 17, and 24, respectively.

Table 4.17. Number of violations of Lipinski's rule of five (receptor: 2JDO, database: Hits of DRRR.62 hypothesis match).

	CoCoCo ID	**MW**	**LogP**	**donorHB**	**accptHB**	**Lipinski Violations**
	95% of drugs					
	MIN.	130.0	-2.0	0.0	2.0	
	MAX.	725.0	6.5	6.0	20.0	
1	2290040	342.38	1.25	3.00	7.00	0
2	4849420	377.49	2.70	1.00	6.50	0
3	5611052	458.43	-0.90	4.25	**14.35**	1
4	5609932	366.42	-0.09	**6.25**	6.00	1
5	3399013	397.43	1.47	2.00	10.40	0
6	1629090	377.53	3.49	2.00	5.70	0
7	1642127	379.50	2.90	2.00	6.45	0
8	1273283	390.48	3.03	2.00	6.00	0
9	1318556	353.46	2.67	2.00	6.20	0
10	5356769	330.39	1.35	2.00	7.00	0
11	1327900	355.50	2.81	2.00	5.70	0
12	4703230	318.38	3.42	1.00	5.00	0
13	5717141	**616.43**	-0.18	**7.00**	**14.05**	3
14	5242298	404.51	3.17	1.00	7.25	0
15	5658764	323.35	1.41	3.50	6.00	0
16	5331047	316.36	1.17	2.00	7.00	0
17	5657276	422.46	2.94	4.25	4.75	0
18	5581393	401.46	1.68	3.00	8.95	0
19	5657271	440.45	3.33	4.25	4.75	0
20	370431	337.40	3.39	1.00	4.75	0
21	4586762	295.35	1.49	1.00	6.50	0
22	5331049	316.36	1.26	2.00	7.00	0
23	1573035	295.35	1.54	1.00	7.00	0
24	5403832	372.34	-0.828	4.00	**12.60**	1
25	4849433	377.49	2.958	1.00	6.50	0

Table 4.18. Number of violations of Lipinski's rule of five (receptor: 2JDR, database: Hits of DRRR.62 hypothesis match).

	CoCoCo ID	**MW**	**LogP**	**donorHB**	**accptHB**	**Lipinski Violations**
	95% of drugs					
	MIN.	130.0	-2.0	0.0	2.0	
	MAX.	725.0	6.5	6.0	20.0	
1	5326362	358.44	2.10	2.00	7.00	0
2	5341958	388.47	1.37	4.00	10.00	0
3	5609932	366.42	-0.24	**6.25**	6.00	1
4	1120440	296.33	1.94	1.00	4.75	0
5	1542071	333.44	3.44	2.00	5.00	0
6	4454000	312.29	0.55	2.00	9.00	0
7	4586703	295.35	1.17	1.00	7.00	0
8	5331049	316.36	1.22	2.00	7.00	0
9	5403837	372.34	-0.58	4.00	**12.60**	1
10	4364750	323.35	3.32	1.50	3.25	0
11	4586818	295.35	1.20	1.00	7.00	0
12	4774811	393.49	3.46	1.50	4.00	0
13	4586815	295.35	1.20	1.00	7.00	0
14	5356771	330.39	1.44	2.00	7.00	0
15	5384569	314.36	1.48	3.00	5.50	0
16	5559431	390.44	0.32	**5.25**	4.75	1
17	6372717	333.39	1.37	4.00	3.50	0
18	5326363	358.44	2.21	2.00	7.00	0
19	1542071	333.43	3.18	2.00	5.00	0
21	6177256	290.33	2.50	2.00	5.00	0
22	5657271	440.45	3.25	4.25	4.75	0
23	5559432	390.44	0.13	**5.25**	4.75	1
24	3789656	374.43	1.57	3.00	7.00	0
25	5427909	318.35	0.07	4.00	8.50	0

Some of the other properties evaluated by QikProp were tabulated in Table 4.19 and Table 4.20. Total solvent accessible surface area (SASA) and its components are shown in Table 4.19. FOSA is the hydrophobic component of the SASA, FISA is the hydrophilic component, PISA is the π (carbon and attached hydrogen) component, and WPSA is the weakly polar component of the SASA. Sum of the mentioned components gives the total

SASA. LogS in Table 4.19 and 4.20 are the predicted aqueous solubility, where S is the solute equilibrium concentration in saturated solution. PCaco, is the predicted permeability of Caco2 cell, which is a good model for gut-blood barrier permeability. Number of stars (#stars) shows the drug likeness according to QikProp criteria and it ranges between 0 and 5. A more drug-like molecule has fewer stars. Molecules, that have star/stars and are therefore eliminated, are shown in bold in Table 4.19 and 4.20. As it is seen from Table 4.19 and Table 4.20, in general, docking with 2JDO yields higher SASA values at around 637.3 while the SASA values for docking with 2JDR at around 595.32. This means larger molecules can fit into the binding pocket in 2JDO structure. This is not surprising since residue Phe163 is extended out from the binding site and this conformation leaves more space to the docked poses. Contribution of WPSA term to SASA is very low and PISA term is almost the same for both of the cases (average values were considered). However, it was observed that contribution of FOSA is higher for the docking with 2JDO (27.6% of SASA for 2JDO and 18.9% of SASA for 2JDR) and contribution of FISA is higher for the docking to 2JDR (24.4% of SASA for 2JDO and 30.0% of SASA for 2JDR). Due to the hydrophobic nature of residue Phe163, when it is turned in towards the active site (in the 2JDR structure) it could favor the hydrophobic interactions and it could be expected to give higher FOSA values; however, FOSA values in the case of 2JDR are lower and this shows that hydrophobic interactions in the binding site exceeds the effect of conformation of Phe163.

Table 4.19. Pharmacokinetic properties of top 25 molecules (receptor: 2JDO, database: hits of DRRR.62 hypothesis match).

	SASA	**FOSA**	**FISA**	**PISA**	**WPSA**	**LogS**	**PCaco**	**%Human Oral Absorption**	**#stars**
Min.	300.0	0.0	7.0	0.0	0.0	-6.5	<25 poor	<25% high	
Max.	1000.0	750.0	330.0	450.0	175.0	0.5	>500 great	>80% high	
1	**558.39**	**82.82**	**222.76**	**208.23**	**44.58**	**-3.48**	**76.48**	**67.96**	**1**
2	629.36	216.63	118.03	294.70	0	-2.12	46.82	72.64	0
3	**803.53**	**180.72**	**334.40**	**288.41**	**0**	**-3.40**	**3.44**	**18.30**	**5**
4	**607.10**	**50.46**	**239.07**	**317.57**	**0**	**-0.19**	**5.30**	**26.41**	**1**
5	643.44	244.43	107.55	291.46	0	-1.76	235.99	78.04	0

Table 4.19. Pharmacokinetic properties of top 25 molecules (receptor: 2JDO, database: hits of DRRR.62 hypothesis match) (cont).

	SASA	FOSA	FISA	PISA	WPSA	LogS	PCaco	%Human Oral Absorption	#stars
6	691.16	230.72	84.81	375.63	0	-2.79	96.71	82.92	0
7	656.88	285.50	69.95	301.44	0	-2.13	133.79	81.99	0
8	663.20	242.34	78.45	342.41	0	-2.87	111.12	81.32	0
9	636.37	308.70	66.73	260.93	0	-2.03	143.51	81.17	0
10	521.54	74.52	174.98	239.08	32.96	-2.78	217.07	76.70	0
11	612.78	191.29	73.16	293.08	55.25	-2.02	124.71	80.91	0
12	607.96	188.87	104.61	314.48	0	-5.38	1009.09	100.00	0
13	**793.86**	**198.20**	**301.60**	**181.26**	**112.79**	**-3.36**	**8.83**	**3.97**	**2**
14	759.49	335.35	116.95	307.19	0	-3.79	47.94	75.61	0
15	584.20	33.16	189.28	361.76	0	-2.47	39.61	63.79	0
16	523.76	39.15	187.30	240.60	56.71	-2.97	165.87	73.52	0
17	695.43	145.29	172.99	330.24	46.90	-3.39	34.22	71.63	0
18	720.15	388.16	191.79	140.21	0	-3.44	37.51	64.98	0
19	713.23	150.54	160.83	308.14	93.71	-3.97	46.50	76.31	0
20	590.45	146.74	68.09	353.17	22.45	-3.71	558.64	95.99	0
21	551.50	166.34	127.17	257.99	0	-2.50	153.76	74.80	0
22	533.48	34.61	187.30	247.47	64.10	-3.09	165.87	74.05	0
23	554.73	167.10	98.25	289.38	0	-2.38	289.12	80.03	0
24	627.85	68.43	295.58	263.83	0	-2.95	15.59	30.49	0
25	652.83	231.00	115.96	305.87	0	-2.53	48.99	74.51	0
Avg.	637.31	176.04	155.50	284.58	21.18	-2.86	152.66	68.32	0.36

Table 4.20. Pharmacokinetic properties of top 25 molecules (receptor: 2JDR, database: hits of DRRR.62 hypothesis match).

	SASA	FOSA	FISA	PISA	WPSA	PCaco	logS	%Human Oral Absorption	#stars
Max. Min.	300.0 1000.0	0.0 750.0	7.0 330.0	0.0 450.0	0.0 175.0	<25 poor >500 great	-6.5 0.5	<25% high >80% high	
1	587.72	134.13	168.47	234.05	51.08	250.20	-3.65	82.16	0
2	621.92	143.30	168.75	226.01	83.87	248.69	-3.28	77.81	0

Table 4.20. Pharmacokinetic properties of top 25 molecules (receptor: 2JDR, database: hits of DRRR.62 hypothesis match) (cont).

	SASA	FOSA	FISA	PISA	WPSA	PCaco	logS	%Human Oral Absorption	#stars
3	**615.28**	**71.38**	**250.16**	**293.74**	**0**	**3.79**	**-0.14**	**22.95**	**1**
4	550.85	95.58	140.63	314.64	0	261.03	-2.63	81.58	0
5	660.37	175.99	102.41	381.98	0	264.03	-4.67	90.45	0
6	551.24	87.39	192.43	271.41	0	148.29	-2.80	69.02	0
7	552.13	157.38	139.10	255.65	0	118.49	-2.34	70.92	0
8	536.80	39.08	187.52	253.40	56.81	165.08	-3.11	73.77	0
9	642.06	96.36	279.04	266.66	0	22.38	-3.13	34.77	0
10	577.51	41.61	191.46	344.45	0	151.46	-4.57	85.38	0
11	550.44	154.41	138.52	257.51	0	120.00	-2.31	71.21	0
12	675.61	221.50	162.74	291.37	0	36.12	-3.31	75.05	0
13	553.40	156.23	138.69	258.48	0	119.56	-2.36	71.15	0
14	541.19	71.22	182.24	238.04	49.68	185.23	-3.08	75.94	0
15	576.71	72.65	164.68	322.66	16.72	135.67	-2.72	73.76	0
16	628.33	78.23	196.71	353.39	0	5.59	-2.64	29.23	0
17	570.72	51.63	133.39	385.71	0	34.00	-3.29	62.37	0
18	618.62	121.98	179.26	254.28	63.10	197.68	-4.21	80.96	0
19	630.46	176.82	103.07	350.58	0	260.26	-4.16	88.80	0
20	585.48	90.15	247.07	247.26	0.99	44.97	-3.28	58.70	0
21	556.80	52.92	128.41	375.47	0	600.04	-3.97	91.34	0
22	744.58	176.39	173.27	337.50	57.41	44.58	-4.76	75.48	0
23	635.64	74.74	223.43	337.46	0	3.31	-2.87	24.08	0
24	616.87	189.00	237.18	136.13	54.55	55.81	-4.35	67.39	0
25	**543.04**	**85.98**	**236.70**	**218.80**	**1.57**	**56.40**	**-2.61**	**58.72**	**1**
Avg.	596.95	112.64	178.61	288.27	17.43	141.31	-3.21	67.72	0.08

4.4.2. Strain Energy Calculations

As a post-processing step, strain energies of docked molecules were calculated by using *strain re-dock* utility of Schrodinger Suite. Results of this step are tabulated in Table 4.21 and Table 4.22. Strain energy is the difference between the bound energy and free energy of the molecule. Strain penalty was applied to Glide docking scores for the

molecules which have higher strain energy than 4 kcal/mol. Revised scores are also presented in Table 4.21 and Table 4.22. Rows of molecules that have strain energy higher than 10 kcal/mol are shown in bold in Table 4.21 and Table 4.22 and these molecules were eliminated from further evaluation.

Table 4.21. Strain Energy (receptor: 2JDO).

	bound (kcal/mol)	**free (kcal/mol)**	**strain (kcal/mol)**	**strain penalty**	**strain docking score**
1	62.774	54.457	8.317	1.079	-11.006
2	37.497	29.878	7.620	0.905	-10.892
3	50.379	44.866	5.513	0.378	-11.235
4	8.496	4.320	4.176	0.044	-11.362
5	45.042	37.257	7.785	0.946	-10.431
6	32.590	27.604	4.987	0.247	-11.126
7	31.485	25.680	5.805	0.451	-10.695
8	**75.963**	**50.731**	**25.232**	**5.308**	**-5.763**
9	27.670	17.772	9.898	1.475	-9.439
10	9.116	4.729	4.388	0.097	-10.674
11	23.881	18.397	5.485	0.371	-10.190
12	36.690	35.015	1.675	0.000	-10.550
13	43.807	36.478	7.329	0.832	-9.682
14	38.159	37.082	1.077	0.000	-10.459
15	**19.392**	**9.347**	**10.044**	**1.511**	**-8.931**
16	11.488	7.601	3.887	0.000	-10.427
17	8.537	2.241	6.295	0.574	-9.838
18	48.233	43.399	4.834	0.208	-10.081
19	10.789	2.206	8.583	1.146	-9.105
20	**39.173**	**28.760**	**10.413**	**1.603**	**-8.628**
21	34.155	31.104	3.051	0.000	-10.182
22	8.842	8.586	0.256	0.000	-10.152
23	41.152	39.672	1.480	0.000	-10.144
24	46.124	38.254	7.870	0.967	-9.169
25	33.607	31.603	2.003	0.000	-10.076

Table 4.22. Strain Energy (receptor: 2JDR).

	bound (kcal/mol)	**free (kcal/mol)**	**strain (kcal/mol)**	**strain penalty**	**strain docking score**
1	9.974	9.198	0.777	0.000	-11.387
2	**31.454**	**18.207**	**13.247**	**2.312**	**-8.922**
3	15.367	8.714	6.653	0.663	-10.451
4	40.896	31.993	8.903	1.226	-9.822
5	**65.412**	**32.844**	**32.568**	**7.142**	**-3.623**
6	23.111	18.060	5.050	0.263	-10.498
7	34.305	30.455	3.850	0.000	-10.095
8	10.782	7.980	2.801	0.000	-10.030
9	44.574	36.659	7.915	0.979	-8.928
10	19.010	15.878	3.133	0.000	-9.817
11	36.198	30.236	5.963	0.491	-9.239
12	29.044	25.291	3.753	0.000	-9.710
13	36.426	30.236	6.190	0.548	-9.158
14	10.642	5.471	5.172	0.293	-9.372
15	18.082	16.819	1.263	0.000	-9.662
16	8.948	2.017	6.931	0.733	-8.802
17	8.431	6.966	1.465	0.000	-9.420
18	12.019	7.970	4.050	0.012	-9.407
19	35.529	32.850	2.680	0.000	-9.411
20	**27.872**	**9.574**	**18.298**	**3.575**	**-5.804**
21	20.135	19.504	0.631	0.000	-9.343
22	4.942	1.978	2.963	0.000	-9.326
23	0.411	-0.418	0.829	0.000	-9.287
24	24.165	23.599	0.566	0.000	-9.231
25	19.366	14.420	4.946	0.237	-8.871

4.4.3. Binding Free Energy Calculation

MM-GBSA calculations were performed to improve the docking scoring. Molecules were re-scored with MM-GBSA method. Binding free energies are tabulated in Table 4.23. MM-GBSA approach gives the binding free energy between the receptor and the ligand. Figure 4.27 shows the graphical view of how MM-GBSA (ΔG bind) values fit into GScore values. Squared correlation coefficients of linear regression were found as 0.0404 for

2JDO and 0.1175 for 2JDR. Thus, no correlation was found between XP GScore and MM-GBSA values.

In literature, there are cases where binding free energy (ΔG bind) yields more reliable results for predicting affinity [122–124], although opposite cases may also exist [125, 126]. Thus, success of re-scoring with Prime MM-GBSA is case-dependent and this approach should be used with caution. For this reason, enrichment studies was carried out (Section 4.5.4), and proposed molecules were selected according to outcome of the enrichment study.

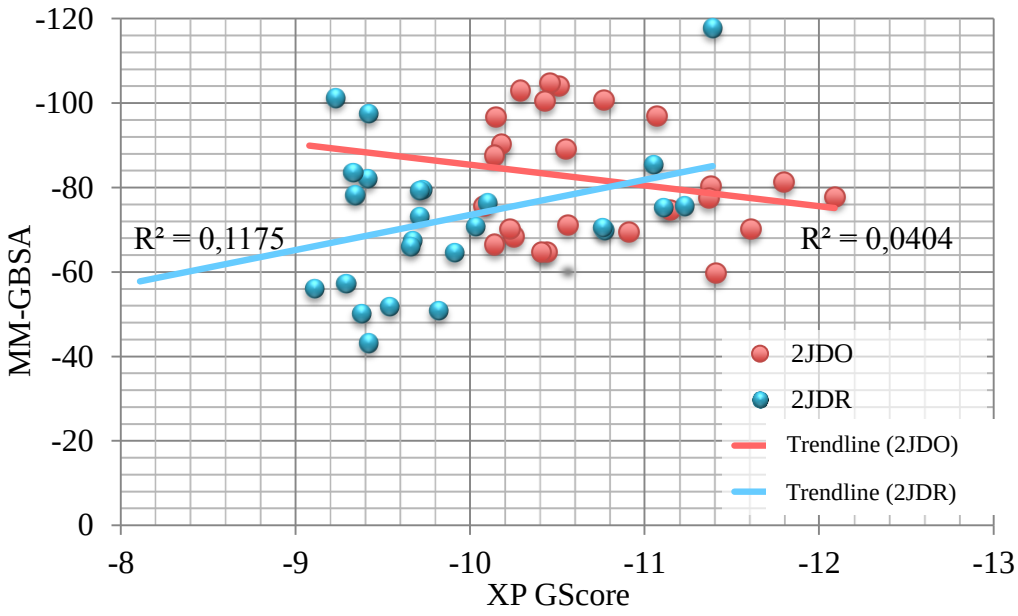

Figure 4.27. Correlation between MM-GBSA and XP GScore.

Table 4.23. Prime MM-GBSA rescoring.

Rank	CoCoCo ID (2JDO)	MM-GBSA (2JDO)	CoCoCo ID (2JDR)	MM-GBSA (2JDR)
1	2290040	-77.79	5326362	-117.71
2	4849420	-81.32	5341958	-75.56
3	5611052	-70.14	5609932	-75.09
4	5609932	-59.69	1120440	-85.41
5	3399013	-80.34	1542071	-69.9
6	1629090	-77.52	4454000	-70.53
7	1642127	-74.72	4586703	-76.23
8	1273283	-96.89	5331049	-70.66

Table 4.23. Prime MM-GBSA rescoring (cont).

Rank	CoCoCo ID (2JDO)	MM-GBSA (2JDO)	CoCoCo ID (2JDR)	MM-GBSA (2JDR)
9	1318556	-69.52	5403837	-64.46
10	5356769	-100.64	4364750	-50.76
11	1327900	-71.07	4586818	-79.46
12	4703230	-89.08	4774811	-73.08
13	5717141	-103.97	4586815	-79.26
14	5242298	-104.73	5356771	-67.28
15	5658764	-64.67	5384569	-66.03
16	5331047	-100.46	5559431	-51.86
17	5657276	-64.77	6372717	-43.11
18	5581393	-102.93	5326363	-97.55
19	5657271	-68.38	1542071	-82.08
20	370431	-70.16	5270832	-50.09
21	4586762	-90.21	6177256	-78.15
22	5331049	-96.62	5657271	-83.46
23	1573035	-87.53	5559432	-57.32
24	5403832	-66.46	3789656	-101.11
25	4849433	-75.65	5427909	-56.04

4.4.4. Enrichment Study

Schrodinger decoy set [85] was used for enrichment calculations. It consists of 1000 drug-like compounds with an average molecular weight of 400 Daltons. Active set that was used in enrichment is composed of 9 co-crystalized AKT-2 kinase inhibitors. For enrichment analysis, Glide XP docking with target 2JDO was performed. Input ligand file consists of 1009 (1000 from decoy set and 9 from active set) compounds.

Although enrichment study is generally used for comparison of different docking and scoring methods, in this research it was used to evaluate the performance of Glide molecular docking and scoring protocol for target AKT-2 kinase protein and to estimate whether Prime MM-GBSA re-scoring could enhance the Glide docking score.

Receiver Operating Characteristic (ROC) curve for XP GScore and MM-GBSA are indicated in Figure 4.28. Area under the ROC (AU-ROC) curve was calculated by

Schrodinger docking post-processing scripts of enrichment calculator [127] and AU-ROC value was found as 0.93 for XP GScore. AU-ROC values higher than 0.9 is classified as excellent according to Hevener et al [116]. Then it can be stated that Glide is a reliable docking and scoring procedure to discriminate actives from inactives. Enrichment study was also conducted to evaluate Prime MM-GBSA re-scoring. AU-ROC value for this case was considerably decreased and found as 0.85. This indicates Glide XP scoring is a more reliable tool to predict activity and ranking of molecules. As a result, proposed molecules were chosen by XP GScore ranking. Detailed ranking information is summarized in Table 4.24 and Table 4.25.

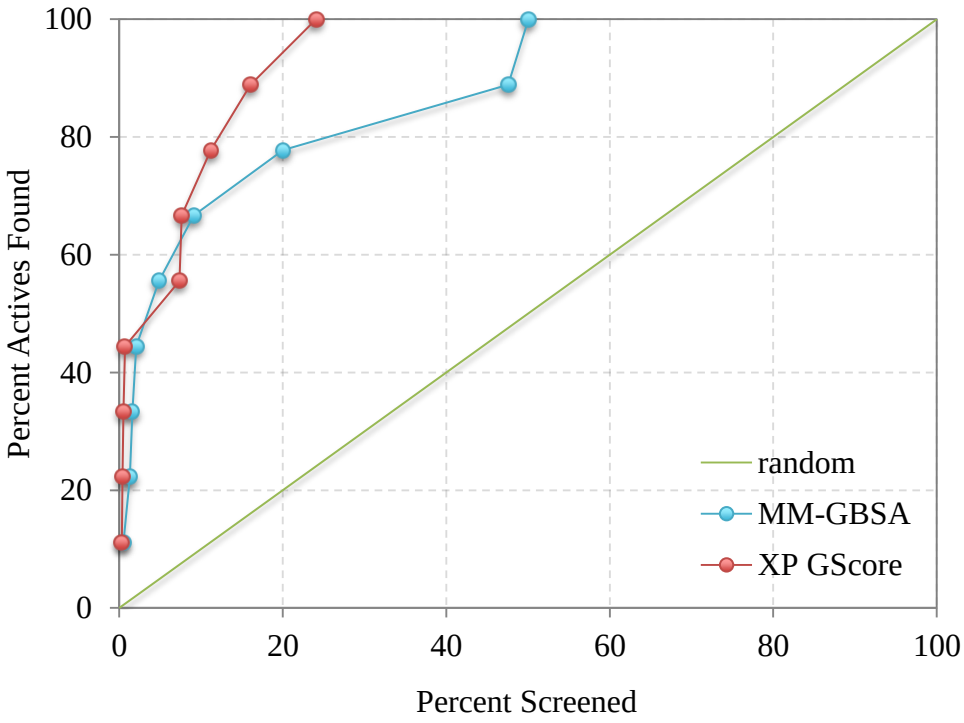

Figure 4.28. ROC curves for MM-GBSA and XP GScore.

Ranking of the actives in the decoy set is represented in Table 4.24. All known actives were ranked in the top 243 according to Glide XP scores, whereas this ranking increased to 505 for ΔG bind values.

Table 4.24. Rank of native ligands in the decoy set with respect to XP GScore and MM-GBSA.

	XP GScore Rank	**MM-GBSA Rank**
G93	243	13
G95	7	202
G96	77	16
G98	113	5
GVP	162	505
I5S	5	49
L20	4	21
X37	74	480
X39	3	92

Number and percentage of actives in the 1%, 2%, 5%, 10%, and 20% of the decoy set are indicated in Table 4.25. Five actives (55.6% of actives) were identified within the top 1% of the decoy set for XP Gsore ranking, and number of actives reduced to one (11.1% of actives) for MM-GBSA ranking.

Finally, enrichment studies suggest that in the case of AKT-2 protein, Prime MM-GBSA (ΔG bind) re-scoring did not enhance the docking results, and Glide XP scoring is superior to MM-GBSA.

Table 4.25. Number and percentage of actives.

Percentage of Decoy Set						
		1%	**2%**	**5%**	**10%**	**20%**
Number of Actives	**XP GScore**	5	5	5	6	8
	DG bind	1	4	5	6	7
Percentage of Actives	**XP GScore**	55.6 %	55.6 %	55.6 %	66.7 %	88.9 %
	DG bind	11.1 %	44.4 %	55.6 %	66.7 %	77.8 %

4.4.5. Discarded Molecules According to Post-processing Results

In summary, the molecules that have higher than 10 kcal/mol strain energy and that are not drug-like according to Lipinski's rule of five and QikProp (# stars>0) from XP docking with receptor 2JDO were eliminated from further analysis. These molecules (XP rank_CoCoCo ID) are 1_2290040 (rank_CoCoCo ID), 3_5611052, 4_5609932, 8_1273283, 13_5717141, 15_5658764, 20_370431, and 24_5403832 for 2JDO, and 2_5341958, 3_5609932, 5_1542071, 9_5403837, 16_5559431, 20_5270832, 23_5559432, and 25_5427909 for receptor 2JDR.

4.5. Binding Mode Analysis of Proposed Molecules

Proposed molecules were selected based on high docking score from the remaining molecules after elimination by calculating the strain energy and examining the ADME properties. Five molecules were proposed for each docking result (2JDO and 2JDR). Proposed 10 molecules are listed in Table 4.26 with XP GScore ranking, CoCoCo ID and IUPAC name.

Table 4.26. Names and identifiers of proposed 10 molecule.

Docking Result	Proposed Molecule	XP Ranking	CoCoCo ID	IUPAC Name
2JDO	**O1**	2	4849420	(1S,3S,4R)-4-[3-(1H-indazol-3-ylformamido)propyl]-1-methyl-3-phenylpiperazine-1,4-diium
	O2	5	3399013	(R)-[(2S)-3-(2H-1,3-benzodioxol-5-ylmethoxy)-2-hydroxypropyl](methyl)[(4-oxo-1,4-dihydroquinazolin-2-yl)methyl]azanium
	O3	6	1629090	(1R,2R)-2-(2-hydroxyethyl)-4-(1H-indol-3-ylmethyl)-1-(3-phenylpropyl)piperazin-1-ium
	O4	7	1642127	(1R,2R)-2-(2-hydroxyethyl)-4-(1H-indol-3-ylmethyl)-1-[(3-methoxyphenyl)methyl]piperazin-1-ium
	O5	9	1318556	(1S,2R,4R)-2-(2-hydroxyethyl)-4-(1H-indol-3-ylmethyl)-1-[(5-methylfuran-2-yl)methyl]piperazine-1,4-diium

Table 4.26. Names and identifiers of proposed 10 molecule (cont).

Docking Result	Proposed Molecule	XP Ranking	CoCoCo ID	IUPAC Name
2JDR	**R1**	1	5326362	6-{[4-(9H-purin-6-ylsulfanyl)butyl]sulfanyl}-7H-purin-3-ium
	R2	4	1120440	3-{2-[2-(2H-indazol-3-yl)acetamido]ethoxy}pyridin-1-ium
	R3	6	4454000	2-{[(1S)-1-[(7H-purin-6-yl)carbamoyl]ethoxy]carbonyl}pyridin-1-ium
	R4	7	4586703	4-{1H-pyrazolo[3,4-d]pyrimidin-4-yl}-1-(pyridin-1-ium-4-ylmethyl)piperazin-1-ium
	R5	8	5331049	6-{[(9H-purin-6-ylsulfanyl)methyl]sulfanyl}-7H-purin-3-ium

4.5.1. Selectivity Studies

Hinge region H-bond constraint (Ala232 or Glu230) was imposed to increase the success rate of the docking results. However, H-bond interactions in the hinge region are not specific to AKT-2 kinase protein and this may result in nonselective hits. Therefore, to assess the effect of the applied constraint, proposed molecules are re-docked with other protein kinase structures.

Protein Kinase A (PKA) has high degree of sequence identity to PKB-β, namely 45% sequence identity of kinase domains and 80% sequence identity of ATP binding site [71] and PKA also favors the hinge region H-bond interactions. In addition, highly homologous isoforms of AKT-2 share up to 90% sequence identity in the catalytic domain. These similarities put forward the problem of finding PKB-β selective inhibitors.

In order to test selectivity, the top five molecules with the best Glide XP score were docked to PKA and PKB-α/AKT-1 (crystal structure of PKB-γ/AKT-3is not available in PDB). To compare results of docking with receptor of 2JDO (PKB-β+I5S) with docking to PKA, PDB file that has PKA in complex with ligand I5S (PDB code: 2JDT) was used for docking experiment. PKB-α in complex with ligand I5S is not available in PDB, therefore an arbitrary complex structure of PKB-α was used. Docking experiments with PKA and PKB-α were done without any constraints and in the protein preparation step all waters were deleted. XP GScores of docking to PKA, PKB-α, and PKB-β are comparatively

shown in Table 4.27 (Scores for PKB-β are the same as in Table 4.13). The XP scores for the five proposed ligands are lower with PKB-β compared with those of PKA and PKB-α suggesting that the five molecules bind more selectively to PKB-β. In relation to difference between the XP GScores, it can be said that the most PKB-β selective molecule is O1 and the least one is O2.

Co-crystallized ligand I5S was re-docked with extra precision mode to its native protein 2JDO with the same constraints used in Glide XP docking in Section 4.3.5 and docking resulted in a score of -11.693 kcal/mol. This result suggests that molecules O1-O5 may have similar degrees of affinity to 2JDO as the native ligand I5S.

Table 4.27. Comparison of Glide XP scores of docking with receptor PKA, PKB-α and PKB-β (2JDO) for selected five molecules.

Proposed Molecule	**XP GScore**		
	2JDO(PKB-β+I5S)	**2JDT (PKA+I5S)**	**3OCB (PKB-α+XM1)**
O1	-11.797	-6.832	-5.217
O2	-11.377	-9.215	-7.023
O3	-11.373	-7.506	-7.796
O4	-11.146	-7.374	-7.894
O5	-10.913	-7.321	-6.265

The Glide XP docking results with receptor 2JDR (PKB-β+L20) were also compared with PKA and PKB-α. PDB file that has PKA in complex with ligand L20 was used for this docking experiment, which was done in Glide XP mode with no constraint and by deleting all waters in the protein preparation step. PKB-α in complex with ligand I5S is not available in PDB, therefore an arbitrary complex structure of PKB-α was used in docking experiments with the same parameter that was used for PKA docking. XP GScores of docking experiments with receptors PKA and PKB-α were tabulated in Table 4.28 in comparison with those of PKB-β (Scores are same as Table 4.14).

Co-crystallized ligand, L20, was also re-docked to its native protein 2JDR. Glide XP docking with the same constraints resulted in a score of -12.772 kcal/mol. Although all proposed molecules have relatively high scores, it is seen in Table 4.28 that none of the

proposed molecules can achieve a score as high as that of the native ligand. This may be a result of the U-shaped binding mode of L20, which is mentioned in Section 4.1.

Table 4.28. Comparison of Glide XP scores of docking with receptor PKA, PKB-α and PKB-β (2JDR) for selected five molecules.

Proposed Molecule	**XP GScore**		
	2JDR (PKB-β+L20)	**2JDV (PKA+L20)**	**3OCB (PKB-α+XM1)**
R1	-11.387	-10.530	-7.550
R2	-11.047	-8.665	-5.668
R3	-10.760	-8.772	-4.996
R4	-10.095	-7.152	-6.619
R5	-10.030	-9.799	-7.905

4.5.2. Interactions of Proposed Ligands with PKB- β (2JDO)

Molecules listed in Table 4.27 are analyzed in more detail to obtain more information about their interactions with protein AKT-2 summarized in Figure 4.29 to Figure 4.33. The 3D binding poses of the proposed molecules for 2JDO, O1-O5, along with hydrogen bond interactions are represented in Appendix B (Figure B.1).

The molecule O1 with chemical formula $C_{22}H_{29}N_5O$ has 57 atoms and 60 bonds of which 6 are rotatable. Figure 4.29 shows the interactions between O1 and AKT-2. Indazole ring of molecule O1 makes a H-bond with Glu230 backbone. Indazole ring is also in hydrophobic contact with residues Met282, Phe439, Try231, Ala232, Ala179, Leu158, and Val 166. Positively charged groups of the molecule also make H-bonds with residues Glu236 and Asp293 in the ribose binding region. Phenyl group of the molecule makes π-cation interaction with conserved Lys181 residue.

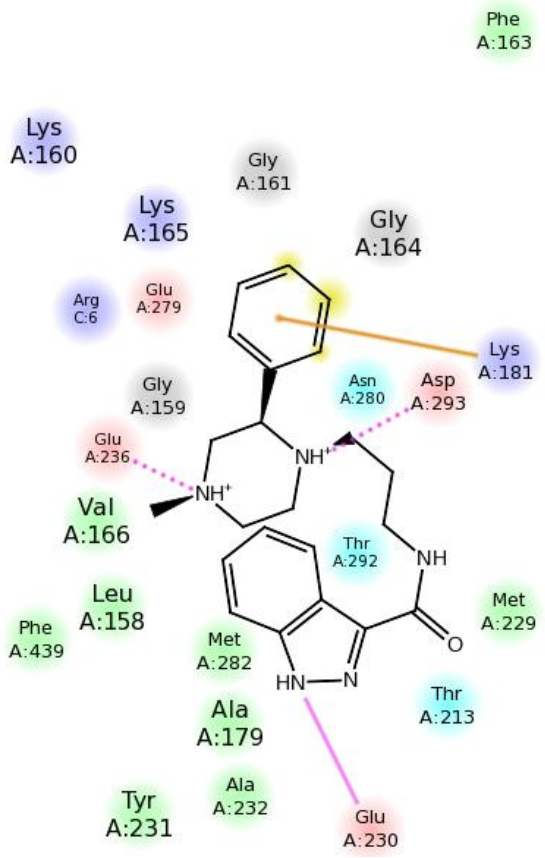

Figure 4.29. Interaction diagram between O1 and protein (receptor:2JDO).

The molecule O2 with chemical formula $C_{21}H_{24}N_3O_5$ has 53 atoms and 56 bonds of which 8 are rotatable. Figure 4.30 shows the interactions between the molecule and the protein AKT-2. 1,3-benzodioxole of O2 makes a H-bond with the backbone of hinge region residue Ala232. In the acidic, ribose binding region of the protein, Glu279 makes a H-bond with alkynol –OH group of the molecule, and Asp293 makes a H-bond with the two amine groups of the molecule. Benzodioxole group is in hydrophobic contact with residues Val166, Leu158, Ala179, and Met282. 1H-Quinazolin-4-one makes π-cation interaction with conserved Lys181 residue.

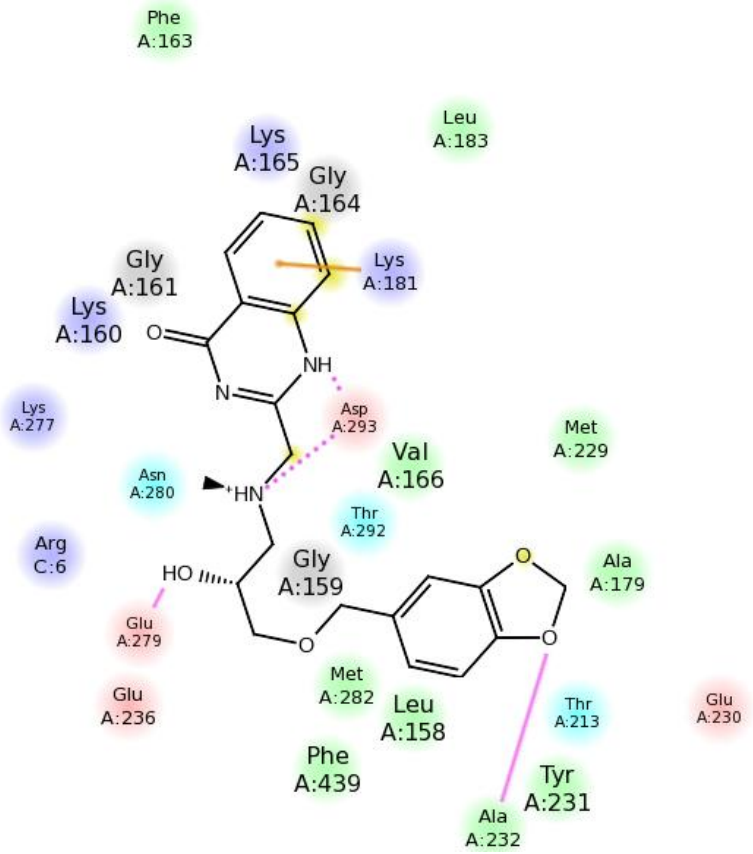

Figure 4.30. Interaction diagram between O2 and protein (receptor:2JDO).

The molecule O3 with chemical formula $C_{24}H_{32}N_3O$ has 60 atoms and 63 bonds of which 8 are rotatable. Figure 4.31 shows the interactions between the molecule and the protein AKT-2. Indole ring of O3 forms a H-bond with backbone of hinge region residue of Glu230 of AKT-2, and it is in hydrophobic contact with residues Met282, Val166, Phe439, Leu158, Ala179, and Tyr231. In the acidic, ribose binding region of the protein, Glu279 makes a H-bond with alkynol –OH group of the molecule, and Asp293 make a H-bond with ammonium of the molecule. Phenyl group makes π-cation interaction with conserved Lys181 residue.

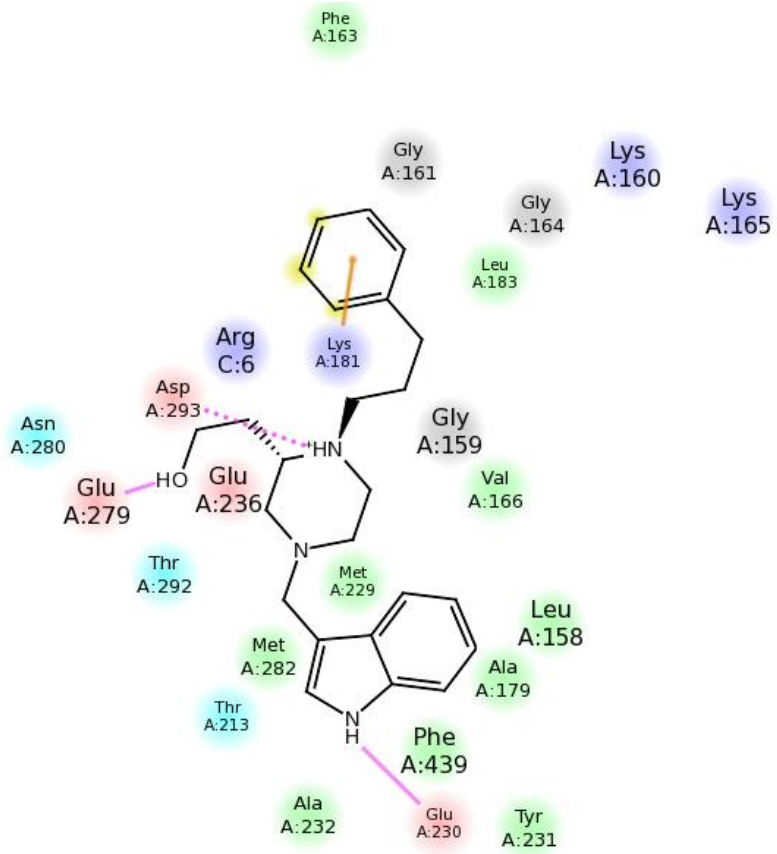

Figure 4.31. Interaction diagram between O3 and protein (receptor:2JDO).

The molecule O4 with chemical formula $C_{23}H_{30}N_3O_2$ has 58 atoms and 61 bonds of which 7 are rotatable. Figure 4.32 shows the interactions between the molecule and the protein AKT-2. Chemical structure of O4 is similar to that of molecule O3. Indole ring of O4 forms a H-bond with the backbone of hinge region residue Glu230 of AKT-2, and it is in hydrophobic contact with residues Met282, Ala179, Met229, Leu158, Thr231, and Phe439. In the acidic, ribose binding region of the protein, Glu236 makes a H-bond with alkynol –OH group of the molecule, and Asp293 makes a H-bond with ammonium of the molecule.

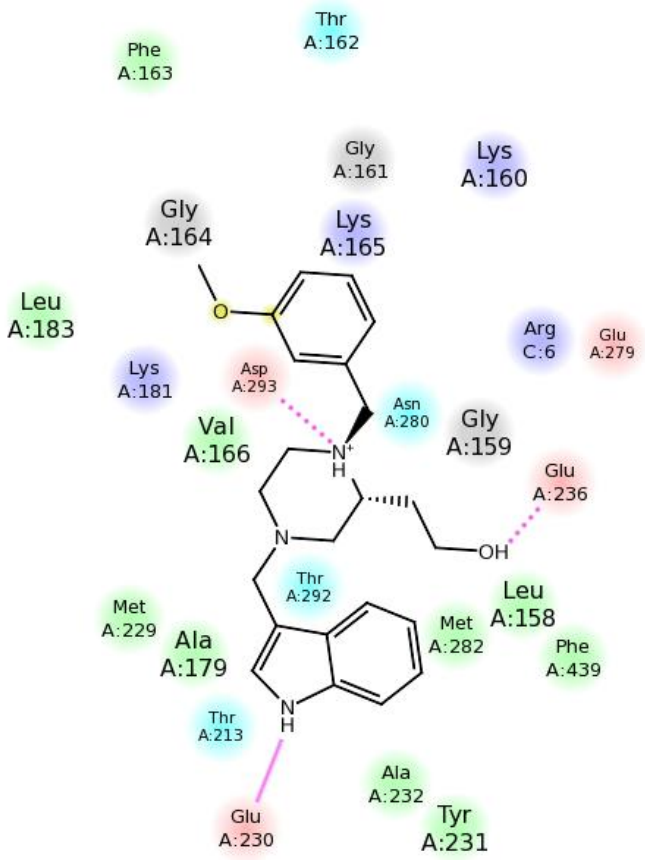

Figure 4.32. Interaction diagram between O4 and protein (receptor:2JDO).

The molecule O5 with chemical formula $C_{21}H_{29}N_3O_2$ has 55 atoms and 58 bonds of which 6 are rotatable. Figure 4.33 shows the interactions between the molecule and the protein AKT-2. Indole ring and ammonium group of O5 is similar to those of molecules O3 and O4. Indole ring of O5 forms a H-bond with the backbone of hinge region residue of Glu230 of AKT-2, and it is in hydrophobic contact with residues Met282, Ala179, Met229, Leu158, Thr231, and Phe439. In the acidic, ribose binding region of the protein, Glu236 makes a H-bond with alkynol –OH group of the molecule, and Asp293 makes a H-bond with ammonium of the molecule.

Figure 4.34a shows 2D structures of O1-O5 and the native ligand of 2JDO, I5S. 3D alignment of O1-O5 in the active site is represented in Figure 4.34b.

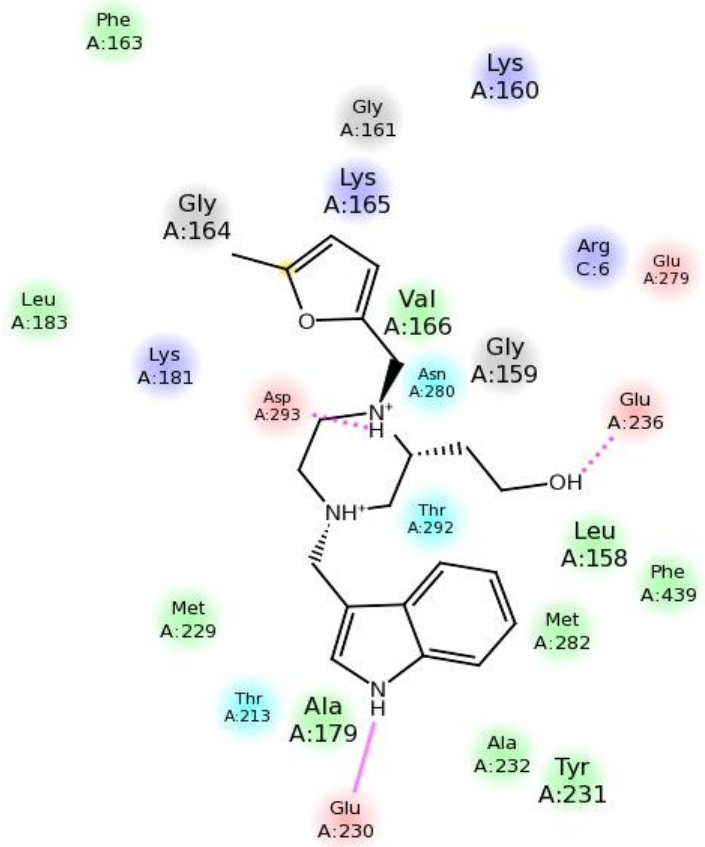

Figure 4.33. Interaction diagram between O5 and protein (receptor:2JDO).

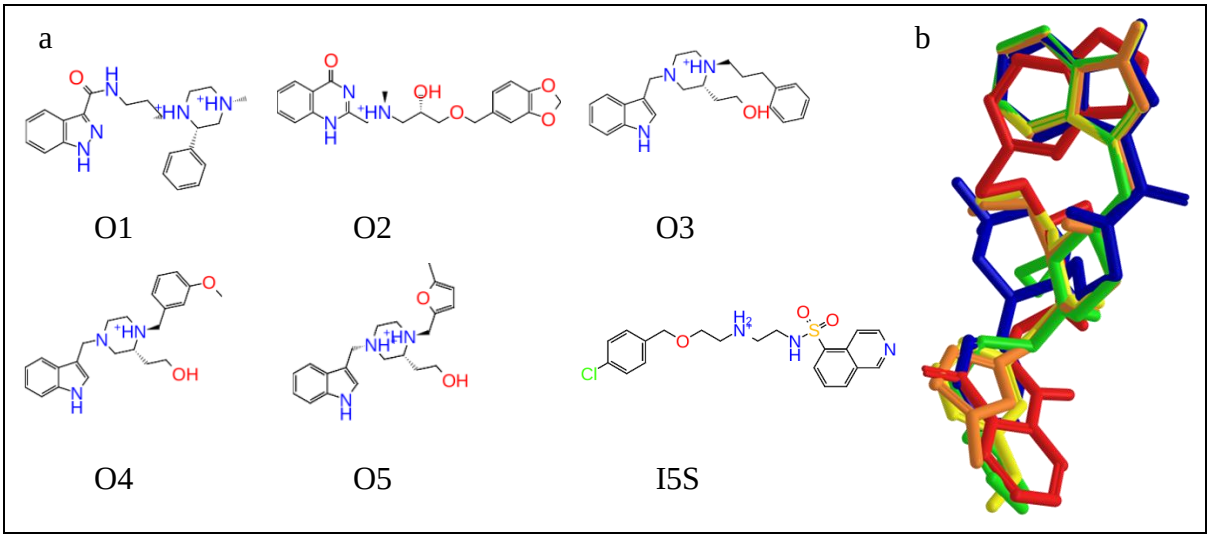

Figure 4.34. (a) 2D structures of O1-O5 and I5S, (b) 3D alignment of O1-O5 in the active site (O1-blue, O2-red, O3-green,O4-yellow, O5-orange).

4.5.3. Interactions of Proposed Ligands with PKB- β (2JDR)

The five proposed molecules, listed in Table 4.28 are analyzed in more detail to obtain more information about their interactions with protein AKT-2, summarized in Figure 4.35 to Figure 4.39. The 3D binding poses of the proposed molecules for 2JDR, R1-R5, along with hydrogen bond interactions are represented in Appendix B (Figure B.2).

The molecule R1 with chemical formula $C_{14}H_{15}N_8S_2$ has 39 atoms and 42 bonds of which 7 are rotatable. Figure 4.35 shows the interactions between the R1 and AKT-2. Purine ring of R1 forms a H-bond with the backbone of hinge region residue of Glu230 and Ala232 of AKT-2, and it is in hydrophobic contact with residues Ala179, Met229, Leu158, Thr231, and Phe439. In the acidic, ribose binding region of the protein, Asp293 makes a H-bond with ammonium of the molecule.

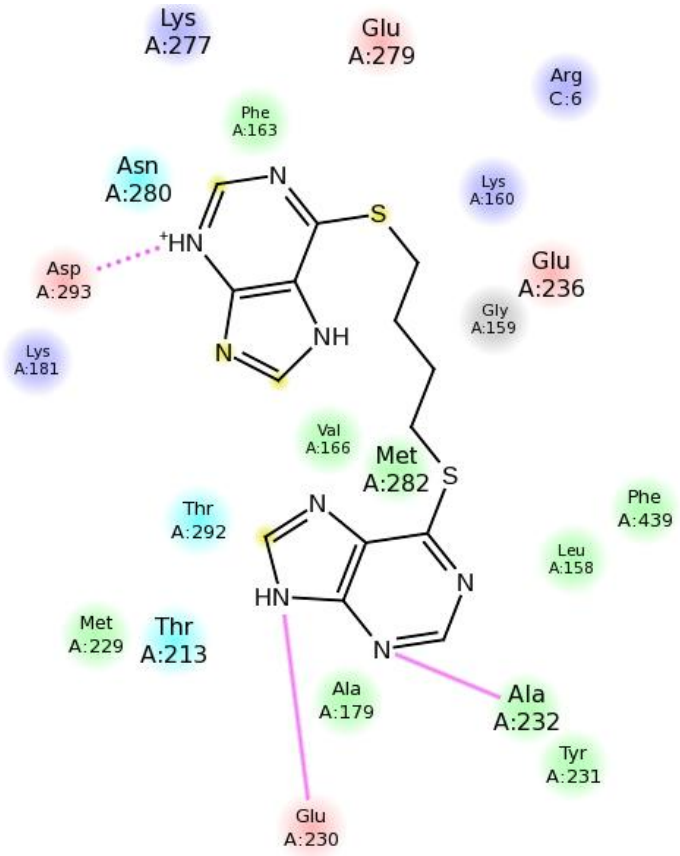

Figure 4.35. Interaction diagram between R1 and protein (receptor:2JDR).

The molecule R2 with chemical formula $C_{16}H_{17}N_4O_2$ has 39 atoms and 41 bonds of which 6 are rotatable. Figure 4.36 shows the interactions between the molecule and AKT-2. R2 forms a H-bond with Ala232 backbone. This part of the molecule is in hydrophobic contact with residues Tyr231, Met282, Leu158, Ala179, and Phe439. Ammonium on the pyridine ring makes a H-bond with residue Asn280 and pyridine ring is in hydrophobic contact with residue Phe163, which is turned towards the active site in the 2JDR structure.

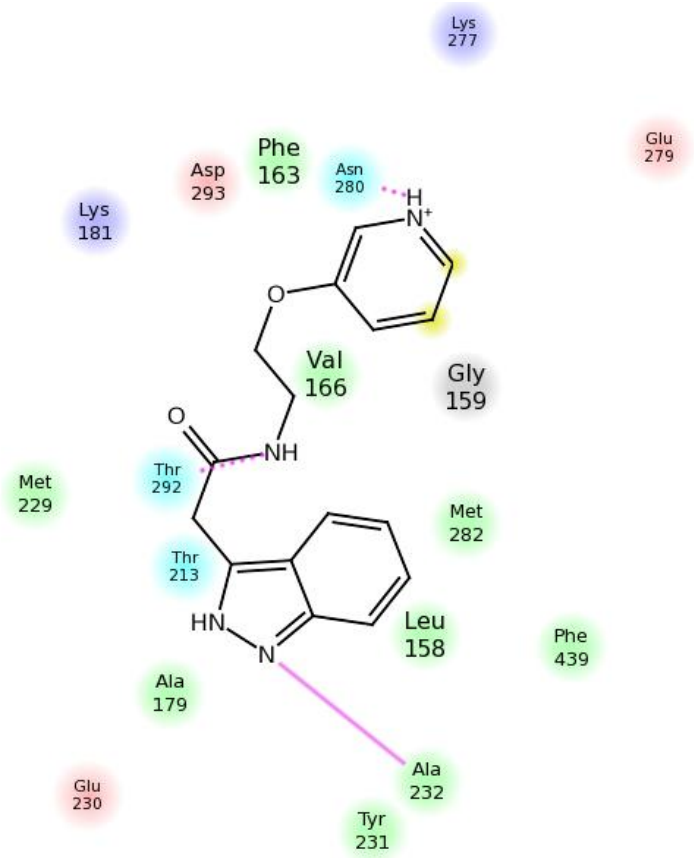

Figure 4.36. Interaction diagram between R2 and protein (receptor:2JDR).

The molecule R3 with chemical formula $C_{14}H_{13}N_6O_3$ has 36 atoms and 38 bonds of which 5 are rotatable. Figure 4.37 shows the interactions between the molecule and the protein AKT-2. Purine group of the R3 forms H-bond with the backbone of Ala232 of the AKT-2. Purine group is also in contact with residues Phe439, Leu158, Val166, Ala179, and Met282. Amine group of R3 makes a H-bond with Thr292, and ketone group makes a H- bond with Lys181. Another H-bond is observed between ammonium of the solvent

exposure region of the molecule and residue Asp293 of the protein. This region is also in hydrophobic contact with the residues Phe163, Val166 and Met282.

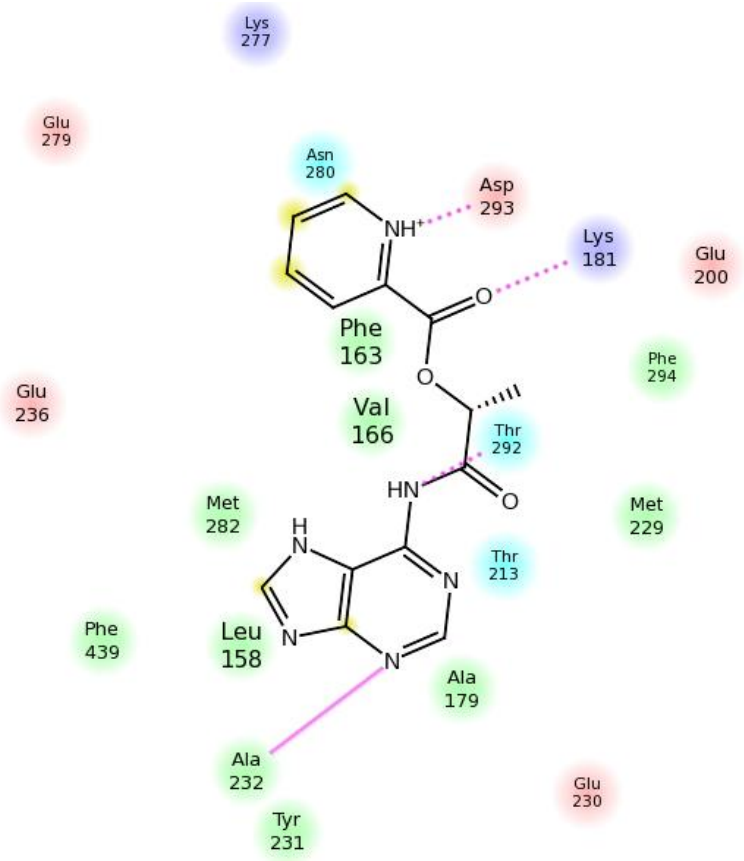

Figure 4.37. Interaction diagram between R3 and protein (receptor:2JDR).

The molecule R4 with chemical formula $C_{15}H_{19}N_7$ has 41 atoms and 44 bonds of which 3 are rotatable. Figure 4.38 shows the interactions between the R4 and the protein AKT-2. Pyrazole ring of the R4 makes a H-bond with residue Glu230, and pyrimidine ring of the molecule makes a H-bond with the other hinge region residue Ala232. This part of the ligand is in hydrophobic contact with Phe439, Tyr231, Met229, and Leu158. Pyridine ring on the solvent exposure side of the molecule is in hydrophobic contact with the residue Phe163.

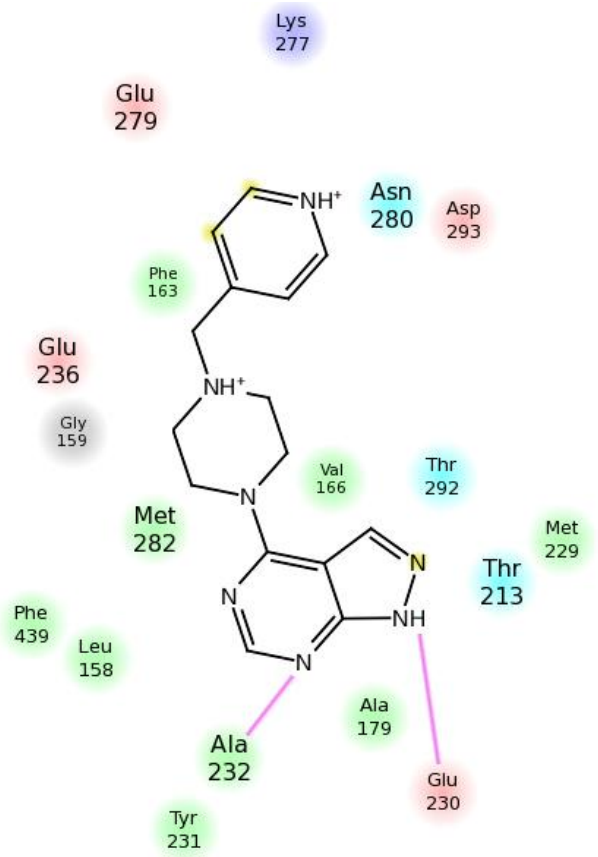

Figure 4.38. Interaction diagram between R4 and protein (receptor:2JDR).

The molecule R5 with chemical formula $C_{11}H_9N_8S_2$ has 30 atoms and 33 bonds of which 4 are rotatable. Figure 4.39 shows the interactions between the R5 and the protein AKT-2. Purine ring of R5 makes a H-bond interaction with hinge region residues of Ala232 and Glu230. This part of the molecule is in hydrophobic contact with residues Met229, Tyr231, Phe439, Ala179, and Leu158. Purine ring in the solvent exposed region of the molecule makes a H-bond with residue Glu236.

Figure 4.40a shows 2D structures of R1-R5 and the native ligand of 2JDR, L20. 3D alignment of R1-R5 in the active site is represented in Figure 4.40b.

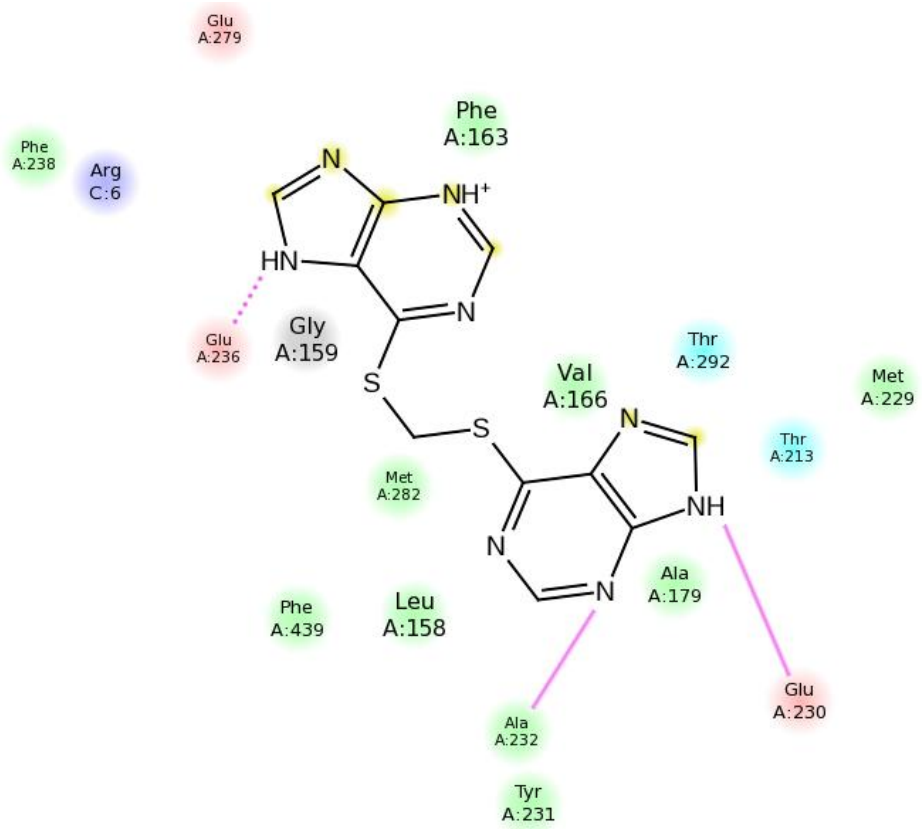

Figure 4.39. Interaction diagram between R5 and protein (receptor:2JDR).

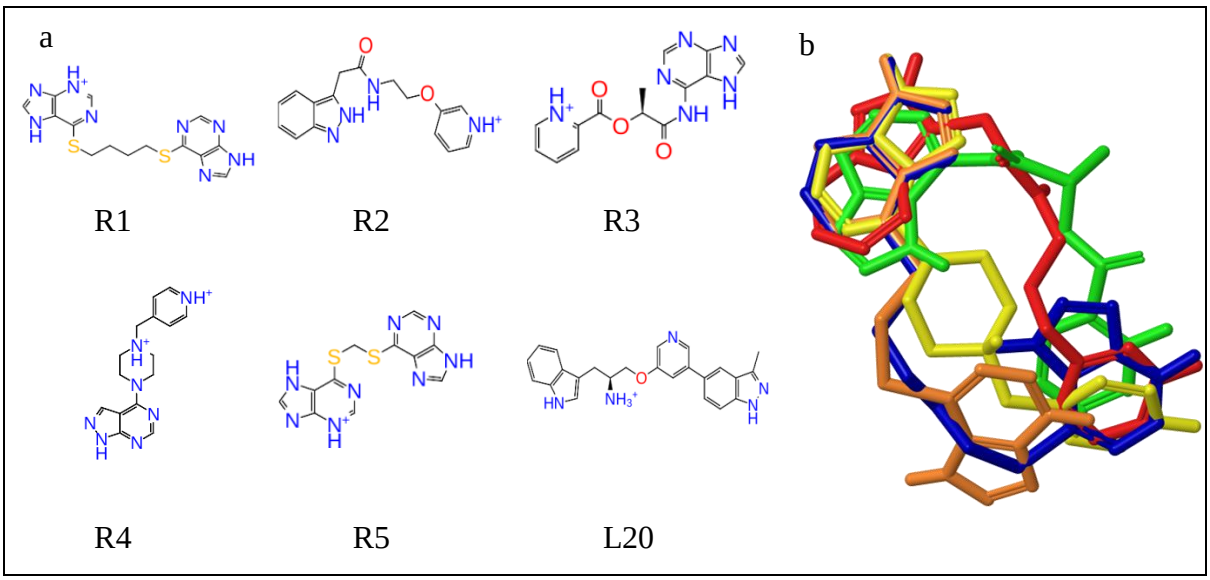

Figure 4.40. (a) 2D structures of R1-R5 and L20, (b) 3D alignment of R1-R5 in the active site (R1-blue, R2-red, R3-green,R4-yellow, R5-orange).

4.5.4. Comparison of Ten Selected Molecules

When the proposed five molecules from docking with the structure of 2JDO were compared, it was found out that four of the molecules (except O2) have indole or indazole groups that occupy the same position in the active site and interact with Glu230 in the hinge region. Furthermore, binding mode of O4 is remarkably alike with the molecule O5.

Proposed five molecules from docking with the structure of 2JDR were also examined, and it was detected that four of the molecules (except R2) have considerably overlapping purine or pyrazole group that make interaction with hinge region residues. Molecules R1 and R5 adapt a similar binding mode. The chain that links the solvent exposed part of the molecule and the deep binding components of the molecules is longer in the case of R1 and this allows to make a H-bond with Asp293 instead of Glu236. This difference may be responsible for better docking score of R1 compared to R2 to R5.

From the analysis of binding poses of proposed molecules, it was observed that none of the molecules (O1-O5) from docking with 2JDO is in hydrophobic contact with the residue Phe163, whereas R2, R3, and R4 are in a direct hydrophobic contact with Phe163 in case of docking with 2JDR, in which Phe163 is turned down towards the active site. O1-O5 have extra ring that is occupied by Phe163 in 2JDR, whereas R1-R5 have more compact form. This is an expected result as also mentioned in Section 4.3.5.

Summary of chemical properties of proposed molecules and their interactions with AKT-2 residues are shown in Table 4.29 and Table 4.30, respectively. Table 4.29 was taken from the public web service of chemicalize.org [106] which is created by ChemAxon. Number of bonds in the molecule including hydrogens is given in “# of bonds” column, where number in the parenthesis shows the number of rotatable bonds. It was observed that docking with open loop conformation (2JDO) resulted in more flexible ligand structures which have approximately seven rotatable bonds, and docking with closed loop conformation (2JDR) resulted in less flexible ligand structures with about five rotatable bonds. In addition, average molecular weight of the proposed molecules for docking with 2JDO was found to 377.08 while it is 315.75 for docking with 2JDR (Table 4.29). These are expected results since conformation of Phe163 leaves more space to the

docked poses in the binding region of 2JDO. In addition, the total number of interactions of proposed molecules is higher for docking with 2JDO (Table 4.30), possibly due to a larger cavity in receptor 2JDO, which accepts larger molecules in the binding site. Longer molecules can fit in the active site, have higher chance to make contact, and show greater binding affinity. This also explains the higher XP GScore of docking with 2JDO when compared to 2JDR. As the total number of interactions with receptor is increased the docked molecule may become more specific to its target protein. The result of docking experiment with PKA (Table 4.27 and Table 4.28) is in agreement with the finding proposed molecules O1-O5 have higher specificity to their target (AKT-2).

As it is seen from Table 4.30, molecules make a π-cation interaction with residue Lys181 as there is a benzene ring of the docked poses in the corresponding part of the binding site. None of the proposed molecules make H-bond with residues Glu200 and Phe294 which were set as constraint in the XP docking experiments. Like native ligands, there is still a high tendency among proposed molecules to make H-bond with hinge region residues of Ala232 and Glu230 which were set as constraints in both SP and XP docking experiments. It was found that the tendency to make H-bond with Asp293 is increased compared to interactions of native ligands (Table 4.5) suggesting that proposed molecules possibly adapt a new binding mode.

Table 4.29. Summary of chemical properties of proposed molecules.

Molecule	**# of atoms**	**# of bonds**	**H-bond acceptors**	**H-bond donors**	**MW**	**LogP**	**Lipinski rule (Drug-like)**
O1	57	60 (6)	6.5	1.00	377.49	2.70	+
O2	53	56 (8)	10.4	2.00	397.43	1.47	+
O3	60	63 (8)	5.70	2.00	377.53	3.49	+
O4	58	61 (7)	6.45	2.00	379.50	2.90	+
O5	55	58 (6)	6.20	2.00	353.46	2.67	+
R1	39	42 (7)	7.00	2.00	358.44	2.10	+
R2	39	41 (6)	4.75	1.00	296.33	1.94	+
R3	36	38 (5)	9.00	2.00	312.29	0.55	+
R4	41	44 (3)	7.00	1.00	295.35	1.17	+
R5	30	33 (4)	7.00	2.00	316.36	1.22	+

Table 4.30. Summary of17 interactions of proposed molecules.

Molecule	Lys181	Glu200	Glu230	Ala232	Glu236	Glu279	Asn280	Met282	Thr292	Asp293	Phe294	Total
O1	π -cation		H-bond		H-bond					H-bond		4
O2	π -cation			H-bond		H-bond				H-bond		4
O3	π -cation		H-bond			H-bond				H-bond		4
O4			H-bond		H-bond					H-bond		3
O5			H-bond		H-bond					H-bond		3
R1			H-bond	H-bond						H-bond		3
R2				H-bond			H-bond		H-bond			3
R3	H-bond			H-bond					H-bond	H-bond		4
R4			H-bond	H-bond								2
R5			H-bond	H-bond	H-bond							3
Total	4	0	7	6	4	2	1	0	2	7	0	

Pairwise molecular similarities between proposed molecules and native ligands of I5S and L20 were calculated with ChemMine Tools [128], which is available at http://chemmine.ucr.edu. 2D similarity search within ChemMine Tools uses atom pair algorithm with the Tanimoto similarity metrics. Tanimoto coefficient (also known as Jaccard coefficient) calculates the degree of similarity between two molecules and has a range from 0 to 1. Higher Tanimoto value means greater similarity. Obtained Tanimoto coefficients of proposed molecules along with I5S and L20 are summarized in Table 4.31. Hierarchical clustering tree analysis was carried out by ChemMine Tools, shown in Figure 4.41, and molecules are clustered by structural similarity. Similarity matrix, which is obtained from Tanimoto coefficients, is converted to distance matrix. Distance values are calculated by substracting Tanimoto coefficient values from 1, and clustering is done by hclust function with R program.

According to Table 4.31, O4 and O5 are the most similar compounds while O3 and R5 are the least similar compounds. As expected, molecules O1-O5 have higher similarity to I5S, which is the ligand in 2JDO, than to L20, which is the native ligand in 2JDR. Similarly R1-R5 have higher degree of similarity to L20 than to I5S. As it is seen from Table 4.31 and Figure 4.41, molecules O1-O5 have greater similarity within each other than the similarity within molecules R1-R5. Among molecules R1-R5, R2 is the most similar compound to O1-O5.

Table 4.31. Pairwise molecular similarity of proposed molecules, I5S, and L20 by Tanimoto coefficient.

Tanimoto	O1	O2	O3	O4	O5	R1	R2	R3	R4	R5	I5S	L20
O1	1	0.304	0.392	0.392	0.378	0.213	0.333	0.173	0.266	0.105	0.268	0.262
O2		1	0.281	0.289	0.293	0.166	0.251	0.154	0.177	0.083	0.281	0.251
O3			1	0.546	0.518	0.160	0.199	0.071	0.211	0.058	0.266	0.203
O4				1	0.719	0.178	0.263	0.123	0.285	0.077	0.225	0.264
O5					1	0.192	0.255	0.116	0.284	0.081	0.222	0.222
R1						1	0.245	0.173	0.303	0.296	0.135	0.183
R2							1	0.312	0.269	0.164	0.245	0.301
R3								1	0.207	0.272	0.131	0.244
R4									1	0.212	0.136	0.189
R5										1	0.083	0.173
I5S											1	0.221
L20												1

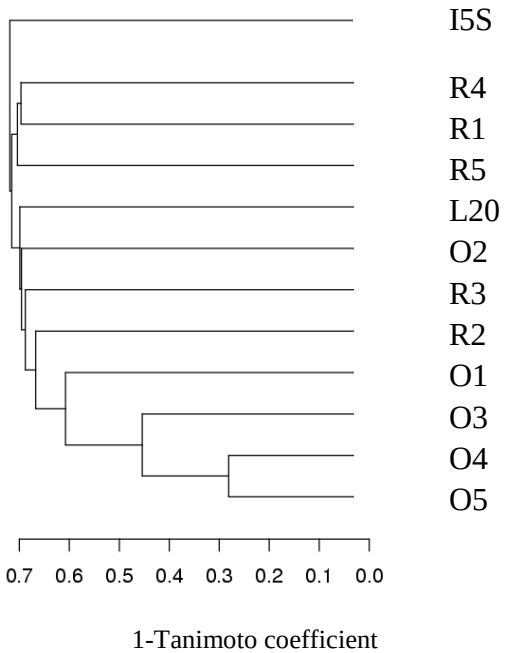

Figure 4.41. Hierarchical clustering tree of proposed molecules, I5S and L20.

4.6. Induced Fit Docking

Proposed ten molecules were subjected to induced fit docking (IFD) with receptors 2JDO and 2JDR to re-generate the binding poses of proposed molecules and to examine their binding poses, protein-ligand interactions and predicted binding affinity in terms of docking score. Induced fit allows conformational changes in the active site upon binding and this protocol assumes both receptor and ligand flexibility. IFD scores of best poses of the proposed molecules are listed in Table 4.32.

Table 4.32. IFD Score of proposed molecules in kcal/mol.

Molecule	IFD Score	Molecule	IFD Score
O1	-11.661	**R1**	-11.429
O2	-9.440	**R2**	-14.217
O3	-9.413	**R3**	-8.957
O4	-8.937	**R4**	-13.016
O5	-9.017	**R5**	-11.429

The docking scores after IFD are close to or even better than the scores obtained after XP docking. In fact, the ranking of the ten compounds after IFD is also similar to the ranking obtained after XP docking (Table 4.32). Interaction diagram of the poses for O1-O5 obtained after IFD are available in Appendix C (Figure C.1 to Figure C.5). Indazole ring of molecule O1 is near hinge region as in Glide docking and makes H-bonds with residues Glu230 and Ala232. Positively charged group of the molecule makes H-bond with residue Glu279 (IFD docking) instead of Glu236 and Asp293 (XP docking) in the ribose binding region. Alkynol –OH group of O2 is positioned in the hinge region of the protein and makes H-bond with residue Ala232 whereas in the Glide docking it is placed in the ribose binding region. 1,3-benzodioxole and 1H-Quinazolin-4-one of O2 is placed in the solvent exposed region. Alkynol –OH group of O3, like O2, is located in the hinge region of the protein and makes H-bond with residue Ala232 whereas in the GlideXP docking it is placed in the ribose binding region. IFD binding pose of O4 is considerably different from its original binding pose and no H-bond interaction was observed between the molecule and protein. In the acidic, ribose binding region of the protein, instead of Glu236, Asp440 and Leu158 make a H-bond with alkynol –OH group of the O5 for the case of IFD docking, and Glu236 makes a H-bond with ammonium of the molecule.

In the case of receptor 2JDR, the binding modes of proposed molecules (R1-R5) are essentially similar to their Glide XP binding modes (Figure C.6 to Figure C.11). Unlike Glide rigid protein docking, induced fit docking results yield higher scores for receptor 2JDR. Purine ring of the highest IFD scoring binding mode of R1 is able to interact with Glu230 and Ala232, as in Glide docking. However interactions with Asp293 were not observed, instead, Lys277 make a hydrogen bond with the highest scoring binding mode of R1. Orientation of the second highest binding mode of R1 is more similar to Glide XP binding modes with predicting hinge region H-bonds with residues Glu230 and Ala232 (IFD score: -10.950 kcal/mol). This pose of R1 also has π-π interactions between residue Phe163 and ammonium of the molecule. IFD binding mode of R2 with highest score was remarkably similar to its original docking orientation, interacting with Ala232, Asn280, and Thr292 besides an additional H-bond with residue Glu230. Except for the purine group of the R3, highest scoring IFD binding pose displays highly matching orientation with respect to its Glide XP binding pose. H-bond between Ala232 and purine group was not observed for the case for IFD binding pose, however, H-bond between residues Thr292 and Asp293 was observed. The highest scoring docking mode of R4 generated in IFD protocol is similar to its original docking orientation. Pyrazole ring of the R4 is able to make a H-bond with residue Glu230, and pyrimidine ring of the molecule is able to make a H-bond with the other hinge region residue Ala232. Additionally, pyridine ring of R4 interacts with residue Asp293. The purine ring of top IFD scoring pose of R5 overlaps with its Glide XP binding pose, interacting with hinge region residues of Ala232 and Glu230. H-bond with residue Glu236 was not observed in IFD.

Overall, binding mode of proposed molecules (R1-R5) in induced fit docking with receptor 2JDR seems remarkably alike with the poses generated in Glide XP docking, while induced fit docking with receptor 2JDO was failed to predict the identified interactions of Glide XP docking.

5. CONCLUSION AND FUTURE WORK

5.1. Conclusion

The primary aim of this study is to carry out a molecular docking process of novel inhibitors for AKT-2 which belongs to serine/threonine kinase subfamily. AKT-2 is in oncogenic activity and plays a role in cell growth, survival, and progression of tumor. Inhibition of this protein was aimed since it is an important therapeutic target for the treatment of cancer.

Computer-aided drug design methodologies were applied to find putative inhibitors of AKT-2 kinase. Ligand-based and structure-based approaches were used to filter molecular database and to identify novel drug candidates. Virtual screening studies were performed by Schrodinger Suite 2011 module. In this study, a small molecule database was first pre-filtered by ligand-based virtual screening and then structure-based virtual screening was applied.

3D pharmacophore method was employed for ligand-based virtual screening. Pharmacophore hypothesis was built by Phase with the nine AKT-2 native ligands, for which the complex structure are available in the PDB. Ligand-based excluded volumes were generated and added to pharmacophore hypothesis. In the screening process, ligands which occupy a region on the excluded volume were rejected. CoCoCo_Phase database of 3.7 million compounds was screened via ligand-based pharmacophore model to find molecules that have similar 3D property to applied hypothesis.

Molecular docking approach was employed for structure-based virtual screening. Glide application of Schrodinger Suite 2011 was used to perform docking experiments. 3D structures of target proteins were obtained and prepared before molecular docking. Binding site was analyzed and important residues that are critical for binding were identified. To handle the induced fit effect of binding, two different conformations of AKT-2 kinase protein were used in docking experiments; namely, 2JDO (open loop) and 2JDR (close loop). Two step molecular docking was performed to screen filtered database molecules. In

all docking calculations, flexible ligand mode was used and H-bond constraints were applied. Empirical GScore values were used as final scoring function. Filtered database was first screened by SP mode of Glide docking protocol and top 1000 poses were kept. In the second step, these molecules were re-docked to target proteins by extra precision mode of Glide.

Hierarchical computational filters reduced the number of molecules to 394 and 137 after pharmacophore and docking based virtual screening to 2JDO and 2JDR. Post-filtering was performed via examining the pharmacokinetic features of the molecules. By looking at strain energy, ADME properties, and druglikeness undesired molecules are eliminated from further evaluation and totally ten molecules were proposed based on docking score. The multi-step molecular docking yields mainly, purine and pyrazole class of compounds. Proposed molecules for 2JDO inhibition were named as O1, O2, O3, O4, and O5; while R1, R2, R3, R4, and R5 were used to call the proposed molecules for 2JDR inhibition. Names and identifiers of proposed ten molecules can be found in Table 4.26 and the vendor list of the molecules can be obtained from Table 4.15 and Table 4.16. Docking results for 2JDO yield bulkier, more flexible, and more selective ligands. In addition molecules O1-O5 have higher XP GScores and the number of interactions between ligand and protein is also higher for 2JDO docking.

In order to evaluate the performance of Glide docking and scoring protocol for target AKT-2 kinase, enrichment study was conducted. Enrichment calculations yielded a AU-ROC value of 0.93 for GScore ranking, indicating that Glide docking is a reliable tool.

Selectivity studies were carried out to assess whether the proposed molecules are PKB-β selective or not. Hence, proposed molecules were docked to highly homologous proteins, PKA and PKB-α. All of the proposed molecules were found to be AKT-2 selective with respect to PKA and PKB-α. The most selective compound was determined to be the molecule O1 with CoCoCo ID 48494320, which belongs to indazole class of inhibitor, and also it has the highest XP GScore among the proposed ones.

Tanimoto coefficients were calculated to assess pairwise molecular similarities of proposed molecules. In general, structural similarities among O1-O5 were observed to be

greater than the similarities among R1-R5. Proposed 2JDO inhibitors were structurally more diverse compared to 2JDR inhibitors. Proposed molecules were not subject to in any pharmacological study. Nine co-crystallized PKB-β inhibitors mainly consists of aminofurazan and indazole based inhibitors and the multi-step molecular docking yielded mainly, purine and indole class of compounds where purine derivatives have found as antiviral, antibiotic, anticancer, antiprotozoal agents and indole derivatives have found as antihypertensive, antiproliferative, antiviral, antitumor, analgesic, anti-inflammatory, antimicrobial activities [129–131].

5.2. Recommendations

In this work, one pharmacophore hypothesis was selected and used in the pharmacophore filtering step. In future, pharmacophore database screening can be performed with other hypotheses and docking procedure can be repeated. Employing more than one hypothesis is expected to yield compounds that are more diverse compared to previously found ones.

Although the same molecules were used as input for docking with each structure (2JDO and 2JDR), only three out of the top 25 hits were identified as common. Docking with two PKB-β structures that have different loop conformations allowed the screening and identification of a more diverse set of molecules. Then, additional docking study with different protein conformations can be performed.

MD simulations can be performed to determine the stability of the complex structures. In MD simulations, ligand and receptor are allowed to be flexible so induced-fit effect can be handled. Since MD simulations are run in a water-mediated environment, solvation effect would be readily taken into account. MD simulations can also be used to assess the consistency of the docked poses. Accurately docked ligand poses can be differentiated from the unstable ones [132].

To validate the results, proposed molecules can be tested experimentally for inhibition of AKT-2 (PKB-β), PKA and PKB-α, and experimental inhibitory data could be utilized to improve docking calculations.

Ligand and structure-based virtual screening procedure can be repeated to design new type of inhibitors which target PH domain of AKT-2 kinase. This allosteric type of inhibition is non-competitive and it is expected to yield more isoform specific inhibitors to its target protein.

APPENDIX A: ENRICHMENT REPORT

Enrichment report according to XP GScore values is given below.

Enrichment Report

```
-----------------
Actives file: /home/pinarderin/Desktop/enrichment/actives.maegz
     Results:/home/pinarderin/Desktop/enrichment/2JDO_enrich_schrod__glid
     e-dock_XP_33_pv.maegz
Total actives: 9
Total ligands(actives+decoys): 1009
Number of ranked actives: 9
BEDROC(alpha=160.9, alpha*Ra=1.4352): 0.461
BEDROC(alpha=20.0, alpha*Ra=0.1784): 0.585
BEDROC(alpha=8.0, alpha*Ra=0.0714): 0.708
ROC: 0.93
RIE: 10.71
Area under accumulation curve: 0.93
Ave. Number of outranking decoys: 64
Minimum Tc over all active pairs: n/a
Count and percentage of actives in top N% of decoy results.
% Decoys | 1%| 2%| 5%| 10%| 20%|
# Actives | 5| 5| 5| 6| 8|
% Actives | 55.6| 55.6| 55.6| 66.7| 88.9|
Count and percentage of actives in top N% of results.
% Results | 1%| 2%| 5%| 10%| 20%|
# Actives | 4| 5| 5| 6| 8|
% Actives | 44.4| 55.6| 55.6| 66.7| 88.9|
Enrichment Factors with respect to N% sample size.
% Sample | 1%| 2%| 5%| 10%| 20%|
EF | 45| 28| 11| 6.7| 4.4|
EF* | 56| 28| 11| 6.7| 4.4|
EF' | 76| 51| 22| 12| 7.6|
DEF | n/a| n/a| n/a| n/a| n/a|
DEF* | n/a| n/a| n/a| n/a| n/a|
DEF' | n/a| n/a| n/a| n/a| n/a|
Eff | 0.965| 0.931| 0.835| 0.739| 0.633|
Enrichment Factors with respect to N% actives recovered.
% Actives | 40%| 50%| 60%| 70%| 80%| 90%| 100%|
```

EF | 64| 40| 40| 8.7| 6.9| 5.5| 4.2|
EF* |1.5e+02| 62| 62| 9.4| 7.3| 5.8| 4.3|
EF' | 1e+02| 79| 79| 16| 12| 9| 6.8|
FOD | 0.002| 0.004| 0.004| 0.01| 0.03| 0.04| 0.06|
Rank Title
------ --
3 X39__2X39-PPW-noWAT_noPEPTIDE
4 L20__2JDR--PPW-noWAT_noPEPTIDE
5 I5S__2JDO-PPW-noWAT_noPEPTIDE
7 G95__3E87-PPW-noWAT_noPEPTIDE
14 X37__2XH5-PPW-noWAT_noPEPTIDE
77 G96__3E88-PPW-noWAT_noPEPTIDE
113 G98__3E8D-PPW-noWAT_noPEPTIDE
162 GVP__2UW9-PPW-noWAT_noPEPTIDE
242 G93__3D0E-PPW-noWAT_noPEPTIDE
Enrichment report according to ΔG bind values is given below.
Enrichment Report

Actives file: /home/pinarderin/Desktop/NEW/enrichment/actives.maegz
Results: enrichment_from_project_selection.mae.gz
Total actives: 9
Total ligands(actives+decoys): 1009
Number of ranked actives: 9
BEDROC(alpha=160.9, alpha*Ra=1.4352): 0.157
BEDROC(alpha=20.0, alpha*Ra=0.1784): 0.444
BEDROC(alpha=8.0, alpha*Ra=0.0714): 0.577
ROC: 0.85
RIE: 8.14
Area under accumulation curve: 0.85
Ave. Number of outranking decoys: 148
Minimum Tc over all active pairs: n/a
Count and percentage of actives in top N% of decoy results.
% Decoys | 1%| 2%| 5%| 10%| 20%|
# Actives | 1| 4| 5| 6| 7|
% Actives | 11.1| 44.4| 55.6| 66.7| 77.8|
Count and percentage of actives in top N% of results.
% Results | 1%| 2%| 5%| 10%| 20%|
# Actives | 1| 3| 5| 6| 6|
% Actives | 11.1| 33.3| 55.6| 66.7| 66.7|
Enrichment Factors with respect to N% sample size.

% Sample | 1%| 2%| 5%| 10%| 20%|
EF | 11| 17| 11| 6.7| 3.9|
EF* | 11| 22| 11| 6.7| 3.9|
EF' | 16| 18| 15| 10| 6.2|
DEF | n/a| n/a| n/a| n/a| n/a|
DEF* | n/a| n/a| n/a| n/a| n/a|
DEF' | n/a| n/a| n/a| n/a| n/a|
Eff | 0.835| 0.914| 0.835| 0.739| 0.591|
Enrichment Factors with respect to N% actives recovered.
% Actives | 40%| 50%| 60%| 70%| 80%| 90%| 100%|
EF | 21| 11| 11| 7.3| 3.9| 1.9| 2|
EF* | 26| 13| 13| 7.8| 4| 1.9| 2|
EF' | 18| 15| 15| 11| 6.3| 3.2| 3|
FOD | 0.01| 0.02| 0.02| 0.03| 0.05| 0.1| 0.1|
Rank Title
------ --
5 G98__3E8D-PPW-noWAT_noPEPTIDE
13 G93__3D0E-PPW-noWAT_noPEPTIDE
16 G96__3E88-PPW-noWAT_noPEPTIDE
21 L20__2JDR--PPW-noWAT_noPEPTIDE
49 I5S__2JDO-PPW-noWAT_noPEPTIDE
92 X39__2X39-PPW-noWAT_noPEPTIDE
202 G95__3E87-PPW-noWAT_noPEPTIDE
480 X37__2XH5-PPW-noWAT_noPEPTIDE
505 GVP__2UW9-PPW-noWAT_noPEPTIDE

APPENDIX B: 3D BINDING POSES OF PROPOSED MOLECULES

The 3D binding poses Glide XP docking for ten proposed compounds to AKT-2 were given in below figures. In Figure B.1 and B.2, AKT-2 is shown in ribbon representation, ligands and interacting residues are shown in stick representation, and hydrogen bonds between ligands and AKT-2 are indicated by red dashed lines.

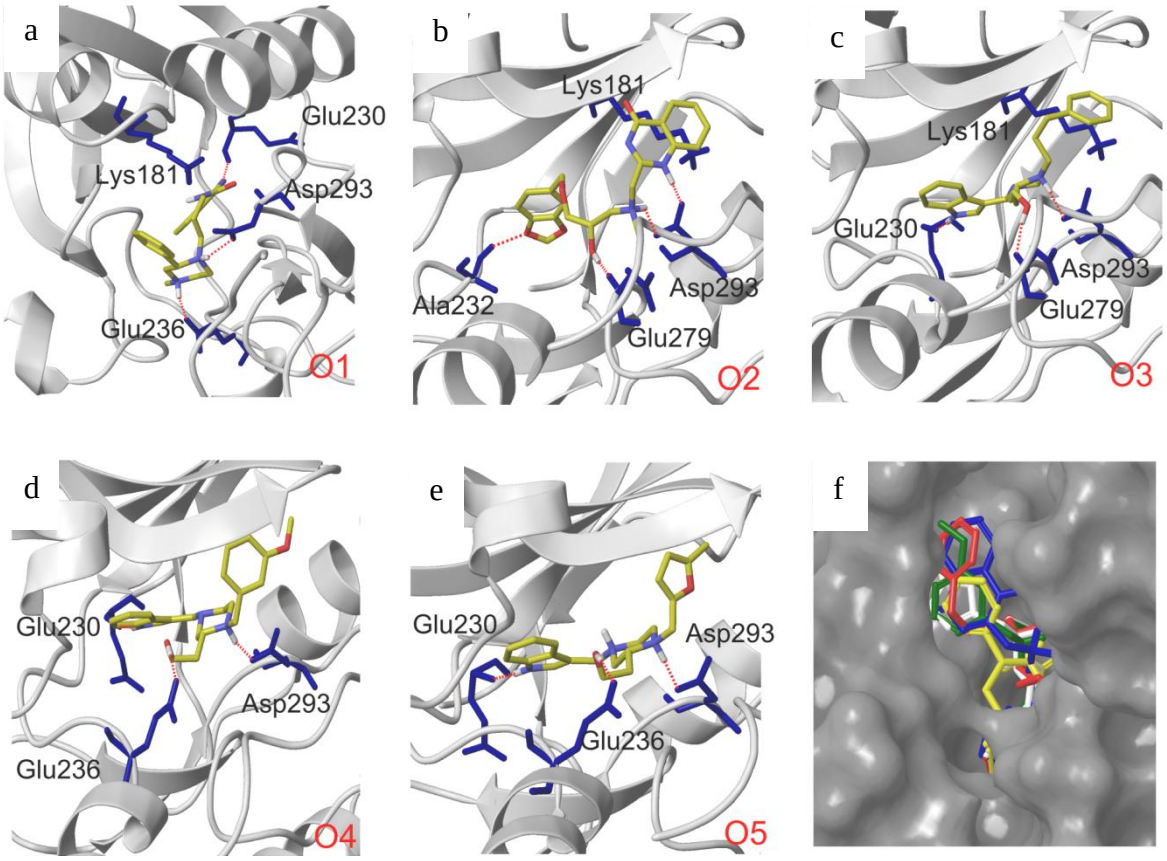

Figure B.1. (a)-(e) Glide XP binding modes of proposed molecules O1-O5 in ATP binding site of AKT-2 (PDB code: 2JDO). (f) Superimposed poses of five proposed molecules. AKT-2 is in surface representation and ligands are colored by molecule.

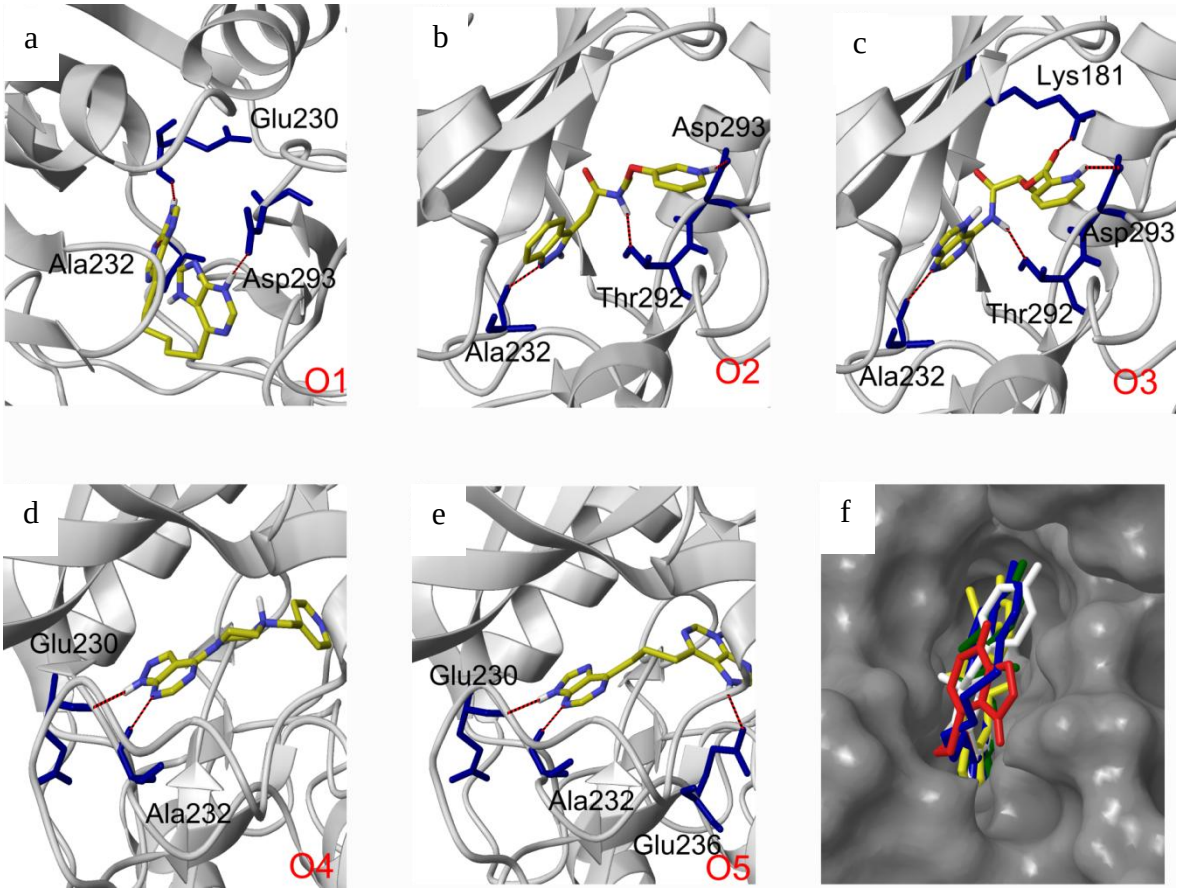

Figure B.2. (a)-(e) Glide XP binding modes of proposed molecules R1-R5 in ATP binding site of AKT-2 (PDB code: 2JDR). (f) Superimposed poses of five proposed molecules. AKT-2 is in surface representation and ligands are colored by molecule.

APPENDIX C: INDUCED FIT DOCKING

The ligand interaction diagrams of induced fit docking ten proposed compounds to AKT-2 were given in below figures.

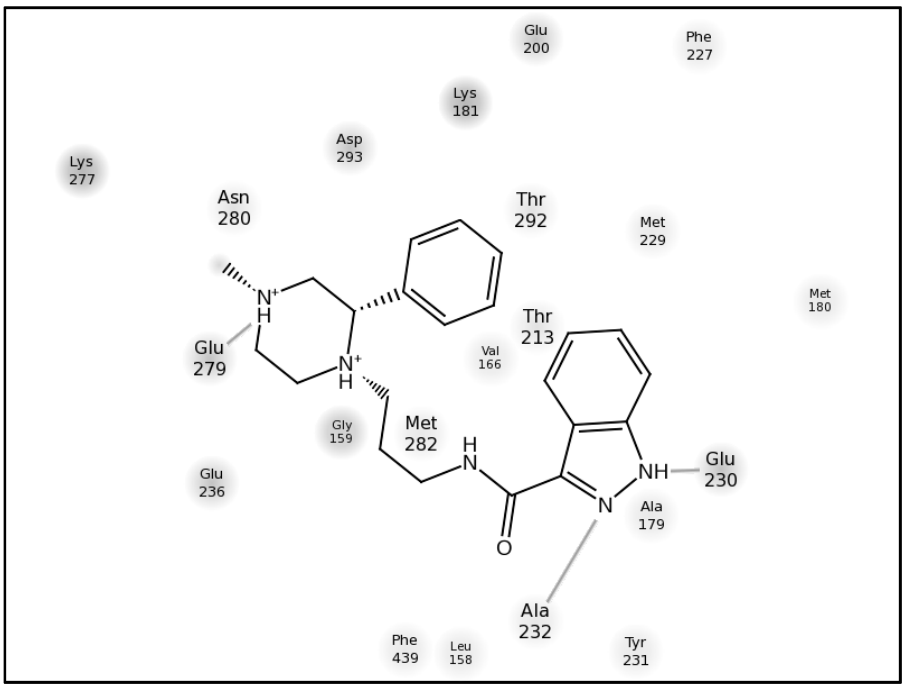

Figure C.1. Induced fit docking ligand interaction map of compound O1.

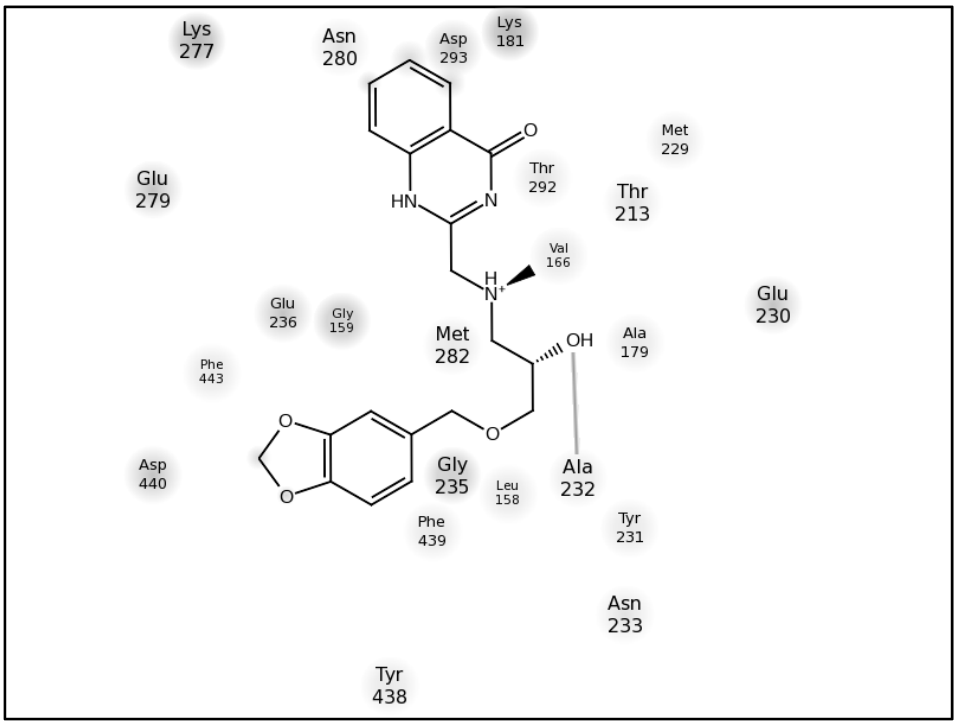

Figure C.2. Induced fit docking ligand interaction map of compound O2.

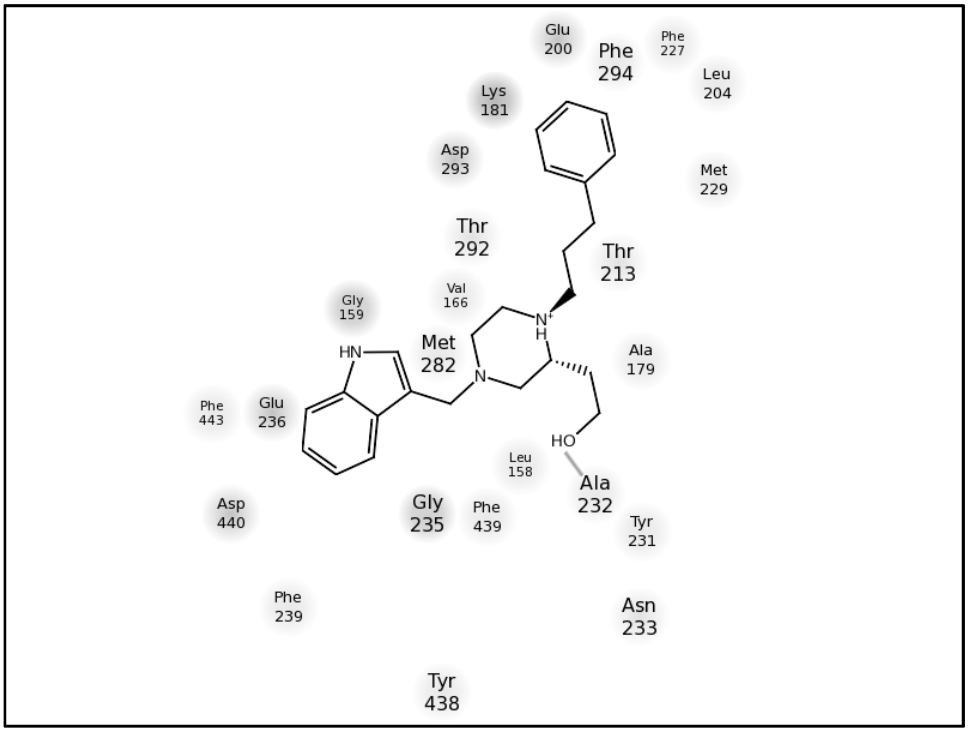

Figure C.3. Induced fit docking ligand interaction map of compound O3.

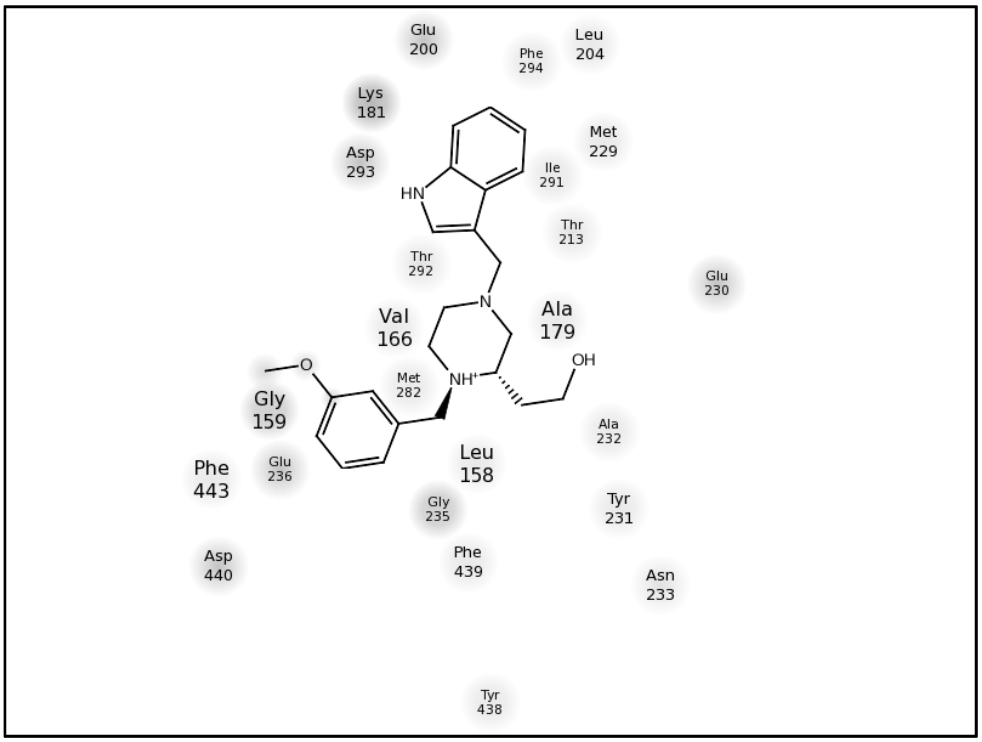

Figure C.4. Induced fit docking ligand interaction map of compound O4.

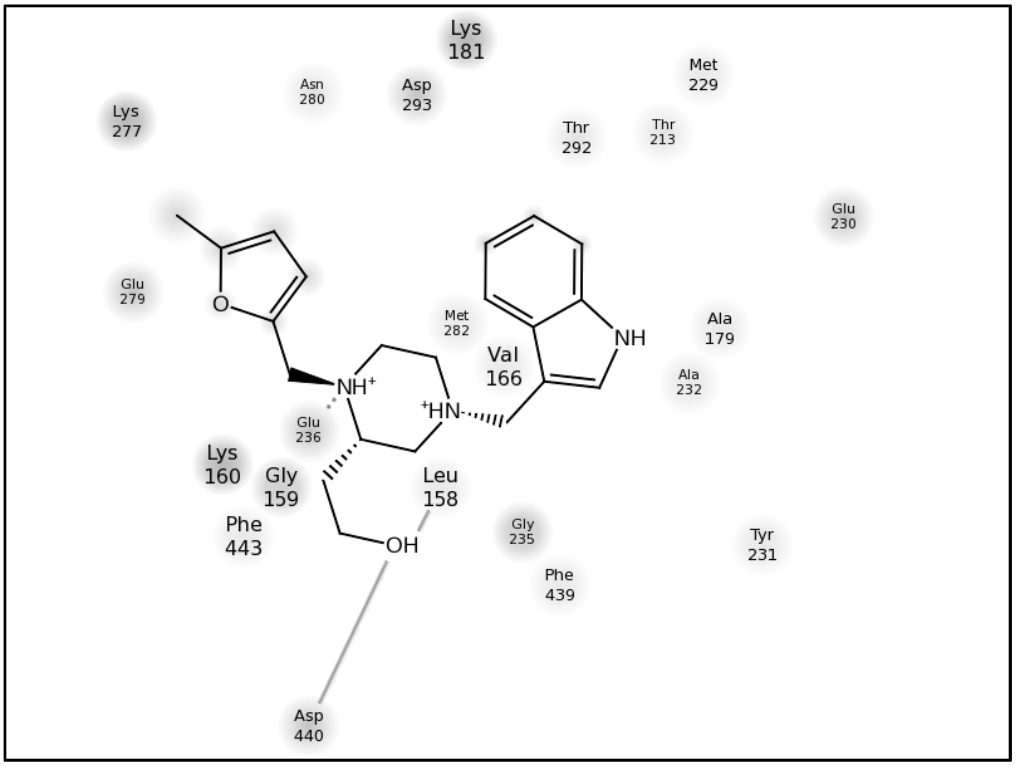

Figure C.5. Induced fit docking ligand interaction map of compound O5.

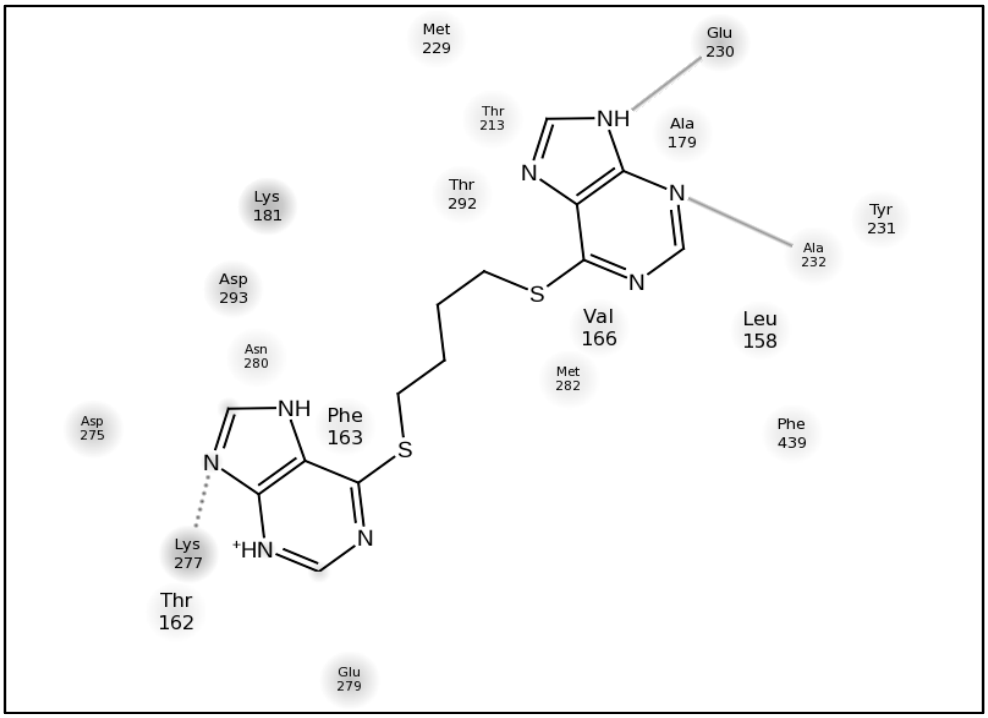

Figure C.6. Induced fit docking ligand interaction map of compound R1 (highest scoring pose).

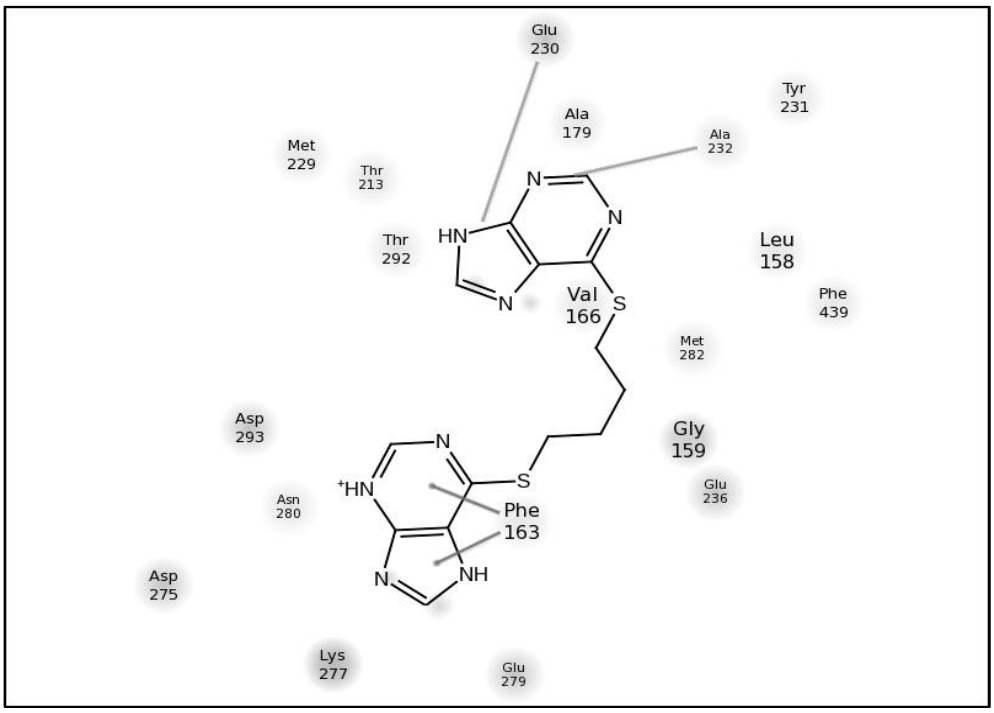

Figure C.7. Induced fit docking ligand interaction map of compound R1 (second highest scoring pose).

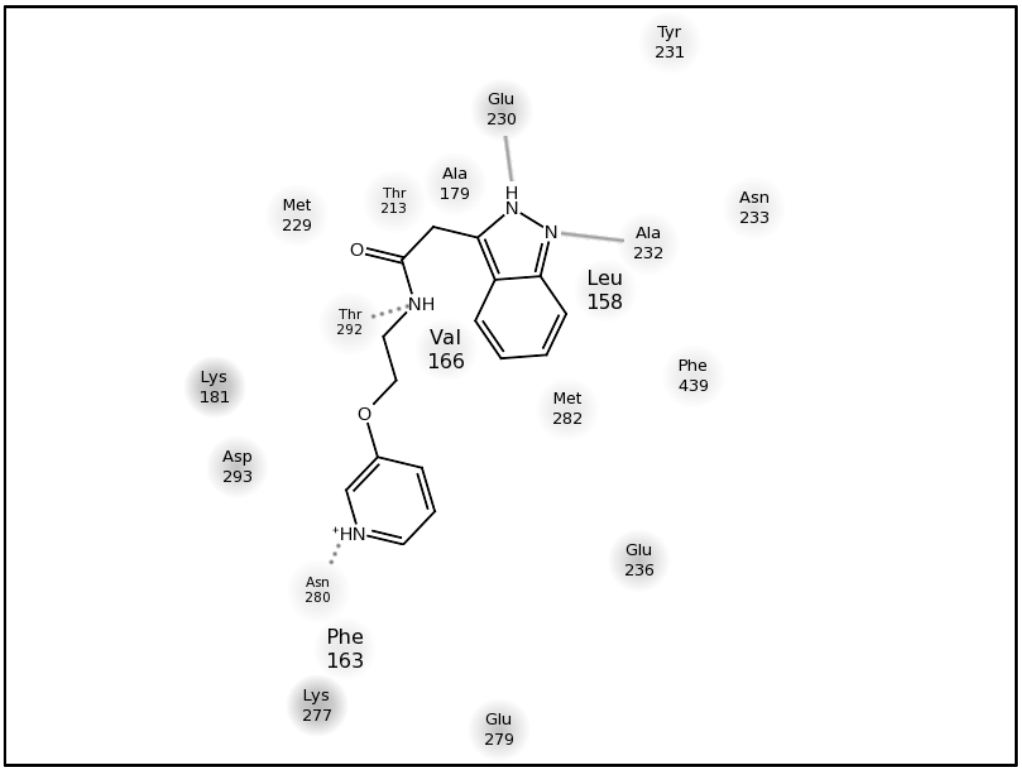

Figure C.8. Induced fit docking ligand interaction map of compound R2.

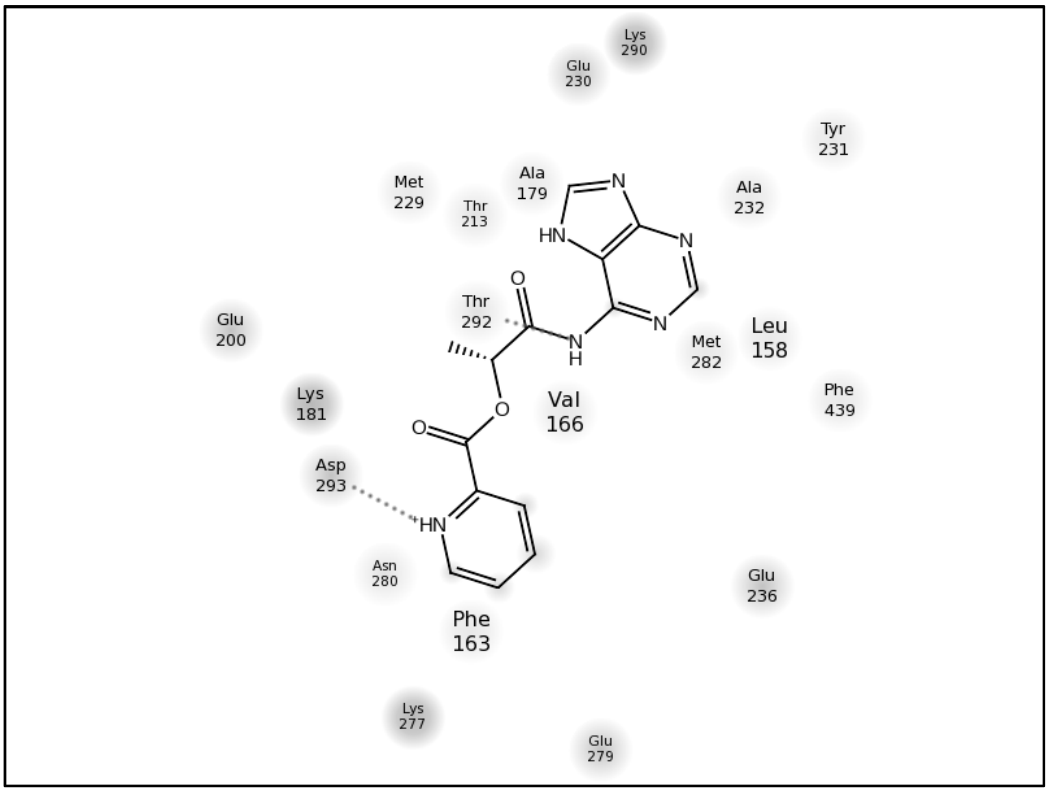

Figure C.9. Induced fit docking ligand interaction map of compound R3.

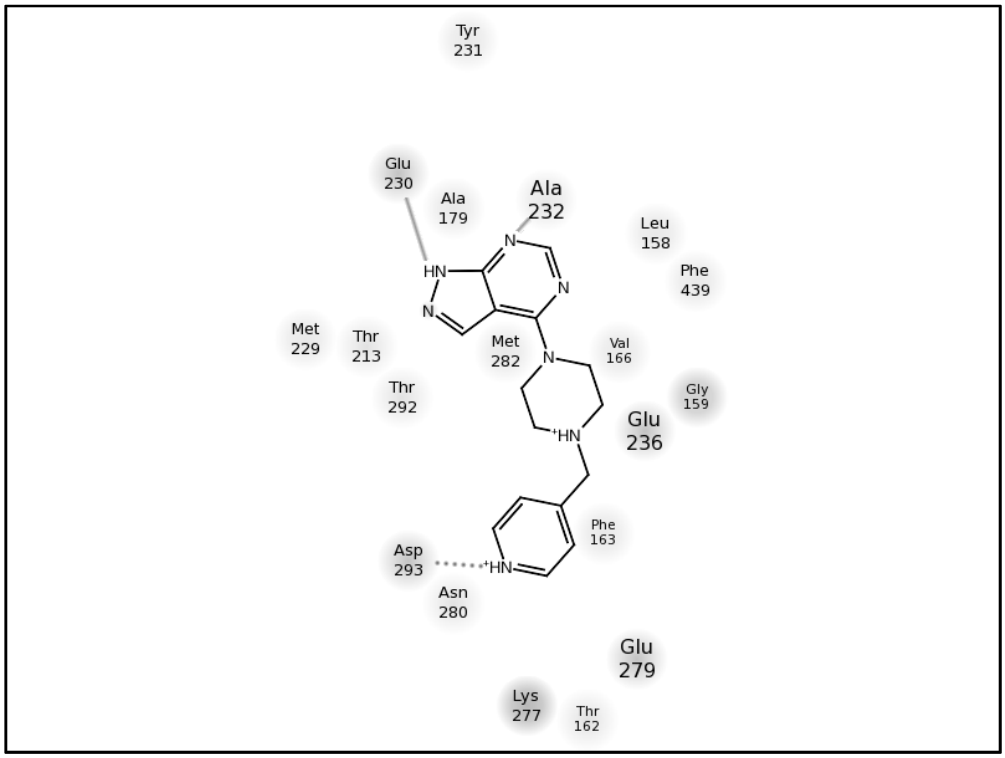

Figure C.10. Induced fit docking ligand interaction map of compound R4.

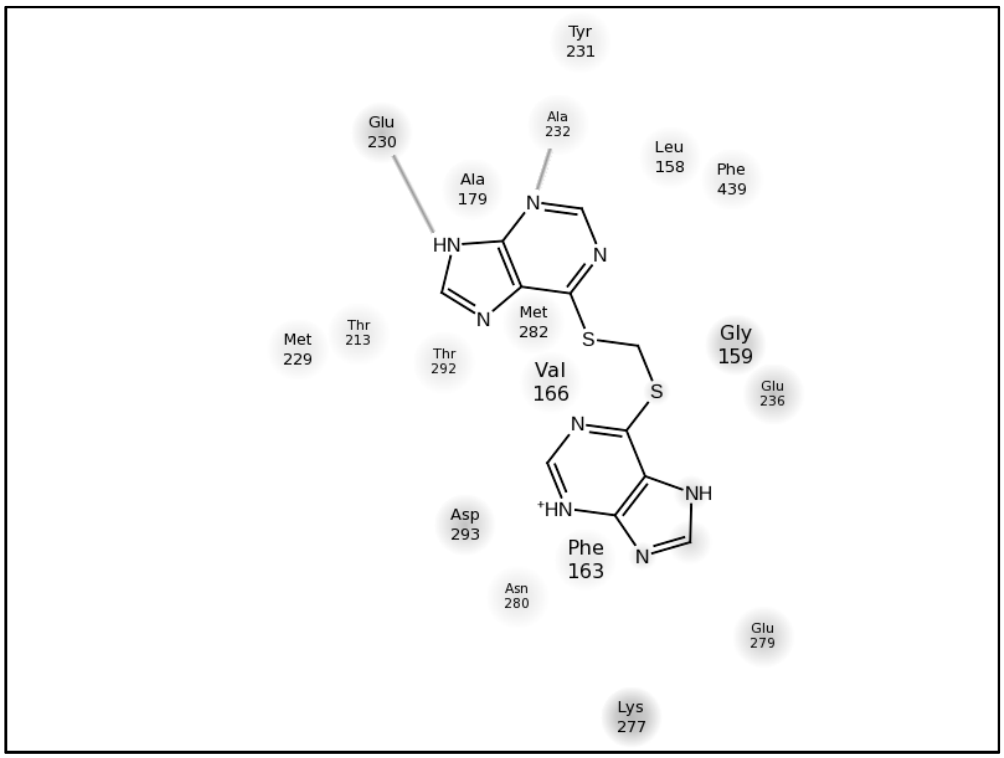

Figure C.11. Induced fit docking ligand interaction map of compound R4.

REFERENCES

1. Myers S. and A. Baker, "Drug Discovery — An Operating Model for a New Era", *Nature Biotechnology*, Vol. 19, No. 8, pp. 727–730, 2001.

2. DiMasi J. A., R. W. Hansen, and H. G. Grabowski, "The Price of Innovation: New Estimates of Drug Development Costs", *Journal of Health Economics*, Vol. 22, No. 2, pp. 151–185, 2003.

3. Otto S., R. L. E. Furlan, and J. K. M. Sanders, "Dynamic Combinatorial Chemistry", *Drug Discovery Today*, Vol. 7, No. 2, pp. 117–125, 2002.

4. Walters W. P. and M. A. Murcko, "Prediction of Drug-likeness", *Advanced Drug Delivery Reviews*, Vol. 54, No. 3, pp. 255–271, 2002.

5. Manning G., G. D. Plowman, T. Hunter, and S. Sudarsanam, "Evolution of Protein Kinase Signaling from Yeast to Man", *Trends in Biochemical Sciences*, Vol. 27, No. 10, pp. 514–520, 2002.

6. Brognard J. and T. Hunter, "Protein Kinase Signaling Networks in Cancer", *Current Opinion in Genetics & Development*, Vol. 21, No. 1, pp. 4–11, 2011.

7. Del Rio A., A. J. M. Barbosa, F. Caporuscio, and G. F. Mangiatordi, "CoCoCo: A Free Suite of Multiconformational Chemical Databases for High-throughput Virtual Screening Purposes", *Molecular BioSystems*, Vol. 6, No. 11, pp. 2122–2128, 2010.

8. Berman H. M., J. Westbrook, Z. Feng, G. Gilliland, T. N. Bhat, H. Weissig, I. N. Shindyalov, and P. E. Bourne, "The Protein Data Bank", *Nucleic Acids Research*, Vol. 28, No. 1, pp. 235–242, 2000.

9. Ripphausen P., B. Nisius, L. Peltason, and J. Bajorath, "Quo Vadis, Virtual Screening? A Comprehensive Survey of Prospective Applications", *Journal of Medicinal Chemistry*, Vol. 53, No. 24, pp. 8461–8467, 2010.

10. Varnek A., and A. Tropsha, *Chemoinformatics Approaches to Virtual Screening*, Royal Society of Chemistry, Cambridge, United Kingdom, 2008.

11. Gonzalez P., C. Acharya, A. MacKerell Jr., and J. Polli, "Inhibition Requirements of the Human Apical Sodium-dependent Bile Acid Transporter (hASBT) Using Aminopiperidine Conjugates of Glutamyl-Bile Acids", *Pharmaceutical Research.*, Vol. 26, No. 7, pp. 1665–1678, 2009.

12. Bernard D., A. Coop, and A. D. MacKerell Jr, "Conformationally Sampled Pharmacophore for Peptidic Delta Opioid Ligands", *Journal of Medicinal Chemistry*, Vol. 48, No. 24, pp. 7773–7780, 2005.

13. Acharya C., A. Coop, and J. Polli, "Recent Advances in Ligand-Based Drug Design: Relevance and Utility of the Conformationally Sampled Pharmacophore Approach", *Current Computer Aided Drug Design*, Vol. 7, No. 1, pp. 10–22, 2011.

14. McInnes C., "Virtual Screening Strategies in Drug Discovery", *Current Opinion in Chemical Biology*, Vol. 11, No. 5, pp. 494–502, 2007.

15. Lyne P. D., "Structure-Based Virtual Screening: An Overview", *Drug Discovery Today*, Vol. 7, No. 20, pp. 1047–1055, 2002.

16. Johnson, M. A. and G. M. Maggiora, *Concepts and Application of Molecular Similarity*, John Wiley & Sons, New York, 1990.

17. Willett P., "Similarity-Based Virtual Screening Using 2D Fingerprints", *Drug Discovery Today*, Vol. 11, No. 23–24, pp. 1046–1053, 2006.

18. Lee C. H., H. C. Huang, and H. F. Juan, "Reviewing Ligand-Based Rational Drug Design: The Search for an ATP Synthase Inhibitor", *International Journal of Molecular Sciences*, Vol. 12, No. 8, pp. 5304–5318, 2011.

19. Scior T., J. L. Medina-Franco, Q. T. Do, K. Martínez-Mayorga, J. A. Yunes Rojas, and P. Bernard, "How to Recognize and Workaround Pitfalls in QSAR Studies: A Critical Review", *Current Medicinal Chemistry*, Vol. 16, No. 32, pp. 4297–4313, 2009.

20. Ehrlich, P., "Über den Jetzigen Stand der Chemotherapie", *Berichte der Deutschen Chemischen Gesellschaft*, Vol. 42, No. 1, p. 17-47, 1909.

21. Patel Y., V. Gillet, and G. Bravi, "A Comparison of the Pharmacophore Identification Programs: Catalyst, DISCO and GASP," *Journal of Computer-Aided Molecular Design*, Vol. 16, No. 8-9, pp. 653–681, 2002.

22. Dixon S. L., A. M. Smondyrev, and S. N. Rao, "PHASE: A Novel Approach to Pharmacophore Modeling and 3D Database Searching", *Chemical Biology & Drug Design*, Vol. 67, No. 5, pp. 370–372, 2006.

23. Dixon S. L., A. M. Smondyrev, E. H. Knoll, S. N. Rao, D. E. Shaw, and R. a Friesner, "PHASE: A New Engine for Pharmacophore Perception, 3D QSAR Model Development, and 3D Database Screening: 1. Methodology and Preliminary Results.," *Journal of Computer-Aided Molecular Design*, Vol. 20, No. 10–11, pp. 647–671, 2006.

24. Bemporad D., C. Luttmann, and J. W. Essex, "Behaviour of Small Solutes and Large Drugs in a Lipid Bilayer from Computer Simulations", *Biochimica et Biophysica Acta*, Vol. 1718, No. 1–2, pp. 1–21, 2005.

25. Cheng T., Q. Li, Z. Zhou, Y. Wang, and S. H. Bryant, "Structure-Based Virtual Screening for Drug Discovery: A Problem-Centric Review", *The AAPS Journal*, Vol. 14, No. 1, pp. 133–141, 2012.

26. Morris G., D. Goodsell, and R. Halliday, "Automated Docking Using a Lamarckian Genetic Algorithm and an Empirical Binding Free Energy Function", *Journal of Computational Chemistry*, Vol. 19, No. 14, pp. 1639–1662, 1998.

27. Ewing T. J. A., S. Makino, A. G. Skillman, and I. D. Kuntz, "DOCK 4 .0 : Search Strategies for Automated Molecular Docking of Flexible Molecule Databases", *Journal of Computer-Aided Molecular Design*, Vol. 15, No. 5, pp. 411–428, 2001.

28. Rarey M., B. Kramer, T. Lengauer, and G. Klebe, "A Fast Flexible Docking Method Using an Incremental Construction Algorithm", *Journal of Molecular Biology*, Vol. 261, No. 3, pp. 470–489, 2002.

29. Friesner R. A, J. L. Banks, R. B. Murphy, T. A Halgren, J. J. Klicic, D. T. Mainz, M. P. Repasky, E. H. Knoll, M. Shelley, J. K. Perry, D. E. Shaw, P. Francis, and P. S. Shenkin, "Glide: A New Approach for Rapid, Accurate Docking and Scoring. 1. Method and Assessment of Docking Accuracy", *Journal of Medicinal Chemistry*, Vol. 47, No. 7, pp. 1739–1749, 2004.

30. Jones G., P. Willett, R. C. Glen, A. R. Leach, R. Taylor, and K. B. R. Uk, "Development and Validation of a Genetic Algorithm for Flexible Docking", *Journal of Molecular Biology*, Vol. 267, No. 3, pp. 727–748, 1997.

31. Jain A. N., "Surflex: Fully Automatic Flexible Molecular Docking Using a Molecular Similarity-Based Search Engine", *Journal of Medicinal Chemistry*, Vol. 46, No. 4, pp. 499–511, 2003.

32. Abagyan R., M. Totrov, and D. Kuznetsov, "ICM? A New Method for Protein Modeling and Design: Applications to Docking and Structure Prediction from the Distorted Native Conformation", *Journal of Computational Chemistry*, Vol. 15, No. 5, pp. 488–506, 1994.

33. Venkatachalam C. M., X. Jiang, T. Oldfield, and M. Waldman, "Ligandfit: A Novel Method for the Shape-Directed Rapid Docking of Ligands to Protein Active Sites", *Journal of Molecular Graphics & Modelling*, Vol. 21, No. 4, pp. 289–307, 2003.

34. Zsoldos Z., I. Szabo, Z. Szabo, and A. P. Johnson, "Software Tools for Structure Based Rational Drug Design", *Journal of Molecular Structure: THEOCHEM*, Vol. 666–667, No. 1, pp. 659–665, 2003.

35. Cummings M. D., A. C. Gibbs, and R. L. DesJarlais, "Processing of Small Molecule Databases for Automated Docking", *Medicinal Chemistry*, Vol. 3, No. 1, pp. 107–113, 2007.

36. Coffer P. J. and J. R. Woodgett, "Molecular Cloning and Characterisation of a Novel Putative Protein-Serine Kinase Related to the Camp-Dependent and Protein Kinase C Families", *European Journal of Biochemistry / FEBS*, Vol. 201, No. 2, pp. 475–481, 1991.

37. Staal S., “Molecular Cloning of the Akt Oncogene and Its Human Homologues AKT1 and AKT2: Amplification of AKT1 in a Primary Human Gastric Adenocarcinoma”, *Proceedings of the National Academy of Sciences of the United States of America*, Vol. 84, No. 14, pp. 5034–5037, 1987.

38. Kohn A. D., K. S. Kovacina, and R. A Roth, “Insulin Stimulates the Kinase Activity of RAC-PK, a Pleckstrin Homology Domain Containing Ser/Thr Kinase”, *The EMBO Journal*, Vol. 14, No. 17, pp. 4288–4295, 1995.

39. Kumar C. C. and V. Madison, “AKT Crystal Structure and AKT-Specific Inhibitors”, *Oncogene*, Vol. 24, No. 50, pp. 7493–501, 2005.

40. Cheng J. Q., A. K. Godwin, A. Bellacosa, T. Taguchi, T. F. Franke, T. C. Hamilton, P. N. Tsichlis, and J. R. Testa, “AKT2, a Putative Oncogene Encoding a Member Of a Subfamily Of Protein-Serine/Threonine Kinases, is Amplified in Human Ovarian Carcinomas”, *Proceedings of the National Academy of Sciences of the United States of America*, Vol. 89, No. 19, pp. 9267–9271, 1992.

41. Testa J. R. and a Bellacosa, “AKT Plays a Central Role in Tumorigenesis”, *Proceedings of the National Academy of Sciences of the United States of America*, Vol. 98, No. 20, pp. 10983–5, 2001.

42. Tamgüney T., C. Zhang, D. Fiedler, K. Shokat, and D. Stokoe, “Analysis of 3-Phosphoinositide-Dependent Kinase-1 Signaling and Function in ES Cells”, *Experimental Cell Research*, Vol. 314, No. 11–12, pp. 2299–2312, 2008.

43. Testa J. and A. Bellacosa, “Membrane Translocation and Activation of the Akt Kinase in Growth Factor-Stimulated Hematopoietic Cells”, *Leukemia Research*, Vol. 21, No. 12, pp. 1027–1031, 1997.

44. Matheny R. W. and M. L. Adamo, “Current Perspectives on Akt Akt-Ivation and Akt-Ions”, *Experimental Biology and Medicine*, Vol. 234, No. 11, pp. 1264–1270, 2009.

45. Miller M., K. Ginalski, B. Lesyng, N. Nakaigawa, L. Schmidt, and B. Zbar, “Structural Basis of Oncogenic Activation Caused by Point Mutations in the Kinase Domain of the MET Proto-Oncogene: Modeling Studies”, *Proteins*, Vol. 44, No. 1, pp. 32–43, 2001.

46. Klippel A., W. M. Kavanaugh, D. Pot, and L. T. Williams, “A Specific Product of Phosphatidylinositol 3-Kinase Directly Activates the Protein Kinase Akt through Its Pleckstrin Homology Domain”, *Molecular and Cellular Biology*, Vol. 17, No. 1, pp. 338–344, 1997.

47. Stokoe D., L. R. Stephens, T. Copeland, P. R. Gaffney, C. B. Reese, G. F. Painter, a B. Holmes, F. McCormick, and P. T. Hawkins, “Dual Role of Phosphatidylinositol-3,4,5-Trisphosphate in the Activation of Protein Kinase B”, *Science*, Vol. 277, No. 5325, pp. 567–570, 1997.

48. Matte B. M. and J. Downward, “PKB / Akt : Connecting Phosphoinositide 3-Kinase to Cell Survival and Beyond”, *Trends in Biochemical Sciences*, Vol. 22, No. 9, pp. 355–358, 1997.

49. Frech M., M. Andjelkovic, E. Ingley, K. K. Reddy, J. R. Falck, and B. A. Hemmings, “High Affinity Binding of Inositol Phosphates and Phosphoinositides to the Pleckstrin Homology Domain of RAC/Protein Kinase B and Their Influence on Kinase Activity”, *The Journal of Biological Chemistry*, Vol. 272, No. 13, pp. 8474–8481, 1997.

50. Thomas A. T., F. Franke, D. R. Kaplan, and L. C. Cantley, “Direct Regulation of the Akt Proto-Oncogene Product by Phosphatidylinositol-3,4-Bisphosphate”, *Science*, Vol. 275, No. 5300, pp. 665–668, 1997.

51. Alessi D. R., F. B. Caudwell, M. Andjelkovic, B. A. Hemmings, and P. Cohen, “Molecular Basis for the Substrate Specificity of Protein Kinase B; Comparison with MAPKAP Kinase-1 and P70 S6 Kinase”, *FEBS Letters*, Vol. 399, No. 3, pp. 333–338, 1996.

52. Huang X., M. Begley, K. A. Morgenstern, Y. Gu, P. Rose, H. Zhao, and X. Zhu, “Crystal Structure of an Inactive Akt2 Kinase Domain”, *Structure*, Vol. 11, No. 1, pp. 21–30, 2003.

53. Alessi D. R., M. Deak, A. Casamayor, F. B. Caudwell, N. Morrice, D. G. Norman, P. Gaffney, C. B. Reese, N. Colin, D. Harbison, A. Ashworth, and M. Bownes, “3-Phosphoinositide-Dependent Protein Kinase-1 (PDK1): Structural and Functional Homology with the Drosophila DSTPK61 Kinase”, *Current Biology*, Vol. 7, No. 10, pp. 776–789, 1997.

54. Stephens L., K. Anderson, D. Stokoe, H. Erdjument-Bromage, G. F. Painter, A. B. Holmes, P. R. Gaffney, C. B. Reese, F. McCormick, P. Tempst, J. Coadwell, and T. Hawkins, P., “Protein Kinase B Kinases That Mediate Phosphatidylinositol 3,4,5-Trisphosphate-Dependent Activation of Protein Kinase B”, *Science*, Vol. 279, No. 5351, pp. 710–714, 1998.

55. Millward T. A., S. Zolnierowicz, and B. A. Hemmings, “Regulation of Protein Kinase Cascades by Protein Phosphatase 2A”, *Trends in Biochemical Sciences*, Vol. 24, No. 5, pp. 186–191, 1999.

56. Hers I., E. E. Vincent, and J. M. Tavaré, “Akt Signalling in Health and Disease”, *Cellular Signalling*, Vol. 23, No. 10, pp. 1515–1527, 2011.

57. Nicholson K. M. and N. G. Anderson, “The Protein Kinase B/Akt Signalling Pathway in Human Malignancy” *Cellular Signalling*, Vol. 14, No. 5, pp. 381–395, 2002.

58. Bellacosa A., D. de Feo, A. K. Godwin, D. W. Bell, J. Q. Cheng, D. A. Altomare, M. Wan, L. Dubeau, G. Scambia, V. Masciullo, G. Ferrandina, P. Benedetti Panici, S. Mancuso, G. Neri, and J. R. Testa, “Molecular Alterations of the AKT2

Oncogene in Ovarian and Breast Carcinomas", *International Journal of Cancer*, Vol. 64, No. 4, pp. 280–285, 1995.

59. Cheng J. Q., B. Ruggeri, W. M. Klein, G. Sonoda, D. A. Altomare, D. K. Watson, J. R. Testa "Amplification of AKT2 in Human Pancreatic Cells and Inhibition of AKT2 Expression and Tumorigenicity by Antisense RNA", *Proceedings of the National Academy of Sciences of the United States of America*, Vol. 93, No. 8, pp. 3636–3641, 1996.

60. Nakatani K., D. A. Thompson, A. Barthel, H. Sakaue, W. Liu, R. J. Weigel, and R. A. Roth, "Up-Regulation of Akt3 in Estrogen Receptor-Deficient Breast Cancers and Androgen-Independent Prostate Cancer Lines", *The Journal of Biological Chemistry*, Vol. 274, No. 31, pp. 21528–21532, 1999.

61. Heerding D. A., N. Rhodes, J. D. Leber, T. J. Clark, R. M. Keenan, L. V. Lafrance, M. Li, I. G. Safonov, D. T. Takata, J. W. Venslavsky, D. S. Yamashita, A. E. Choudhry, R. A. Copeland, Z. Lai, M. D. Schaber, P. J. Tummino, S. L. Strum, E. R. Wood, D. R. Duckett, D. Eberwein, V. B. Knick, T. J. Lansing, R. T. Mcconnell, S. Zhang, E. A. Minthorn, N. O. Concha, G. L. Warren, and R. Kumar, "Identification of 4-(2-(4-Amino-1,2,5-Oxadiazol-3-Yl)-1-Ethyl-7-{[(3S)-3-Piperidinylmethyl]Oxy}- 1H-Imidazo[4,5-C]Pyridin-4-Yl)-2-Methyl-3-Butyn-2-Ol (GSK690693), a Novel Inhibitor of AKT Kinase", *Journal of Medicinal Chemistry*, Vol. 51, No. 18, pp. 5663–5679, 2008.

62. Kim D., H. Dan, S. Park, L. Yang, Q. Liu, and S. Kaneko, "AKT/PKB Signaling Mechanisms in Cancer and Chemoresistance", *Frontiers in Bioscience*, Vol. 10, No. 1, pp. 975–987, 2005.

63. Cheng J. Q., C. W. Lindsley, G. Z. Cheng, H. Yang, and S. V. Nicosia, "The Akt/PKB Pathway: Molecular Target for Cancer Drug Discovery", *Oncogene*, Vol. 24, No. 50, pp. 7482–7492, 2005.

64. Mahadevan D., G. Powis, E. a Mash, B. George, V. M. Gokhale, S. Zhang, K. Shakalya, L. Du-Cuny, M. Berggren, M. A. Ali, U. Jana, N. Ihle, S. Moses, C. Franklin, S. Narayan, N. Shirahatti, and E. J. Meuillet, "Discovery of a Novel Class of AKT Pleckstrin Homology Domain Inhibitors", *Molecular Cancer Therapeutics*, Vol. 7, No. 9, pp. 2621–2632, 2008.

65. Kumar C. C. and V. Madison, "AKT Crystal Structure and AKT-Specific Inhibitors", *Oncogene*, Vol. 24, No. 50, pp. 7493-7501, 2005.

66. Luo Y., A. R. Shoemaker, X. Liu, K. W. Woods, S. A. Thomas, R. de Jong, E. K. Han, T. Li, V. S. Stoll, J. A. Powlas, A. Oleksijew, M. J. Mitten, Y. Shi, R. Guan, T. P. McGonigal, V. Klinghofer, E. F. Johnson, J. D. Leverson, J. J. Bouska, M. Mamo, R. A. Smith, E. E. Gramling-Evans, B. A. Zinker, A. K. Mika, P. T. Nguyen, T. Oltersdorf, S. H. Rosenberg, Q. Li, and V. L. Giranda, "Potent and Selective Inhibitors of Akt Kinases Slow the Progress of Tumors in Vivo", *Molecular Cancer Therapeutics*, Vol. 4, No. 6, pp. 977–986, 2005.

67. Collins I., J. Caldwell, T. Fonseca, A. Donald, V. Bavetsias, L. J. K. Hunter, M. D. Garrett, M. G. Rowlands, G. W. Aherne, T. G. Davies, V. Berdini, S. J. Woodhead, D. Davis, L. C. A. Seavers, P. G. Wyatt, P. Workman, and E. McDonald, "Structure-Based Design of Isoquinoline-5-Sulfonamide Inhibitors of Protein Kinase B", *Bioorganic & Medicinal Chemistry*, Vol. 14, No. 4, pp. 1255–1273, 2006.

68. Reuveni H., N. Livnah, T. Geiger, S. Klein, O. Ohne, I. Cohen, M. Benhar, G. Gellerman, and A. Levitzki, "Toward a PKB Inhibitor: Modification of a Selective PKA Inhibitor by Rational Design", *Biochemistry*, Vol. 41, No. 32, pp. 10304–10314, 2002.

69. Saxty G., S. J. Woodhead, V. Berdini, T. G. Davies, M. L. Verdonk, P. G. Wyatt, R. G. Boyle, D. Barford, R. Downham, M. D. Garrett, and R. A. Carr, "Identification of Inhibitors of Protein Kinase B Using Fragment-Based Lead Discovery", *Journal of Medicinal Chemistry*, Vol. 50, No. 10, pp. 2293–2296, 2007.

70. Gaßel M., C. B. Breitenlechner, P. Rüger, U. Jucknischke, T. Schneider, R. Huber, D. Bossemeyer, and R. A. Engh, "Mutants of Protein Kinase A That Mimic the ATP-Binding Site of Protein Kinase B (AKT)", *Journal of Molecular Biology*, Vol. 329, No. 5, pp. 1021–1034, 2003.

71. Davies T. G., M. L. Verdonk, B. Graham, S. Saalau-Bethell, C. C. F. Hamlett, T. McHardy, I. Collins, M. D. Garrett, P. Workman, S. J. Woodhead, H. Jhoti, and D. Barford, "A Structural Comparison of Inhibitor Binding to PKB, PKA and PKA-PKB Chimera", *Journal of Molecular Biology*, Vol. 367, No. 3, pp. 882–894, 2007.

72. McHardy T., J. J. Caldwell, K.-M. Cheung, L. J. Hunter, K. Taylor, M. Rowlands, R. Ruddle, A. Henley, A. de Haven Brandon, M. Valenti, T. G. Davies, L. Fazal, L. Seavers, F. I. Raynaud, S. A. Eccles, G. W. Aherne, M. D. Garrett, and I. Collins, "Discovery of 4-Amino-1-(7H-Pyrrolo[2,3-D]Pyrimidin-4-Yl)Piperidine-4-Carboxamides as Selective, Orally Active Inhibitors of Protein Kinase B (Akt)", *Journal of Medicinal Chemistry*, Vol. 53, No. 5, pp. 2239–2249, 2010.

73. Rouse M. B., M. A. Seefeld, J. D. Leber, K. C. McNulty, L. Sun, W. H. Miller, S. Zhang, E. A. Minthorn, N. O. Concha, A. E. Choudhry, M. D. Schaber, and D. A. Heerding, "Aminofurazans as Potent Inhibitors of AKT Kinase", *Bioorganic & Medicinal Chemistry Letters*, Vol. 19, No. 5, pp. 1508–1511, 2009.

74. Castillo S. S., J. Brognard, P. A. Petukhov, C. Zhang, J. Tsurutani, C. A. Granville, M. Li, M. Jung, K. A. West, J. G. Gills, A. P. Kozikowski, and P. A. Dennis, "Preferential Inhibition of Akt and Killing of Akt-Dependent Cancer Cells by Rationally Designed Phosphatidylinositol Ether Lipid Analogues", *Cancer Research*, Vol. 64, No. 8, pp. 2782–2792, 2004.

75. Lindsley C. W., Z. Zhao, W. H. Leister, R. G. Robinson, S. F. Barnett, D. Defeo-Jones, R. E. Jones, G. D. Hartman, J. R. Huff, H. E. Huber, and M. E. Duggan, "Allosteric Akt (PKB) Inhibitors: Discovery and SAR of Isozyme Selective

Inhibitors", *Bioorganic & Medicinal Chemistry Letters*, Vol. 15, No. 3, pp. 761–764, 2005.

76. Zhao Z., W. H. Leister, R. G. Robinson, S. F. Barnett, D. Defeo-Jones, R. E. Jones, G. D. Hartman, J. R. Huff, H. E. Huber, M. E. Duggan, and C. W. Lindsley, "Discovery of 2,3,5-Trisubstituted Pyridine Derivatives as Potent Akt1 and Akt2 Dual Inhibitors", *Bioorganic & Medicinal Chemistry Letters*, Vol. 15, No. 4, pp. 905–909, 2005.

77. Obata T., M. B. Yaffe, G. G. Leparc, E. T. Piro, H. Maegawa, A. Kashiwagi, R. Kikkawa, and L. C. Cantley, "Peptide and Protein Library Screening Defines Optimal Substrate Motifs for AKT/PKB", *The Journal of Biological Chemistry*, Vol. 275, No. 46, pp. 36108–36115, 2000.

78. Feldman R. I., J. M. Wu, M. A. Polokoff, M. J. Kochanny, H. Dinter, D. Zhu, S. L. Biroc, B. Alicke, J. Bryant, S. Yuan, B. O. Buckman, D. Lentz, M. Ferrer, M. Whitlow, M. Adler, S. Finster, Z. Chang, and D. O. Arnaiz, "Novel Small Molecule Inhibitors of 3-Phosphoinositide-Dependent Kinase-1", *The Journal of Biological Chemistry*, Vol. 280, No. 20, pp. 19867–19874, 2005.

79. Semba S., N. Itoh, M. Ito, M. Harada, and M. Yamakhawa, "The in Vitro and in Vivo Effects Oof 2- (4-Morpholinyl) -8-Phenyl- Chromone (LY294002), a Specific Inhibitor of Phosphatidylinositol 3-Kinase, in Human Colon Cancer Cells", *Clinical Cancer Research*, Vol. 8, No. 6, pp. 1957–1963, 2002.

80. Dan H. C., K. Jiang, D. Coppola, A. Hamilton, S. V. Nicosia, S. M. Sebti, and J. Q. Cheng, "Phosphatidylinositol-3-OH Kinase/AKT and Survivin Pathways as Critical Targets for Geranylgeranyltransferase I Inhibitor-Induced Apoptosis", *Oncogene*, Vol. 23, No. 3, pp. 706–715, 2004.

81. Kondapaka S. B., S. S. Singh, G. P. Dasmahapatra, E. A. Sausville, and K. K. Roy, "Perifosine, a Novel Alkylphospholipid, Inhibits Protein Kinase B Activation", *Molecular Cancer Therapeutics*, Vol. 2, No. 11, pp. 1093–1103, 2003.

82. Medina-Franco J. L., M. A. Giulianotti, Y. Yu, L. Shen, L. Yao, and N. Singh, "Discovery of a Novel Protein Kinase B Inhibitor by Structure-Based Virtual Screening", *Bioorganic & Medicinal Chemistry Letters*, Vol. 19, No. 16, pp. 4634–4638, 2009."

83. Hernández-Campos A., I. Velázquez-Martínez, R. Castillo, F. López-Vallejo, P. Jia, Y. Yu, M. a Giulianotti, and J. L. Medina-Franco, "Docking of Protein Kinase B Inhibitors: Implications in the Structure-Based Optimization of a Novel Scaffold", *Chemical Biology & Drug Design*, Vol. 76, No. 3, pp. 269–276, 2010.

84. Phase, version 3.3, Schrödinger, LLC, New York, NY, 2011.

85. Halgren T. A., R. B. Murphy, R. A. Friesner, H. S. Beard, L. L. Frye, W. T. Pollard, and J. L. Banks, "Glide: A New Approach for Rapid, Accurate Docking and

Scoring. 2. Enrichment Factors in Database Screening", *Journal of Medicinal Chemistry*, Vol. 47, No. 7, pp. 1750–1759, 2004.

86. Friesner R. A., R. B. Murphy, M. P. Repasky, L. L. Frye, J. R. Greenwood, T. A. Halgren, P. C. Sanschagrin, and D. T. Mainz, "Extra Precision Glide: Docking and Scoring Incorporating a Model of Hydrophobic Enclosure for Protein-Ligand Complexes", *Journal of Medicinal Chemistry*, Vol. 49, No. 21, pp. 6177–6196, 2006.

87. Glide, version 5.7, Schrödinger, LLC, New York, NY, 2011.

88. Schrödinger Suite 2011 Schrödinger Suite; Epik version 2.2, Schrödinger, LLC, New York, NY, 2011; Impact version 5.7, Schrödinger, LLC, New York, NY, 2011; Prime version 2.3, Schrödinger, LLC, New York, NY, 2011.

89. Maestro, version 9.2, Schrödinger, LLC, New York, NY, 2011.

90. Shelley J. C., Æ. A. Cholleti, Æ. L. L. Frye, J. R. Greenwood, and Æ. M. R. Timlin, "Epik : A Software Program for Pk A Prediction and Protonation State Generation for Drug-Like Molecules", *Journal of Computer-Aided Molecular Design*, Vol. 21, No. 12, pp. 681–691, 2007.

91. Greenwood J. R., D. Calkins, A. P. Sullivan, and J. C. Shelley, "Towards the Comprehensive, Rapid, and Accurate Prediction of the Favorable Tautomeric States of Drug-Like Molecules in Aqueous Solution", *Journal of Computer-Aided Molecular Design*, Vol. 24, No. 6–7, pp. 591–604, 2010.

92. Park M. S., C. Gao, and H. a Stern, "Estimating Binding Affinities by Docking/Scoring Methods Using Variable Protonation States", *Proteins*, Vol. 79, No. 1, pp. 304–314, 2011.

93. Epik, version 2.2, Schrödinger, LLC, New York, NY, 2011.

94. Impact version 5.7, Schrödinger, LLC, New York, NY, 2011.

95. LigPrep, version 2.5, Schrödinger, LLC, New York, NY, 2011.

96. MacroModel, version 9.9, Schrödinger, LLC, New York, NY, 2011.

97. QikProp, version 3.4, Schrödinger, LLC, New York, NY, 2011.

98. Jorgensen,W.L., J. Tirado-Rives, "Molecular Modeling of Organic and Biomolecular Systems Using BOSS and MCPRO", *Journal of Computational Chemistry*, Vol. 26, No. 16, pp.1689–1700, 2005.

99. Schrödinger QikProp (2011) Schrödinger, Inc. http://www.schrodinger.com/products/14/17/, April 2012.

100. Jacobson M. P., D. L. Pincus, C. S. Rapp, T. J. F. Day, B. Honig, D. E. Shaw, and R. A. Friesner, "A Hierarchical Approach to All-Atom Protein Loop Prediction", *Proteins*, Vol. 55, No. 2, pp. 351–367, 2004.

101. Jacobson M. P., R. A. Friesner, Z. Xiang, and B. Honig, "On the Role of the Crystal Environment in Determining Protein Side-Chain Conformations", *Journal of Molecular Biology*, Vol. 320, No. 3, pp. 597–608, 2002.

102. Prime, version 2.1, Schrödinger, LLC, New York, NY, 2009.

103. Sherman W., H. S. Beard, and R. Farid, "Use of an Induced Fit Receptor Structure in Virtual Screening", *Chemical Biology & Drug Design*, Vol. 67, No. 1, pp. 83–84, 2006.

104. Sherman W., T. Day, M. P. Jacobson, R. a Friesner, and R. Farid, "Novel Procedure for Modeling Ligand/Receptor Induced Fit Effects", *Journal of Medicinal Chemistry*, Vol. 49, No. 2, pp. 534–553, 2006.

105. Heerding D. A., N. Rhodes, J. D. Leber, T. J. Clark, R. M. Keenan, L. V. Lafrance, M. Li, I. G. Safonov, D. T. Takata, J. W. Venslavsky, D. S. Yamashita, A. E. Choudhry, R. A. Copeland, Z. Lai, M. D. Schaber, P. J. Tummino, S. L. Strum, E. R. Wood, D. R. Duckett, D. Eberwein, V. B. Knick, T. J. Lansing, R. T. Mcconnell, S. Zhang, E. A. Minthorn, N. O. Concha, G. L. Warren, and R. Kumar, "1H-imidazo [4 , 5-c] pyridin-4-yl) -2-methyl-3-butyn-2-ol (GSK690693), a Novel Inhibitor of AKT Kinase", *Journal of Medicinal Chemistry*, Vol. 51, No. 18, pp. 5663–5679, 2008.

106. ChemAxon.Ltd, "chemicalize.org", *Journal of Chemical Information and Modeling*, Vol. 52, No. 2, pp. 613–615, 2012.

107. Waltenberger B., K. Wiechmann, J. Bauer, P. Markt, S. M. Noha, G. Wolber, J. M. Rollinger, O. Werz, D. Schuster, and H. Stuppner, "Pharmacophore Modeling and Virtual Screening for Novel Acidic Inhibitors of Microsomal Prostaglandin E_2 Synthase-1 (Mpges-1)", *Journal of Medicinal Chemistry*, Vol. 54, No. 9, pp. 3163–3174, 2011.

108. Bagga V., O. Silakari, V. S. Ghorela, M. S. Bahia, G. Rambabu, and J. Sarma, "A Three-Dimensional Pharmacophore Modelling of ITK Inhibitors and Virtual Screening for Novel Inhibitors", *SAR and QSAR in Environmental Research*, Vol. 22, No. 1–2, pp. 171–190, 2011.

109. Niu Y., C. Ma, H. Jin, F. Xu, H. Gao, P. Liu, Y. Li, C. Wang, G. Yang, and P. Xu, "The Discovery of Novel B-Secretase Inhibitors: Pharmacophore Modeling, Virtual Screening, and Docking Studies", *Chemical Biology & Drug Design*, Vol. 79, No. 6, pp. 972–980, 2012.

110. Lu S., H.-C. Liu, Y.-D. Chen, H.-L. Yuan, S.-L. Sun, Y.-P. Gao, P. Yang, L. Zhang, and T. Lu, "Combined Pharmacophore Modeling, Docking, and 3D-QSAR Studies

of PLK1 Inhibitors", *International Journal of Molecular Sciences*, Vol. 12, No. 12, pp. 8713–8739, 2011.

111. Bharatham N., K. Bharatham, and K. W. Lee, "P56 LCK Inhibitor Identification by Pharmacophore Modelling and Molecular Docking", Vol. 28, No. 2, pp. 200–206, 2007.

112. Deng X. Q., H. Y. Wang, Y. L. Zhao, M. L. Xiang, P. D. Jiang, Z. X. Cao, Y. Z. Zheng, S. D. Luo, L. T. Yu, Y. Q. Wei, and S. Y. Yang, "Pharmacophore Modelling and Virtual Screening for Identification of New Aurora-A Kinase Inhibitors", *Chemical Biology & Drug Design*, Vol. 71, No. 6, pp. 533–539, 2008.

113. Rella M., C. A. Rushworth, J. L. Guy, A. J. Turner, T. Langer, and R. M. Jackson, "Structure-Based Pharmacophore Design and Virtual Screening for Novel Angiotensin Converting Enzyme 2 Inhibitors", *Journal of Chemical Information and Modeling*, Vol. 46, No. 2, pp. 708–716, 2006.

114. Barillari C., A. L. Duncan, I. M. Westwood, J. Blagg, and R. L. M. van Montfort, "Analysis of Water Patterns in Protein Kinase Binding Sites", *Proteins*, Vol. 79, No. 7, pp. 2109–2121, 2011.

115. Sanschagrin P. C. and L. A. Kuhn, "Cluster Analysis of Consensus Water Sites in Thrombin and Trypsin Shows Conservation between Serine Proteases and Contributions to Ligand Specificity", *Protein Science*, Vol. 7, No. 10, pp. 2054–2064, 1998.

116. Hevener K., W. Zhao, and D. Ball, "Validation of Molecular Docking Programs for Virtual Screening against Dihydropteroate Synthase", *Journal of Chemical Information and Modeling*, Vol. 49, No. 2, pp. 444–460, 2009.

117. Pierce A. and M. Jacobs, "Docking Study Yields Four Novel Inhibitors of the Protooncogene Pim-1 Kinase", *Journal of Medicinal Chemistry*, Vol. 51, No. 6, pp. 1972–1975, 2008.

118. Thilagavathi R. and R. L. Mancera, "Ligand-Protein Cross-Docking with Water Molecules", *Journal of Chemical Information and Modeling*, Vol. 50, No. 3, pp. 415–421, 2010.

119. Kenyon V., I. Chorny, W. J. Carvajal, T. R. Holman, and M. P. Jacobson, "Novel Human Lipoxygenase Inhibitors Discovered Using Virtual Screening with Homology Models", *Journal of Medicinal Chemistry*, Vol. 49, No. 4, pp. 1356–1363, 2006.

120. Eldridge M. D., C. W. Murray, T. R. Auton, G. V. Paolini, and R. P. Mee, "Empirical Scoring Functions: I. The Development of a Fast Empirical Scoring Function to Estimate the Binding Affinity of Ligands in Receptor Complexes", *Journal of Computer-Aided Molecular Design*, Vol. 11, No. 5, pp. 425–445, 1997.

121. Lipinski C. A., F. Lombardo, B. W. Dominy, and P. J. Feeney, "Experimental and Computational Approaches to Estimate Solubility and Permeability in Drug Discovery and Development Settings", *Advanced Drug Delivery Reviews*, Vol. 23, No. 1–3, pp. 3–25, 1997.

122. Kawatkar S., H. Wang, R. Czerminski, and D. Joseph-McCarthy, "Virtual Fragment Screening: An Exploration of Various Docking and Scoring Protocols for Fragments Using Glide", *Journal of Computer-Aided Molecular Design*, Vol. 23, No. 8, pp. 527–539, 2009.

123. Naik P. K., M. Lopus, R. Aneja, S. N. Vangapandu, and H. C. Joshi, "In Silico Inspired Design and Synthesis of a Novel Tubulin-Binding Anti-Cancer Drug: Folate Conjugated Noscapine (Targetin)", *Journal of Computer-Aided Molecular Design*, Vol. 26, No. 2, pp. 233–247, 2012.

124. Ringe K. M. Jr, D., and C. Reynolds, *Drug design: Structure-and Ligand-Based Approaches*. Cambridge University Press, NewYork, NY, pp. 1–10, 2010.

125. Nichols S. E., R. A. Domaoal, V. V. Thakur, J. Tirado-Rives, K. S. Anderson, and W. L. Jorgensen, "Discovery of Wild-Type and Y181C Mutant Non-Nucleoside HIV-1 Reverse Transcriptase Inhibitors Using Virtual Screening with Multiple Protein Structures", *Journal of Chemical Information and Modeling*, Vol. 49, No. 5, pp. 1272–1279, 2009.

126. Singh K. D., P. Kirubakaran, S. Nagarajan, S. Sakkiah, K. Muthusamy, D. Velmurgan, and J. Jeyakanthan, "Homology Modeling, Molecular Dynamics, E-Pharmacophore Mapping and Docking Study of Chikungunya Virus Nsp2 Protease", *Journal of Molecular Modeling*, Vol. 18, No. 1, pp. 39–51, 2012.

127. Truchon J. F. and C. I. Bayly, "Evaluating Virtual Screening Methods: Good and Bad Metrics for the 'Early Recognition' Problem", *Journal of Chemical Information and Modeling*, Vol. 47, No. 2, pp. 488–508, 2007.

128. Backman T. W. H., Y. Cao, and T. Girke, "Chemmine Tools: An Online Service for Analyzing and Clustering Small Molecules", *Nucleic Acids Research*, Vol. 39, No. 2, pp. 486–491, 2011.

129. Dinesh S., G. Shikha, G. Bhavana, S. Nidhi, and S. Dileep, "Biological Activities of Purine Analogues : A Review", *Journal of Pharmaceutical and Scientific Innovation*, Vol. 1, No. 2, pp. 29–34, 2012.

130. Dhani R., A. Avinash, S. K. Salenaagina, M. V. S. Teja, and P. Masthanaiah, "Indole : The Molecule of Diverse Pharmacological Activities", *Journal of Chemical and Pharmaceutical Research*, Vol. 3, No. 5, pp. 519–523, 2011.

131. Lalit K., B. Shashi, and J. Kamal, "The Diverse Pharmacological Importance of Indole Derivatives : A Review", *International Journal of Research in Pharmacy and Science*, Vol. 2, No. 2, pp. 23–33, 2012.

132. Alonso H., A. A. Bliznyuk, and J. E. Gready, “Combining Docking and Molecular Dynamic Simulations in Drug Design”, *Medicinal Research Reviews*, Vol. 26, No. 5, pp. 531–568, 2006.